



**HAL**  
open science

## **A synthesis of SNAPO-CO<sub>2</sub> ocean total alkalinity and total dissolved inorganic carbon measurements from 1993 to 2022**

Nicolas Metzl, Jonathan Fin, Claire Lo Monaco, Claude Mignon, Samir Alliouane, David Antoine, Guillaume Bourdin, Jacqueline Boutin, Yann Bozec, Pascal Conan, et al.

### ► To cite this version:

Nicolas Metzl, Jonathan Fin, Claire Lo Monaco, Claude Mignon, Samir Alliouane, et al.. A synthesis of SNAPO-CO<sub>2</sub> ocean total alkalinity and total dissolved inorganic carbon measurements from 1993 to 2022. 2023. hal-04292340v1

**HAL Id: hal-04292340**

**<https://hal.science/hal-04292340v1>**

Preprint submitted on 4 Sep 2023 (v1), last revised 17 Nov 2023 (v2)

**HAL** is a multi-disciplinary open access archive for the deposit and dissemination of scientific research documents, whether they are published or not. The documents may come from teaching and research institutions in France or abroad, or from public or private research centers.

L'archive ouverte pluridisciplinaire **HAL**, est destinée au dépôt et à la diffusion de documents scientifiques de niveau recherche, publiés ou non, émanant des établissements d'enseignement et de recherche français ou étrangers, des laboratoires publics ou privés.



1 A synthesis of SNAPO-CO<sub>2</sub> ocean total alkalinity and total dissolved  
2 inorganic carbon measurements from 1993 to 2022.

3

4 Nicolas Metzl<sup>1</sup>, Jonathan Fin<sup>1,2</sup>, Claire Lo Monaco<sup>1</sup>, Claude Mignon<sup>1</sup>, Samir Alliouane<sup>3</sup>,  
5 David Antoine<sup>3,4</sup>, Guillaume Bourdin<sup>5</sup>, Jacqueline Boutin<sup>1</sup>, Yann Bozec<sup>6</sup>, Pascal Conan<sup>7,8</sup>,  
6 Laurent Coppola<sup>3,8</sup>, Frédéric Diaz<sup>\*</sup>, Eric Douville<sup>9</sup>, Xavier Durrieu de Madron<sup>10</sup>, Jean-Pierre  
7 Gattuso<sup>3,11</sup>, Frédéric Gazeau<sup>3</sup>, Melek Golbol<sup>8,12</sup>, Bruno Lansard<sup>9</sup>, Dominique Lefèvre<sup>13</sup>,  
8 Nathalie Lefèvre<sup>1</sup>, Fabien Lombard<sup>3,14</sup>, Férial Louanchi<sup>15</sup>, Liliane Merlivat<sup>1</sup>, Léa Olivier<sup>1</sup>,  
9 Anne Petrenko<sup>13</sup>, Sébastien Petton<sup>16</sup>, Mireille Pujo-Pay<sup>7</sup>, Christophe Rabouille<sup>9</sup>, Gilles  
10 Reverdin<sup>1</sup>, Céline Ridame<sup>1</sup>, Aline Tribollet<sup>1</sup>, Vincenzo Vellucci<sup>8,12</sup>, Thibaut Wagener<sup>13</sup>, Cathy  
11 Wimart-Rousseau<sup>13,17</sup>

12

13 <sup>1</sup> Laboratoire LOCEAN/IPSL, Sorbonne Université-CNRS-IRD-MNHN, Paris, 75005, France

14 <sup>2</sup> OSU Ecce Terra, Sorbonne Université-CNRS, Paris, 75005, France

15 <sup>3</sup> Sorbonne Université, CNRS, Laboratoire d'Océanographie de Villefranche, LOV, F-06230 Villefranche-sur-  
16 Mer, France

17 <sup>4</sup> Remote Sensing and Satellite Research Group, School of Earth and Planetary Sciences, Curtin University,  
18 Perth WA 6845, Australia

19 <sup>5</sup> School of Marine Sciences, University of Maine, Orono, USA

20 <sup>6</sup> Station Biologique de Roscoff, UMR 7144 – EDYCO-CHIMAR, Roscoff, France

21 <sup>7</sup> Sorbonne Université, CNRS, Laboratoire d'Océanographie Microbienne, LOMIC, F-66650 Banyuls-sur-Mer,  
22 France

23 <sup>8</sup> Sorbonne Université, CNRS, OSU Station Marines, STAMAR, Paris, F-75006, France

24 <sup>9</sup> Laboratoire des Sciences du Climat et de l'Environnement, LSCE/IPSL, UMR 8212 CEA- CNRS-UVSQ,  
25 Université Paris-Saclay, 91191 Gif-sur-Yvette, France

26 <sup>10</sup> CEFREM, CNRS-Université de Perpignan Via Domitia, 52 Avenue Paul Alduy, 66860 Perpignan, France

27 <sup>11</sup> Institute for Sustainable Development and International Relations, Sciences Po, 27 rue Saint Guillaume, F-  
28 75007 Paris, France

29 <sup>12</sup> Sorbonne Université, CNRS, Institut de la Mer de Villefranche, IMEV, Villefranche-sur-Mer, F-06230, France

30 <sup>13</sup> Aix Marseille Univ, Université de Toulon, CNRS, IRD, MIO, Marseille, France

31 <sup>14</sup> Research Federation for the study of Global Ocean Systems Ecology and Evolution, FR2022/Tara GOSEE,  
32 75000, Paris, France.

33 <sup>15</sup> CVRM: Laboratoire de Conservation et de Valorisation des Ressources Marines, Ecole Nationale Supérieure  
34 des Sciences de la Mer et de l'Aménagement du Littoral (ENSSMAL), Station de recherche de Sidi Fredj,  
35 Algeria

36 <sup>16</sup> Ifremer, Univ Brest, CNRS, IRD, LEMAR, F-29840 Argenton, France

37 <sup>17</sup> Marine Biogeochemistry, GEOMAR Helmholtz Centre for Ocean Research Kiel, 24105 Kiel, Germany

38 <sup>\*</sup> Passed away 14/3/2021

39 *Correspondence to:* Nicolas Metzl (nicolas.metzl@locean.ipsl.fr)

40 **Abstract.** Total alkalinity ( $A_T$ ) and total dissolved inorganic carbon ( $C_T$ ) in the oceans are important properties  
41 to understand the ocean carbon cycle and its link with climate change (ocean carbon sinks and sources) or global  
42 change (ocean acidification). We present a data-base of more than 44 400  $A_T$  and  $C_T$  observations in various  
43 ocean regions obtained since 1993 mainly in the frame of French projects. This includes both surface and water  
44 columns data acquired in open oceans, coastal zones and in the Mediterranean Sea and either from time-series or  
45 punctual cruises. Most  $A_T$  and  $C_T$  data in this synthesis were measured from discrete samples using the same  
46 closed-cell potentiometric titration calibrated with Certified Reference Material, with an overall accuracy of  $\pm 4$   
47  $\mu\text{mol kg}^{-1}$  for both  $A_T$  and  $C_T$ . Given the lack of observations in the Indian and Southern Oceans, we added sea



48 surface underway  $A_T$  and  $C_T$  data obtained in 1998-2018 in the frame of OISO cruises and in 2019 during the  
49 CLIM-EPARSEES cruise measured onboard using the same technique. Separate datasets for the global ocean, and  
50 for the Mediterranean Sea are provided in a single format (<https://doi.org/10.17882/95414>, Metzl et al., 2023)  
51 that offers a direct use for regional or global purposes, e.g.  $A_T$ /Salinity relationships, long-term  $C_T$  estimates,  
52 constraint and validation of diagnostics  $C_T$ - $A_T$  reconstructed fields or ocean carbon and coupled climate/carbon  
53 models simulations, as well as data derived from BG-ARGO floats. When associated with other properties, these  
54 data can also be used to calculate pH, fugacity of  $\text{CO}_2$  ( $f\text{CO}_2$ ) and other carbon systems properties to derive  
55 ocean acidification rates or air-sea  $\text{CO}_2$  fluxes.

56

## 57 **1 Introduction**

58

59 Since 1750, humans activities have added 700 ( $\pm 75$ ) PgC to the atmosphere by burning fossil fuels,  
60 producing cement and changing land use (Friedlingstein et al., 2022) driving up the atmospheric carbon dioxide  
61 ( $\text{CO}_2$ ) concentration and leading to unequivocal global warming. The ocean plays a major role in reducing the  
62 impact of climate change by absorbing more than 90% of the excess heat in the climate system (Cheng et al.,  
63 2020; von Schuckmann et al., 2020, 2023; IPCC, 2022) and about 25% of human released  $\text{CO}_2$  (Friedlingstein et  
64 al., 2022). However, the oceanic  $\text{CO}_2$  uptake changes the chemistry of seawater reducing its buffering capacity  
65 (Revelle and Suess, 1957) and leading to a process known as ocean acidification with potential impacts on  
66 marine organisms (Fabry et al., 2008; Doney et al., 2009, 2020; Gattuso et al., 2015). With atmospheric  $\text{CO}_2$   
67 concentrations, surface ocean temperature and ocean heat content, sea-level, sea-ice and glaciers, the ocean  
68 acidification (decrease of pH) is now recognized as one of the 7 key properties for global climate indicators  
69 (WMO, 2018). In the frame of the 2030 Agenda, the United Nations established a set of Sustainable  
70 Development Goals (SDG; United Nations, 2020), including a goal dedicated to the ocean (SDG 14, "Life below  
71 water") which calls to "conserve and sustainably use the oceans, seas and marine resources for sustainable  
72 development". Ocean acidification is specifically referred in the SDG indicator 14.3.1 coordinated at the  
73 Intergovernmental Oceanographic Commission (IOC) of UNESCO. Observing the carbonate system in the  
74 oceans and marginal seas and understanding how this system changes over time is thus highly relevant not only  
75 to quantify the global ocean carbon budget, the anthropogenic  $\text{CO}_2$  inventories or ocean acidification rates, but  
76 also to understand and simulate the processes that govern the complex  $\text{CO}_2$  cycle in the ocean and to better  
77 predict future climate and global changes (Eyring et al., 2016; Kwiatkowski et al., 2020; Jiang et al., 2023a).

78 The number and quality of ocean  $f\text{CO}_2$ ,  $A_T$ ,  $C_T$  and pH measurements has increased substantially over  
79 the past few decades. Quality-controlled observations are now regularly assembled in global data syntheses such  
80 as SOCAT (Surface Ocean  $\text{CO}_2$  Atlas, Pfeil et al., 2013; Bakker et al., 2014, 2016) and GLODAP (Global Ocean  
81 Data Analysis Project, Key et al., 2004; Olsen et al., 2016, 2019, 2020; Lauvset et al., 2021). These datasets  
82 allow evaluation of properties trends in the global ocean, including the change of the ocean  $\text{CO}_2$  sink (e.g.  
83 Wanninkhof et al., 2013; Friedlingstein et al., 2022; Watson et al., 2020), anthropogenic  $\text{CO}_2$  inventories (e.g.  
84 Sabine et al., 2004; Khatiwala et al., 2013; Gruber et al., 2019) and ocean acidification (Lauvset et al., 2015,  
85 2020; Jiang et al., 2019). Thanks to the GLODAP data-base, new methods were recently developed (Sauzède et  
86 al., 2017; Bittig et al., 2018) to reproduce  $A_T$  and  $C_T$  distributions from other properties like temperature, salinity  
87 and oxygen more often observed in the water column especially from autonomous floats (Claustre et al., 2020;  
88 Mignot et al., 2023). These methods (named CANYON-B and CONTENT, Bittig et al., 2018) are now also used  
89 to help decisions on GLODAP data quality control or to fill in observational gaps (Olsen et al., 2019, 2020;



90 Tanhua et al., 2019, 2021). The GLODAP data-products were also successfully used to construct new global  
91 ocean  $A_T$  and  $C_T$  climatological monthly fields in surface and water column using neural network method (e.g.  
92 Broullón et al., 2019, 2020).

93 Following pioneer works that produced various global-ocean climatologies of the sea-surface carbonate  
94 system (Millero et al., 1998; Lee et al., 2000, 2006; Takahashi et al., 2002, 2009, 2014; Sasse et al., 2013; Jiang  
95 et al., 2019), the coupling of  $f\text{CO}_2$  data (from SOCAT) and  $A_T$  data (from GLODAP) now enables reconstruction  
96 of the full carbonate system in the surface ocean at monthly scale to investigate temporal trends at decadal scale  
97 (e.g. Gregor and Gruber, 2021; Keppler et al., 2023).

98 International projects such as SOCAT and GLODAP offer important way to synthesize ocean carbon  
99 data. In these projects, each observation is quality controlled offering to users high quality observations for  
100 regional or global analysis, either for processes analysis or to constraint or validate of ocean and coupled  
101 climate/carbon models (CMIP6, e.g. Lerner et al., 2021). SOCAT is a publicly available synthesis product  
102 initiated in 2007 (Metzl et al., 2007) for quality-controlled, surface ocean  $f\text{CO}_2$  (fugacity of carbon dioxide)  
103 observations made by the international marine carbon research community (Bakker et al., 2016). The first  
104 SOCAT version was released in 2011 (Pfeil et al., 2013; Sabine et al., 2013), followed by 6 SOCAT versions  
105 (Bakker et al., 2014, 2016). The last version in 2023 includes more than 40 million  $f\text{CO}_2$  data with accuracy  
106 better than  $5 \mu\text{atm}$  (Bakker et al., 2023). One important product from SOCAT is the use of data to estimate  
107 global air-sea  $\text{CO}_2$  fluxes based on reconstructed  $p\text{CO}_2$  fields (e.g. SOCOM project, Surface Ocean  $p\text{CO}_2$   
108 Mapping Intercomparison, Rödenbeck et al., 2015). Since 2015, these results are included each year for the  
109 global carbon budget (Le Quere et al., 2015; Friedlingstein et al., 2022).

110 On the other hand, following WOCE/JGOFS era in the 90s when almost all observations were started to  
111 be synthesized in a specific recommended format (Joyce and Corry, 1994), GLODAP focusses on water-column  
112 carbon observations (and other properties). Following the original GLODAP data-product (Key et al., 2004), the  
113 project accumulated many new quality controlled observations. One important achievement from GLODAP is  
114 the use of data to estimate the anthropogenic  $\text{CO}_2$  inventory or its change over decades (Sabine et al., 2004;  
115 Gruber et al., 2019). Both products, SOCAT and GLODAP, are relevant tools to detect oceanic acidification  
116 rates (Lauvset et al., 2015; Jiang et al., 2019).

117 Although these projects include many international ocean observations there are ocean  $\text{CO}_2$  related  
118 observations all around the world (published or not published), such as total alkalinity and dissolved inorganic  
119 carbon, not included in SOCAT or GLODAP. This is because SOCAT accepts and controls only  $f\text{CO}_2$  data,  
120 whereas GLODAP includes and controls water-columns data mainly from WOCE/GO-SHIP/CLIVAR cruises. It  
121 should be noticed that many ocean carbon observations in various formats can be also found in dedicated data-  
122 base such as NCEI/OCADS (former CDIAC-Ocean, Jiang et al., 2013b,  
123 <https://www.ncei.noaa.gov/products/ocean-carbon-acidification-data-system>), PANGAEA  
124 (<https://www.pangaea.de/>) or SeaNoe (<https://www.seano.e.org/>). In this context it is recommended to progress in  
125 data synthesis of the ocean carbon observations that would offer new high quality products for the community  
126 (e.g. for GOA-ON, [www.goa-on.org](http://www.goa-on.org), IOC/SDG 14.1.3, <https://oa.iode.org/>, Tilbrook et al., 2019).

127 In this work, we present a synthesis of more than 44 400  $A_T$  and  $C_T$  observations obtained over the  
128 1993-2022 period during various cruises or at time-series stations mainly supported by French projects. This  
129 dataset merges observations measured with the same instruments thus being analytically coherent. Most of the  
130 data have accuracy better than  $\pm 4 \mu\text{mol kg}^{-1}$ , i.e. between the climate ( $\pm 2 \mu\text{mol kg}^{-1}$ ) and weather ( $\pm 10 \mu\text{mol kg}^{-1}$ )



131 <sup>1</sup>) goals (Bockmon and Dickson, 2015). Hereafter this dataset will be cited as SNAPO-CO<sub>2</sub>. We describe the  
132 data assemblage and associated quality control and discuss some potential uses of this dataset.

133

## 134 **2 Data collections**

135

136 The time series projects and research cruises from which data were collated are listed in Table 1 with  
137 references in the Supplementary file (SNAPO-CO<sub>2</sub>-cruises) and the sampling locations displayed in Figure 1.  
138 Sampling was performed either from CTD-Rosette casts (Niskin bottles) or from the ship's seawater supply  
139 (intake at about 5m depth depending the ship and swell). Samples collected in 500 mL borosilicate glass bottles  
140 were poisoned with 100 to 300 µL of HgCl<sub>2</sub> depending on the cruises, closed with greased stoppers (Apiezon®)  
141 and held tight using elastic band following the SOP protocol (Dickson et al., 2007). Some samples were also  
142 collected in 500 mL bottles closed with screw caps. After completion of each cruise, discrete samples were  
143 returned back to the LOCEAN laboratory (Paris, France) and stored in a dark room at 4 °C before analysis  
144 generally within 2-3 months after sampling (sometimes within a week). Some samples were also measured for  
145 specific processes studies on benthic corals (e.g. Maier et al., 2012; McCulloch et al., 2012) or for mesocosm  
146 and culture experiments but the data are not included in this synthesis as they do not represent natural ocean state  
147 (e.g. addition of Sahara dust during the DUNE project, Ridame et al., 2014).

148 As opposed to pCO<sub>2</sub>, surface A<sub>T</sub> or C<sub>T</sub> observations are generally obtained from discrete sampling  
149 (measured onboard or onshore). Few cruises offer sea-surface semi-continuous A<sub>T</sub> or C<sub>T</sub> observations (e.g. Metzl  
150 et al., 2006) but new instrumental developments now enable A<sub>T</sub> measurements on SOOP lines, Ship of  
151 Opportunity Program (Seelmann et al., 2020). In addition to discrete samples analyzed for various projects  
152 conducted mainly in the North Atlantic, Tropical Atlantic, Tropical Pacific, Mediterranean sea and coastal  
153 regions (Table 1), we complemented this synthesis with A<sub>T</sub> and C<sub>T</sub> surface observations obtained in the Indian  
154 and Southern oceans during the OISO cruises in 1998-2018 (Metzl et al., 2006; Leseurre et al., 2022; data also  
155 available at NCEI/OCADS: [www.nodc.noaa.gov/ocads/oceans/VOS\\_Program/OISO.html](http://www.nodc.noaa.gov/ocads/oceans/VOS_Program/OISO.html)) and the recent CLIM-  
156 EPARSEES cruise conducted in the Mozambique Channel in April 2019 (Lo Monaco et al., 2020, 2021). For  
157 OISO cruises the water-column observations are part of the CARINA (CARbon IN the Atlantic) and GLODAP  
158 synthesis products (Lo Monaco et al., 2010; Olsen et al., 2016, 2019, 2020) and not included here. Excepted  
159 when specified, all data in this synthesis were obtained using the same technique used either in laboratory or at  
160 sea (for OISO 1998-2018 and CLIM-EPARSEES 2019 cruises).

161



162 **Table 1:** List of cruises in the SNAPO-CO2 dataset. This is organized by region: Global Ocean and coastal  
 163 zones, and Mediterranean Sea (MedSea). See Tables S1, S2, S4 and S4 in the Supplementary Material for a list  
 164 of laboratories, of CRMs used, for references and for DOI of cruises. Nb = the number of data for each cruise or  
 165 time-series.

166	Cruise/Project	Start	End	Region	Sampling	Nb
167						
168						
169						
170						
171	AWIPEV	2015	2021	Arctic	Surface and sub-surface	195
172	SURATLANT+RREX	1993	2017	North Atlantic	Surface	2832
173	OVIDE	2006	2018	North Atlantic	Surface, Water Column	397
174	STRASSE	2012		North Atlantic	Water Column	205
175	EUREC4A-OA	2020		North Atlantic	Surface, Water Column	135
176	PROTEUS	2010		North Atlantic	Water Column	27
177	CHANNEL	2012	2015	English Channel	Surface	696
178	SOMLIT-Brest	2008	2019	Coastal North Atl	Surface	1174
179	SOMLIT-Roscoff	2009	2019	Coastal North Atl	Surface and 60m	801
180	ECOSCOPIA	2017	2019	Coastal North Atl	Surface	67
181	PENZE	2011	2020	River Brittany	Surface and sub-surface	148
182	AULNE	2009	2010	River Brittany	Surface	27
183	ELORN	2009	2009	River Brittany	Surface	28
184	BIOZAIRE	2003	2004	Trop Atlantic	Water Column	87
185	EGEE	2005	2007	Trop Atlantic	Surface	199
186	PIRATA-FR	2009	2017	Trop Atlantic	Surface, Water Column	513
187	PLUMAND	2007		Trop Atlantic	Surface	38
188	OUTPACE	2015		Trop Pacific	Water Column	240
189	PANDORA	2012		Solomon Sea	Water Column	178
190	TARA-Pacific	2016	2018	Trop Pac, NATL	Surface and sub-surface	325
191	TARA-Ocean	2009	2012	Global Ocean	Surface + 400m	123
192	TARA-Microbiome	2021	2022	Atlantic	Surface, Water Column	216
193	ACE	2016	2017	Southern Ocean	Surface, Water Column	135
194	MOBYDICK	2019		Southern Ocean	Water Column	64
195	CLIM-EPARSESES	2019		Indian	Surface	790
196	OISO	1998	2018	South Indian	Surface	24950
197						
198	DYFAMED	1998	2017	MedSea	Water Column	2118
199	BOUSSOLE	2014	2019	MedSea	Surface + 10m	172
200	SOMLIT-PointB	2007	2015	MedSea Coastal	Surface + 50m	2397
201	ANTARES	2010	2016	MedSea	Water Column	502
202	MOLA	2010	2013	MedSea Coastal	Water Column	66
203	SOLEMIO	2016	2018	MedSea Coastal	Water Column	212
204	MOOSE-GE	2010	2019	MedSea	Water Column	1847
205	LATEX	2010		MedSea	Water Column	51
206	CARBORHONE	2011	2012	MedSea	Water Column	706
207	CASCADE	2011		MedSea	Water Column	218
208	DEWEX	2013		MedSea	Water Column	367
209	SOMBA	2014	2014	MedSea	Water Column	203
210	AMOR-BFLUX	2015		MedSea Coastal	Water Column	6
211	PEACETIME	2017	2017	MedSea	Water Column	233
212	PERLE	2018	2021	MedSea	Water Column	805

213  
 214

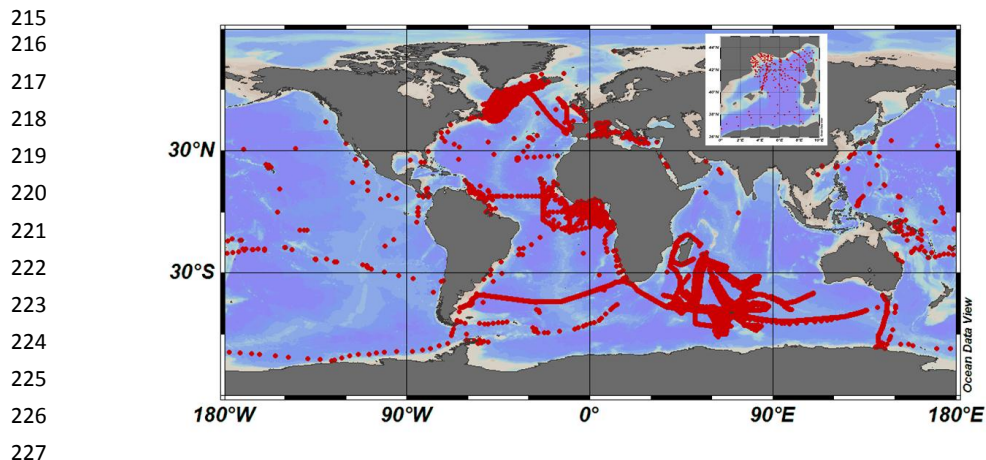


**Figure 1:** Locations of  $A_T$ - $C_T$  data (1993-2022) in the Global Ocean and the Western Mediterranean Sea (insert).  
Figure produced with ODV (Schlitzer, 2018).

### 3 Method, accuracy, reproducibility, intercomparison and quality control

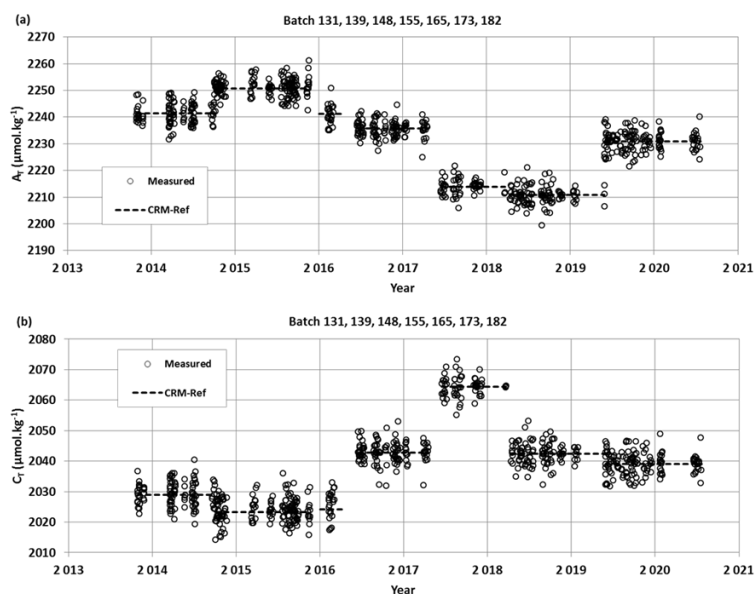
#### 3.1 Method and accuracy

Except for the DYFAMED time-series observations measured between in 1998 and 2000 in the Mediterranean Sea (Copin-Montégut and Bégovic, 2002; Coppola et al., 2020; Lange et al., 2023), the SURATLANT time-series values acquired from 1993 to 1997 in the North Atlantic subpolar gyre (Reverdin et al., 2018) and samples measured in the river Penzé (Brittany) in 2019-2020 (Yann Bozec, SBR/Roscoff, pers. comm.), all discrete samples were measured at LOCEAN laboratory in Paris (SNAPO-CO<sub>2</sub> Service facilities) using the same technique.  $A_T$  and  $C_T$  were analyzed simultaneously by potentiometric titration using a closed cell (Edmond, 1970; Goyet et al., 1991). In the late 1980s the so-called “JGOFS-IOC Advisory Panel on Ocean CO<sub>2</sub>” recommended the need for standard analysis protocols and for developing Certified Reference Materials (CRMs) for inorganic carbon measurements (Poisson et al., 1990; UNESCO, 1990, 1991). The CRMs were provided to international laboratories by Pr. A. Dickson (Scripps Institution of Oceanography, San Diego, USA), starting in 1990 for  $C_T$  and 1996 for  $A_T$ , respectively. These CRMs were thus always available to us and used to calibrate the measurements (CRM Batch numbers used for each cruise are listed in Supplementary file (Table S2)).

Results of analyses performed on 724 CRM bottles (different Batches) in 2013-2020 are presented in Figure 2. The standard deviations of the differences of measurements were on average around  $\pm 3.5 \mu\text{mol kg}^{-1}$  for both  $A_T$  and  $C_T$ . For unknown reasons, the differences were occasionally up to  $10\text{--}15 \mu\text{mol kg}^{-1}$  (0.8% of the data, Figure S2). These few CRM measurements were discarded for the data processing. On average, and excluding some outliers, standard-deviations of the differences for 985 CRM analyses were  $\pm 2.95 \mu\text{mol kg}^{-1}$  for  $A_T$  and  $\pm 3.30 \mu\text{mol kg}^{-1}$  for  $C_T$ , respectively. We did not detect any specific signal for these CRM analyses (e.g., larger uncertainty depending on the Batch number or temporal drifts during analyses, Figure 2) but for some cruises and specific series of samples analyzed over 2 to 7 consecutive days, the accuracy based on CRMs could



256 be slightly better than  $3 \mu\text{mol kg}^{-1}$  ( $\pm 2.5 \mu\text{mol kg}^{-1}$  for both  $A_T$  and  $C_T$ , e.g. Marrec et al., 2014; Touratier et al.,  
257 2016; Ganachaud et al., 2017; Wimart-Rousseau et al., 2020a).



278 **Figure 2:**  $A_T$  (a) and  $C_T$  (b) analyses for different CRM Batches measured in 2013-2020. For these 724 analyses  
279 the mean and standard-deviations of the differences with the CRM reference were  $-0.08 (\pm 3.35) \mu\text{mol.kg}^{-1}$  for  $A_T$   
280 and  $0.15 (\pm 3.61) \mu\text{mol.kg}^{-1}$  for  $C_T$ .

### 281 282 3.2 Reproducibility and repeatability

283  
284 For some projects, duplicates have been regularly sampled (SOMLIT-Point-B, SOMLIT-BREST,  
285 BOUSSOLE/DYFAMED) or replicate bottles sampled at selected depths at fixed stations during the cruises (e.g.  
286 OUTPACE-2015, Wagener et al., 2018; SOMBA-2014, Keraghel et al., 2020). Results of  $A_T$  and  $C_T$   
287 reproducibility or repeatability are synthetized in Table 2. Figure 3 shows example of regular duplicates from the  
288 times-series SOMLIT-Point-B in the coastal Mediterranean Sea (Kapsenberg et al., 2017), SOMLIT-Brest in the  
289 Bay of Brest, coastal Iroise Sea (Salt et al., 2016) and BOUSSOLE/DYFAMED in the Ligurian Sea (Merlivat et  
290 al., 2018; Golbol et al., 2000, 2020). For the 26 OISO cruises conducted between 1998 and 2018 and the CLIM-  
291 EPARSES cruise in April 2019 (Lo Monaco et al., 2020, 2021), the repeatability was evaluated from duplicate  
292 analyses (within 20 minutes time) of continuous sea surface underway sampling at the same location (when the  
293 ship was stopped). Similarly to what was found for the CRM measurements (Figure S2), differences in  
294 duplicates are occasionally higher than  $10\text{-}15 \mu\text{mol kg}^{-1}$  (Figure 3) but most of the duplicates for all projects are  
295 within  $0$  to  $3 \mu\text{mol kg}^{-1}$ . Based on the CRM analyses and replicates for different projects, different regions and  
296 different periods, we estimated the accuracy for both  $A_T$  and  $C_T$  of  $\pm 4 \mu\text{mol kg}^{-1}$ .

297





298  
299  
300  
301  
302  
303  
304  
305  
306  
307  
308  
309  
310  
311  
312  
313  
314  
315  
316  
317  
318  
319  
320  
321  
322  
323  
324  
325  
326  
327  
328  
329  
330  
331  
332  
333  
334  
335  
336  
337  
338  
339  
340  
341  
342

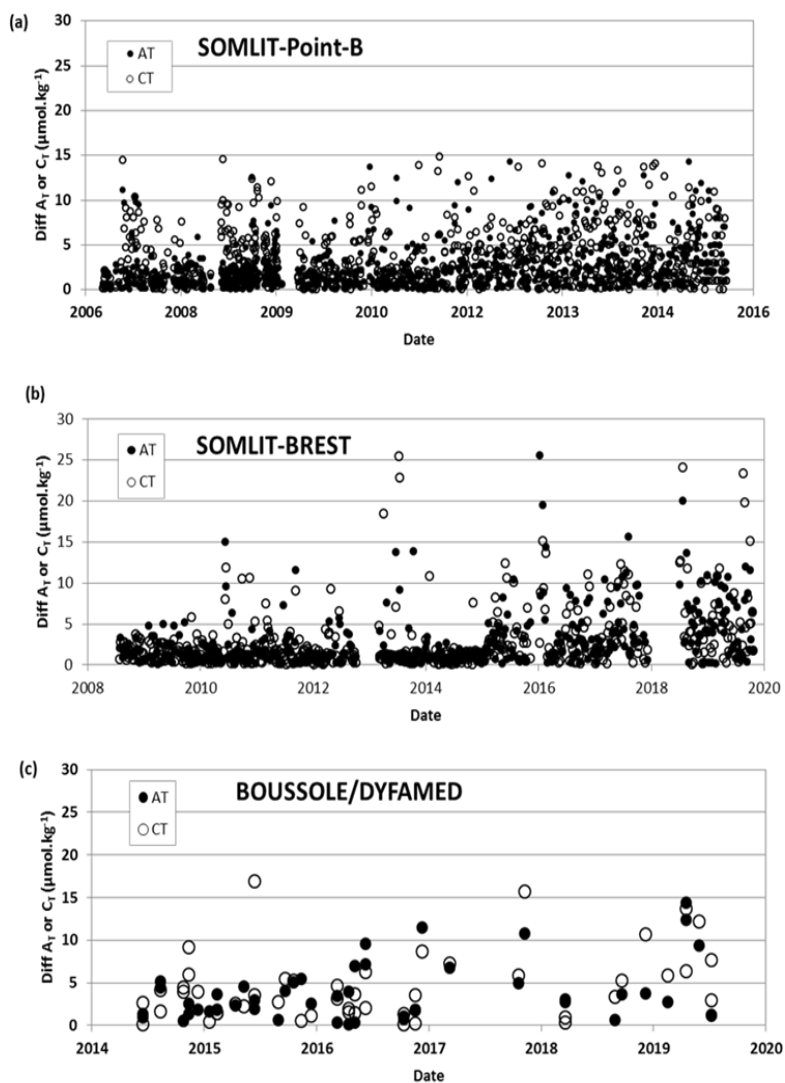


**Figure 3:** Results of duplicate  $A_T$  and  $C_T$  analyses from the time-series (a) SOMLIT-Point-B in the coastal Mediterranean Sea (Kapsenberg et al., 2017), (b) SOMLIT-BREST in the Bay of Brest, coastal Iroise Sea (Salt et al., 2016 and unpublished) and (c) BOUSSOLE/DYFAMED in the Ligurian Sea (Merlivat et al., 2018; Golbol et al., 2020). The plots show differences in duplicates for both  $A_T$  (filled circles) and  $C_T$  (open circles). Standard-deviations of these duplicates are listed in Table 2.



343

344 **Table 2:** Reproducibility of  $A_T$  and  $C_T$  analyses for cruises with duplicate analysis. The results are expressed as  
345 the standard-deviations (Std) of the analysis of replicated samples. Nb = the number of replicates for each Time-  
346 series or Cruise. See Figure 4 for the results of regular duplicates for 3 Time-series (SOMLIT-Point-B,  
347 SOMLIT-BREST, and BOUSSOLE). For OISO and CLIM-EPARSEs cruises the results correspond to repeated  
348 measurements from continuous sea surface underway sampling at the same location (i.e. within 20 minutes time  
349 and when the ship was stopped). For the 26 OISO cruises (1998-2018) and for simplicity we list the mean  
350 repeatability obtained for all cruises. Detail for each OISO cruise could be consulted in the associated metadata  
351 online at NCEI/OCADS, [www.nodc.noaa.gov/ocads/oceans/VOS\\_Program/OISO.html](http://www.nodc.noaa.gov/ocads/oceans/VOS_Program/OISO.html)  
352

353

354

355

356

357

358

359

360

361

362

363

364

365

366

367

368

Project-Cruise	Nb	Std $A_T$ $\mu\text{mol kg}^{-1}$	Std $C_T$ $\mu\text{mol kg}^{-1}$	Reference
OUTPACE	12	3.64	3.68	Wagener et al. (2018)
SOMBA	13	2.00	3.30	Keraghel et al. (2020)
SOMLIT-Point-B	786	2.63	3.10	Kapsenberg et al. (2017)
SOMLIT-Brest	446	3.34	3.67	Salt et al. (2016) + unpub
BOUSSOLE	48	3.47	4.02	Merlivat et al. (2018); Golbol et al. (2020)
CLIM-EPARSEs	122	2.20	2.30	Lo Monaco et al. (2020, 2021)
OISO 1998-2018	1162	2.06	2.28	Metzl et al. (2006) and (*)

367

368

(\*) Data available at [www.nodc.noaa.gov/ocads/oceans/VOS\\_Program/OISO.html](http://www.nodc.noaa.gov/ocads/oceans/VOS_Program/OISO.html)

369

370

371

372

373

374

375

376

377

378

379

380

381

382

383

384

385

386

387

388

389

390

391

392

### 3.3 Inter-comparisons

Inter-comparisons of measurements performed with different technics help to evaluate the quality of the data and detect potential shifts (if any) when merging the data in the same region obtained by different laboratories at different periods. This is especially important to interpret long-term trends of  $A_T$  and  $C_T$  as well as for  $\text{pCO}_2$  and  $\text{pH}$  calculated with  $A_T/C_T$  pairs. For ocean acidification studies, this also refers to the “climate goal” for which an accuracy for  $A_T$  and  $C_T$  better than  $\pm 2 \mu\text{mol kg}^{-1}$  is needed (Newton et al., 2015; Tilbrook et al., 2019). Such inter-comparison thus helps to reflect the quality of the data to achieve either the so-called “weather goal” (for  $A_T$  and  $C_T$ ,  $\pm 10 \mu\text{mol kg}^{-1}$ ) or the “climate goal” ( $\pm 2 \mu\text{mol kg}^{-1}$ ) (Bockmon and Dickson, 2015). For the projects in this data synthesis, inter-laboratory comparisons were performed occasionally and summarized below.

As part of the time-series CHANNEL (2012-2015) in the Western English Channel, Marrec et al. (2014) analyzed surface samples collected bi-monthly in 2011-2013.  $A_T$  analyses were performed with a TA-ALK-2 system (Appolo SciTech.) while  $C_T$  measurements were acquired with an AIRICA system (Marianda Inc.) Based on CRM analyses (Batch #92) the accuracy was estimated  $\pm 3 \mu\text{mol kg}^{-1}$  for  $A_T$  and  $\pm 1.5 \mu\text{mol kg}^{-1}$  for  $C_T$  (Marrec et al., 2014). When comparing with the samples measured at LOCEAN/Paris for the year 2012, Marrec et al. (2014) concluded that between the two methods the concentrations were within  $\pm 2 \mu\text{mol kg}^{-1}$  and  $\pm 3 \mu\text{mol kg}^{-1}$  for  $A_T$  and  $C_T$  respectively. This is close to the “climate goal” offering confident results for long-term trend analysis of the carbonate system in this region.

In the frame of the SURATLANT project in the Sub-Polar North Atlantic gyre, some samples collected at the same time (in 2005, 2006, 2010, 2015, and 2016) were also analyzed onshore for  $A_T$  and/or  $C_T$  by other laboratories using different technics (e.g. coulometric method) and the results summarized by Reverdin et al. (2018). For  $C_T$ , the mean differences between LOCEAN values and from 4 other laboratories range between -0.7 ( $\pm 4.6$ ) and -6.5 ( $\pm 3.4$ )  $\mu\text{mol kg}^{-1}$  depending on the cruise. For  $A_T$  the mean differences with 2 other laboratories



393 range from  $-0.6 (\pm 4.1) \mu\text{mol kg}^{-1}$  to  $+2.3 (\pm 4.8) \mu\text{mol kg}^{-1}$ . These results range between the “climate goal” and  
394 the “weather goal”. See Reverdin et al. (2018) for details on these inter-comparisons.

395 During OVIDE cruises conducted since 2002 in the North Atlantic along a section from Greenland to  
396 Portugal (Lherminier et al., 2007; Mercier et al., 2015) samples have been taken (since 2006) to complement, for  
397 summer, the SURATLANT time-series in the North Atlantic Sub-Polar gyre (NASPG). The OVIDE samples at  
398 the surface and along the water-column at a few stations were measured back at LOCEAN for  $A_T$  and  $C_T$  (Metzl  
399 et al., 2018). This enables us to compare our data with the measurements performed on-board by the IIM group  
400 in Vigo/Spain (e.g. Pérez et al., 2010, 2013, 2018; Vazquez-Rodriguez et al., 2012). The OVIDE data have been  
401 regularly quality controlled in CARINA and GLODAP data products (Velo et al., 2009; Key et al., 2010; Olsen  
402 et al., 2016, 2019, 2020). The results of inter-comparisons are gathered in Table 3. For OVIDE in 2006 we  
403 identified (for unknown reason) a large difference between our original  $A_T$  values compared to the  $A_T$  data  
404 qualified in GLODAP and we thus corrected our  $A_T$  data by  $+7.2 \mu\text{mol kg}^{-1}$ . However, no correction was applied  
405 for  $C_T$ . For other OVIDE cruises, differences for  $A_T$  range between  $-4.5 (\pm 4.11) \mu\text{mol kg}^{-1}$  and  $-0.05 (\pm 3.43)$   
406  $\mu\text{mol kg}^{-1}$  depending on the cruise (i.e.  $A_T$  measured at LOCEAN was always slightly lower than onboard  
407 measurements). For  $C_T$ , we compared our measurements onshore with  $C_T$  values calculated with  $A_T$  and pH  
408 measured onboard. Most of the mean  $C_T$  differences are slightly positive (i.e.  $C_T$  measured at LOCEAN was  
409 always higher, except for 2010). Taking into account all errors associated with the sampling, the transport of  
410 samples, the instrumentations, the data processing, or the calculations for  $C_T$ , the comparisons between  
411 LOCEAN and IIM data for OVIDE cruises are deemed acceptable and large differences for both  $A_T$  and  $C_T$  ( $> 4$   
412  $\mu\text{mol kg}^{-1}$ ) are far from being systematic (Table 3). The data from SURATLANT and OVIDE can then be  
413 merged to complete the time-series in the NASPG in summer and to better describe the seasonality of the  
414 oceanic carbonate system. For example, in 2010, when the North Atlantic Oscillation (NAO) was strongly  
415 negative, the SURATLANT data showed a rapid decrease of  $C_T$  concentrations in the NASPG between early  
416 June and August (Figure 4), with  $C_T$  concentrations in August much lower than other years (Racapé et al., 2014).  
417 This leads to a rapid drop in  $f\text{CO}_2$  in 2009-2010, such that the NASPG was a strong  $\text{CO}_2$  sink (Leseurre et al.,  
418 2020). The winter-to-summer seasonal decrease of  $C_T$  in 2010 in the north NASPG was on average  $-77 \mu\text{mol}$   
419  $\text{kg}^{-1}$  (Figure 4) much larger than in the climatology (range  $-50$  to  $-55 \mu\text{mol kg}^{-1}$ , Takahashi et al., 2014; Reverdin  
420 et al., 2018). The OVIDE data in late June 2010 and SURATLANT in August 2010 confirmed this signal that  
421 was linked to a pronounced primary productivity in that period (Figure 4, Henson et al., 2013; Racapé et al.,  
422 2014; Mc Kinley et al., 2018). Notice that for this period no  $p\text{CO}_2$  observations were available in July-September  
423 2010 in SOCAT data-product and the  $A_T$ - $C_T$  data presented here could be used to calculate  $p\text{CO}_2$  to complement  
424 the  $p\text{CO}_2$  dataset in this region like was done for other periods (Mc Kinley et al., 2011).

425



426  
 427  
 428  
 429  
 430  
 431  
 432  
 433  
 434  
 435  
 436  
 437  
 438  
 439  
 440  
 441  
 442  
 443  
 444  
 445  
 446  
 447  
 448  
 449  
 450  
 451  
 452  
 453  
 454  
 455  
 456  
 457  
 458  
 459  
 460  
 461  
 462  
 463  
 464  
 465  
 466  
 467  
 468  
 469  
 470  
 471  
 472  
 473  
 474  
 475  
 476  
 477  
 478  
 479  
 480  
 481

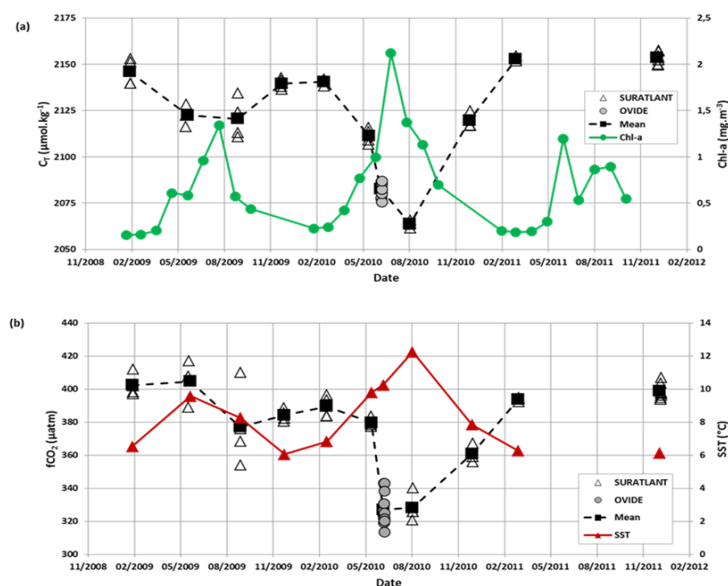


**Figure 4:** (a) Time-series of  $C_T$  concentrations ( $\mu\text{mol.kg}^{-1}$ ) for 2009-2011 in surface waters in the North Atlantic Sub-Polar gyre (zone  $59^\circ\text{N}$ - $33^\circ\text{W}$ ) based on SURATLANT (open triangles) and OVIDE-2010 (grey circles) data. In 2009, SURATLANT data were available in February, June, September and December, while in 2010 data available in March, June, August and December and in 2011 data only available for March and December. The OVIDE data in late June 2010 completed the temporal cycle and confirmed the strong seasonal signal and low  $C_T$  concentrations in summer 2010 not seen in 2009 (or in 2011 as there is no data in summer). The mean observations for each period describe the  $C_T$  seasonal cycles in 2009 and 2010 (Black squares, dashed line). The monthly surface chlorophyll-a concentrations (Chl-a,  $\text{mg.m}^{-3}$ ) averaged in the same region based on MODIS are also shown (Green dots and line) highlighting the high productivity during the summer 2010. Chl-a monthly data extracted from MODIS (Giovanni/NASA, last access 3/5/19). (b): Time-series of  $f\text{CO}_2$  ( $\mu\text{atm}$ ) for the same cruises (same symbols) calculated with  $A_T$ - $C_T$ . Mean SST ( $^\circ\text{C}$ ) indicated (red triangles). In June 2010 oceanic  $f\text{CO}_2$  decreased by  $53 \mu\text{atm}$  in 2 weeks.

**Table 3:** Comparisons of  $A_T$  and  $C_T$  samples measured back at LOCEAN with measurements onboard by IIM Laboratory (F. Pérez, Vigo, Spain) for OVIDE cruises in the North Atlantic. Nb= Number of samples. ND= No Data. The results listed indicate the mean and standard deviations of the differences (LOCEAN-IIM). For  $A_T$ , IIM values were measured on-board. For  $C_T$ , IIM values were calculated from  $A_T$  and pH both measured onboard. The IIM data were quality controlled and here taken from the GLODAP data-products (Olsen et al, 2016, 2019).

Cruise Year	Nb $A_T$	$A_T$ (LOCEAN) - $A_T$ (IIM) $\mu\text{mol.kg}^{-1}$	Nb $C_T$	$C_T$ (LOCEAN) - $C_T$ (IIM) $\mu\text{mol.kg}^{-1}$
OVIDE-2006	14	-2.04 ( $\pm$ 5.84) (*)	14	1.12 ( $\pm$ 2.49)
OVIDE-2008	29	-4.53 ( $\pm$ 4.11)	29	3.76 ( $\pm$ 3.11)
OVIDE-2010	41	-1.96 ( $\pm$ 2.26)	41	-2.42 ( $\pm$ 3.35)
OVIDE-2012	37	-0.12 ( $\pm$ 8.85)	ND	ND
GEOVIDE-2014	57	-0.05 ( $\pm$ 3.43)	54	2.36 ( $\pm$ 7.89)

(\*) for the OVIDE 2006 cruise original difference for  $A_T$  was  $-9.0 (\pm 5.8) \mu\text{mol.kg}^{-1}$  and LOCEAN  $A_T$  data were corrected by  $+7.2 \mu\text{mol.kg}^{-1}$  based on the mean concentrations in deep layers. No corrections were applied for  $A_T$  and  $C_T$  for other cruises.



482 The comparisons described above concern the open ocean region with  $A_T$  and  $C_T$  concentrations in a  
483 range of concentrations close to the CRM references (used by the different laboratories). Another example of  
484 comparison is presented here for samples obtained along a river and thus for waters with low salinity and  $A_T$   
485 concentrations (river Penzé in North Brittany). In 2019,  $A_T$  was measured at SBR laboratory (Station Biologique  
486 de Roscoff) by a potentiometric method (using a Titrino-847 plus Metrohm) calibrated with CRM (Batch #131)  
487 for a final accuracy of  $\pm 2.1 \mu\text{mol kg}^{-1}$  (Gac et al., 2020). Although the samples were measured with different  
488 techniques the  $A_T$ /Salinity relationships are very coherent for both datasets (Figure 5). Therefore we added the  $A_T$   
489 data measured in 2019-2020 to complete the synthesis for this location (river Penzé).

490

491

492

493

494

495

496

497

498

499

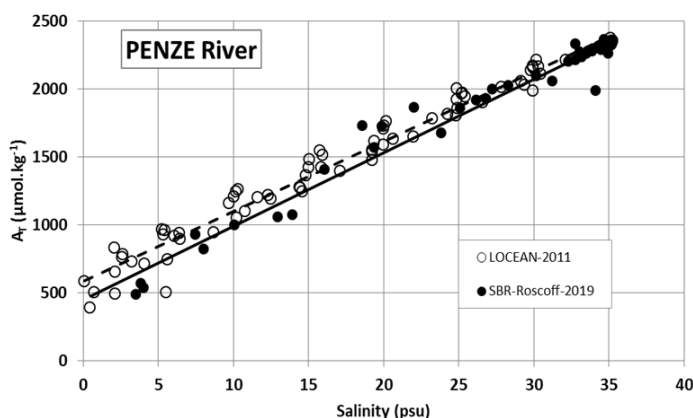
500

501

502

503

504



505

506

507

508

509

510

511

512

513

514

515

516

517

518

519

520

521

522

523

524

525

**Figure 5:** Total alkalinity ( $A_T$ ) versus salinity for samples measured in 2011 and 2019 in the river Penzé, North Brittany (Gac et al., 2020).  $A_T$  samples were measured at LOCEAN in 2011 (open circles, dashed-line) and at SBR laboratory (Roscoff) in 2019 (filled circles, black line).

### 3.4 Quality control and flags

511

512

513

514

515

516

517

518

519

520

521

522

523

524

525

Identifying each data with an appropriate flag is very convenient for selecting the data (good, questionable or bad). Here we used 4 Flags for each property (Flags 2, 3, 4, and 9) following the WOCE program and used in other data products such as SOCAT (Bakker et al., 2016) or GLODAP (Olsen et al., 2016, 2019, 2020; Lauvset et al., 2021). During the data-processing, we first assigned a flag for each  $A_T$  and  $C_T$  data based on the standard error in the calculation of  $A_T$  and  $C_T$  concentrations (non-linear regression, Dickson et al. 2007). By default, if the standard-deviation on the regression is  $> 1 \mu\text{mol kg}^{-1}$ , we assigned a flag 3 (questionable) although the data could be acceptable and then used for interpretations. Flag 3 was also assigned when salinity was doubtful or when differences of duplicates were large (e.g.  $\pm 20 \mu\text{mol kg}^{-1}$ ). Flags 4 (bad or certainly bad) were assigned when clear anomalies were detected for unknown reason (e.g. a sample probably not fixed with  $\text{HgCl}_2$ ). A secondary quality control was performed by the PIs of each project based on data inspection, duplicates,  $A_T$ /Salinity relationship, or the mean observations in deep layers where large variability in  $A_T$  and  $C_T$  is unlikely to occur from year to year. An example presents all data from the MOOSE-GE cruises conducted in 2010-2019 in the Mediterranean Sea (Coppola et al., 2020; Testor et al., 2010) where clear outliers have been identified (Figure S3). For the 10 MOOSE-GE cruises and a total of 1847  $A_T$  and  $C_T$  analyses, 26 were identified flagged as bad (flag 4), 139 for  $A_T$  and 141 for  $C_T$  listed as questionable (flag 3) and 1682 for  $A_T$  and



526 1680 for  $C_T$  considered as good data (flag 2, i.e. more than 90%). Similar control was performed for each  
 527 project.

528 The synthesis of various cruises in the same region and period also offers verification and secondary  
 529 control of the data. For example, several cruises were conducted in the Mediterranean Sea in 2014 (MOOSE-GE,  
 530 SOMBA, ANTARES and DYFAMED). The mean values of  $C_T$  and  $A_T$  in the deep layers (> 1800m) for each  
 531 cruise confirmed the coherence of the data (Table 4). This enabled to merge the different datasets for  
 532 interpretations of the temporal trends and processes driving the  $CO_2$  cycle (Coppola et al., 2019, 2020; Ulses et  
 533 al., 2022) or to train and validate a regional neural network to reconstruct the carbonate system (e.g. CANYON-  
 534 MED, Fourier et al., 2020, 2022).

535  
 536  
 537  
 538  
 539  
 540  
 541  
 542  
 543

**Table 4:** Mean observations in the deep layers (> 1800m) of the western Mediterranean Sea for different cruises  
 conducted in 2014. Results in deep layers (> 1800m) for the DEWEX cruise in 2013 and the PEACETIME  
 cruise in 2017 in the same region are also listed.  $N-A_T$  and  $N-C_T$  are  $A_T$  and  $C_T$  normalized at Salinity = 38. Nb =  
 number of data (with flag 2). Standard-deviations are in brackets. References for these cruises are listed in  
 Supplementary Material.

Cruise	Period	Nb	Pot. Temp C	Salinity PSU	$N-A_T$ $\mu\text{mol kg}^{-1}$	$N-C_T$ $\mu\text{mol kg}^{-1}$
All cruises	Feb/Dec-2014	76	12.905 (0.007)	38.486 (0.005)	2562.9 (5.3)	2303.7 (4.7)
ANTARES	Feb/Nov-2014	14	12.913 (0.004)	38.488 (0.006)	2564.0 (3.8)	2301.9 (3.5)
DYFAMED	Mar/Dec-2014	9	12.905 (0.0016)	38.487 (0.004)	2560.1 (5.0)	2304.3 (6.8)
MOOSE-GE	Jul-2014	21	12.909 (0.004)	38.487 (0.005)	2565.6 (4.6)	2303.5 (4.1)
SOMBA	Aug/Sep-2014	32	12.899 (0.005)	38.483 (0.005)	2561.5 (5.6)	2304.6 (4.8)
DEWEX	Feb/Apr-2013	44	12.903 (0.010)	38.588 (0.006)	2556.0 (4.3)	2294.0 (5.7)
PEACETIME	May/Jun-2017	7	12.904 (0.002)	38.486 (0.003)	2567.2 (10.6)	2308.1 (8.9)

569  
 570

571 The total number of data for the Global Ocean and the Mediterranean Sea are gathered in Table 5 with  
 572 corresponding flags for each property. Overall, the synthesis includes more than 94% of good data for both  $A_T$   
 573 and  $C_T$ . About 5% are questionable and 2% are likely bad. Overall, we believe that all data (with Flag 2) in this  
 574 synthesis have an accuracy better than  $4 \mu\text{mol kg}^{-1}$  for both  $A_T$  and  $C_T$ , the same as for quality-controlled data in  
 575 GLODAP (Olsen et al., 2020; Lauvset et al., 2021). The uncertainty ranges between the “Climate goal” ( $2 \mu\text{mol}$   
 576  $\text{kg}^{-1}$ ) and the “Weather Goal” ( $10 \mu\text{mol kg}^{-1}$ ) for ocean acidification studies (Newton et al., 2015; Tilbrook et al.,  
 577 2019). This accuracy is also relevant to validate or constraint data-based methods that reconstruct  $A_T$  and  $C_T$



578 fields with an error of around 10-15  $\mu\text{mol kg}^{-1}$  for both properties (Bittig et al., 2018; Broullón et al., 2019, 2020;  
579 Fourier et al., 2020; Chau et al., 2023).

580  
581 **Table 5:** Number of Temperature, Salinity,  $A_T$  and  $C_T$  data in the synthesis identified for Flags 2, 3, 4, 9. The  
582 data are given for the full data-set Global Ocean and for the Mediterranean Sea. Last column is the percentage of  
583 Flag 2 (Good).

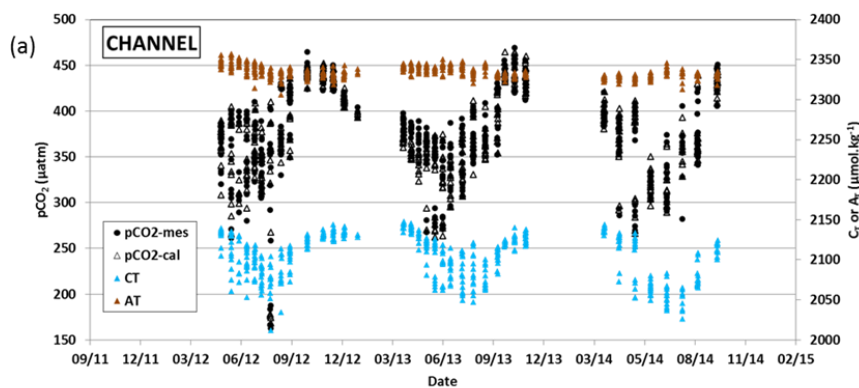
	Flag 2	Flag 3	Flag 4	Flag 9	% Flag 2
Global Ocean					
Temperature	43538	410	0	478	0.9907
Salinity	44033	319	2	71	0.9928
$A_T$	39331	2144	1165	1787	0.9224
$C_T$	39921	2091	1148	1279	0.9250
Mediterranean Sea					
Temperature	9843	1	0	65	0.9999
Salinity	9879	8	2	20	0.9999
$A_T$	8853	425	411	220	0.9137
$C_T$	8854	451	389	211	0.9133

### 3.5 Using $A_T$ - $C_T$ to calculate $p\text{CO}_2$ and pH and compare with $p\text{CO}_2$ and pH measurements

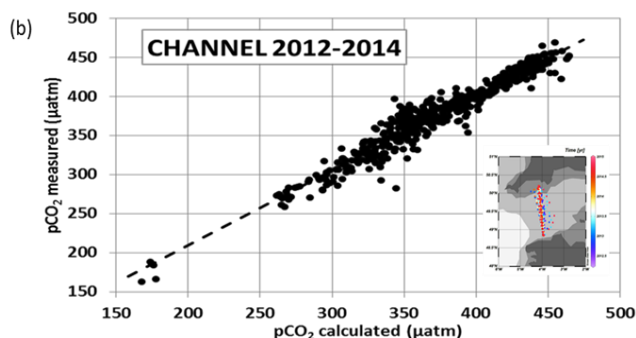
607  
608 For some projects, the  $A_T$ - $C_T$  data presented in this synthesis were used to calibrate or validate in situ  
609  $p\text{CO}_2$  sensors (Bozec et al., 2011; Marrec et al., 2014; Merlivat et al., 2018). The  $A_T$ - $C_T$  data were also used to  
610 calculate  $p\text{CO}_2$  and to derive associated air-sea  $\text{CO}_2$  fluxes, especially during periods when no direct  $p\text{CO}_2$   
611 measurements were available (e.g. in the North Atlantic, Figure 4, Watson et al., 2009; Mc Kinley et al., 2011).  
612 For example, Marrec et al. (2014) successfully used the calculated  $p\text{CO}_2$  (with  $A_T$ - $C_T$  pairs) to adjust the drift of  
613 the  $p\text{CO}_2$  data recorded with a Contros-HydroC/CO2 FT sensor mounted on a FerryBox for regularly sampling  
614 the Western English Channel. Here we show the results for the period 2012-2014 (Figure 6). In this region the  
615 alkalinity is relatively constant over time; the average of  $A_T$  for 528 samples at different seasons and years is  
616 2334.4 ( $\pm 7.2$ )  $\mu\text{mol kg}^{-1}$ . On the opposite, the  $C_T$  concentrations show distinctive seasonality, with higher  
617 concentrations in winter and lower in summer when biological activity is pronounced (Marrec et al., 2013, 2014;  
618 Kitidis et al., 2019). This controls the seasonal  $p\text{CO}_2$  distribution revealed each year in both measured and  
619 calculated  $p\text{CO}_2$  (Figure 6). For 528 co-located samples the mean difference between calculated and measured  
620  $p\text{CO}_2$  is -1.9 ( $\pm 11.9$ )  $\mu\text{atm}$  with no distinct differences depending on the season and year.  
621



622  
 623  
 624  
 625  
 626  
 627  
 628  
 629  
 630  
 631  
 632  
 633  
 634



635  
 636  
 637  
 638  
 639  
 640  
 641  
 642  
 643  
 644  
 645  
 646  
 647



648 **Figure 6:** (a): Time-series of  $A_T$  (brown triangles, right Y-axis),  $C_T$  (blue triangles, right Y-axis),  $pCO_2$   
 649 calculated (open triangles, left Y-axis) and  $pCO_2$  measured (filled circles) in the Western English Channel in  
 650 2012-2014 (Marrec et al., 2014). (b): Measured  $pCO_2$  versus calculated  $pCO_2$  for the same samples. The mean  
 651 difference ( $pCO_{2cal} - pCO_{2mes}$ ) for 528 samples is  $-1.9 \mu atm (\pm 11.9) \mu atm$ . Data from Marrec and Bozec (2016  
 652 a,b; 2017). Localization of the samples is shown in the inserted map.  
 653

654 In the Ligurian Sea, following the first high frequency in situ  $fCO_2$  measurements in 1995-1997 at the  
 655 DYFAMED time-series station (Hood and Merlivat, 2001), a new CARIOCA  $fCO_2$  sensor was deployed at that  
 656 location in 2013 (BOUSSOLE project, Merlivat et al., 2018). The CARIOCA sensor was calibrated with regular  
 657  $A_T$ - $C_T$  analyses performed at LOCEAN. Based on these data, the mean difference between CARIOCA- $fCO_2$   
 658 measurements and calculated- $fCO_2$  data was estimated to be around  $\pm 4.4 \mu atm$  for 2013-2015, i.e. the same  
 659 order than the precision of the CARIOCA sensor ( $\pm 5 \mu atm$ , Merlivat et al., 2018). Here we extend the results for  
 660 the period 2013-2018 (Golbol et al., 2020; data also in SOCAT version v2021, Bakker et al., 2016) and  
 661 compared the CARIOCA  $fCO_2$  time-series with  $A_T$  and  $C_T$  data from different cruises (BOUSSOLE,  
 662 DYFAMED and MOOSE-GE) selected in the layer 0-20m at that location (Figure S4). For 67 co-located  
 663 samples at different seasons and years, the mean difference between calculated and measured  $fCO_2$  ( $fCO_{2cal}$ -  
 664  $fCO_{2mes}$ ) was  $-3.7 \mu atm (\pm 10.8) \mu atm$ . At that location, the alkalinity is relatively constant over 2013-2018 with  
 665 an average concentration of  $2569.8 (\pm 13.2) \mu mol kg^{-1}$ .  $C_T$  concentrations show a clear seasonality, decreasing by  
 666 around  $50 \mu mol kg^{-1}$  from winter to late summer driving the large seasonal cycle of  $fCO_2$  (range  $80 \mu atm$ )  
 667 revealed in both measured and calculated values (here  $fCO_2$  is normalized at  $13^\circ C$ , Figure S4). In addition to  
 668 calibration purposes, a regional  $A_T$ /Salinity relationship was derived from the  $A_T$  data measured at that location  
 669 and successfully used to construct time-series of  $C_T$  and pH calculated from the high-frequency CARIOCA  $fCO_2$





670 data to investigate and interpret the long-term change of  $f\text{CO}_2$  and acidification in the Ligurian Sea (Merlivat et  
671 al., 2018; Coppola et al., 2020).

672 A CARIOCA sensor was also deployed in 2003 near the SOMLIT-Brest time-series site in the Bay of  
673 Brest (Bozec et al., 2011; Salt et al., 2016). As for BOUSSOLE in the Ligurian Sea, samples collected for  $A_T$ - $C_T$   
674 were used for validation of the  $p\text{CO}_2$  recorded by the CARIOCA sensor and the comparison with calculated  
675  $p\text{CO}_2$  showed a good agreement, i.e.  $p\text{CO}_{2\text{cal}} = 0.98 * p\text{CO}_{2\text{mes}} + 7 \mu\text{atm}$  (Bozec et al., 2011). CARIOCA  
676 sensors were also deployed on moorings in the Tropical Atlantic (PIRATA project, e.g. Lefèvre et al., 2008,  
677 2016; Parard et al., 2010). With the discrete  $A_T$  and  $C_T$  data included in this synthesis (EGEE and PIRATA-FR  
678 cruises), the  $f\text{CO}_2$  data from CARIOCA sensor associated with an adapted  $A_T$ /Salinity relationship were used to  
679 derive pH (Lefèvre et al., 2016) or  $C_T$  time-series to evaluate net community production in the eastern tropical  
680 Atlantic (Parard et al., 2010; Lefèvre and Merlivat 2012).

681 Although this is not a direct instrumental inter-comparison, differences between  $p\text{CO}_2$  (or  $f\text{CO}_2$ )  
682 calculated using  $A_T$ - $C_T$  pairs with direct  $p\text{CO}_2$  measurements give a glimpse of the quality of  $A_T$  and  $C_T$  data in  
683 this synthesis given the uncertainty attached to the  $p\text{CO}_2$  or pH calculations (Orr et al., 2015). For example, in  
684 the frame of the SURATLANT project in the North Atlantic, calculated  $f\text{CO}_2$  data were compared with co-  
685 located  $f\text{CO}_2$  measurements for different seasons and years (Figure S5). The mean differences ( $f\text{CO}_{2\text{cal}} - f\text{CO}_{2\text{mes}}$ )  
686 ranged between  $-4.3 \mu\text{atm} (\pm 12.9) \mu\text{atm}$  (2004-2007, 74 co-located samples) and  $-3.0 (\pm 12.1) \mu\text{atm}$  (2014-2015,  
687 98 co-located samples). The differences are almost the same for different years (and seasons) and are thus  
688 attributed to method uncertainties (including sampling time, measurement errors, and data processing). Based on  
689 these comparisons and the consistency between data we are confident that the  $A_T$ - $C_T$  data presented in this  
690 synthesis could be used to calculate  $f\text{CO}_2$  (and pH) and interpret temporal changes and drivers of these  
691 parameters as well as to estimate air-sea  $\text{CO}_2$  fluxes in the North Atlantic (e.g. Corbière et al., 2007; Schuster et  
692 al., 2009, 2013; Watson et al., 2009; Metzl et al., 2010; Mc Kinley et al., 2011; Reverdin et al., 2018, Kitidis et  
693 al., 2019; Leseurre et al., 2020).

694 The  $A_T$ - $C_T$  data in this synthesis have been also successfully used for  $f\text{CO}_2$  and air-sea  $\text{CO}_2$  fluxes  
695 calculations in other regions: the tropical Atlantic (Koffi et al., 2010), the tropical Pacific (Moutin et al., 2018;  
696 Wagener et al., 2018), the Solomon sea (Ganachaud et al., 2017) or the Mediterranean sea and coastal zones (De  
697 Carlo et al., 2013; Marrec et al., 2015; Kapsenberg et al., 2017; Coppola et al., 2020; Keraghel et al., 2020;  
698 Wimart-Rousseau et al., 2020a; Gattuso et al., 2023).

699 In addition,  $A_T$ - $C_T$  data in the surface and the water-column are also relevant to calculate pH and  
700 evaluate its rate of change for addressing ocean acidification topic in different regions (Kapsenberg et al., 2017;  
701 Ganachaud et al., 2017; Wagener et al., 2018; Coppola et al., 2020; Leseurre et al., 2020; Lo Monaco et al.,  
702 2021). At the time-series station ECOSCOPA in the Bay of Brest (Fleury et al., 2023; Petton et al., 2023), pH  
703 calculated with  $A_T$ - $C_T$  data were compared with direct pH measurements (Figure S6). In 2017-2019, pH (at  
704 standard temperature  $25^\circ\text{C}$ , pH-25C) was always lower than 8 and presented a large seasonal signal of 0.3 (high  
705 pH values in spring, low in winter). The mean difference between calculated and measured pH-25C for 46  
706 samples was equal to  $+0.013 (\pm 0.010)$  which is in the range of the pH uncertainty evaluated by error  
707 propagation when calculated from  $A_T$ - $C_T$  pairs ( $A_T$ - $C_T$  error of  $\pm 3 \mu\text{mol kg}^{-1}$  leads to pH error of  $\pm 0.0144$ ). Part  
708 of these  $A_T$ - $C_T$  data used to calculate pH also helped for interpreting the response of marine species to  
709 acidification, e.g. pteropodes or coccolithophores (*Emiliana huxleyi*) in the Mediterranean Sea (Howes et al.,  
710 2015, 2017; Meier et al., 2014) or in the Southern Ocean (Beaufort et al., 2011). The  $A_T$ - $C_T$  data were also



711 supporting environmental analysis in coral reef ecosystems in the tropical Pacific (TARA Expedition, Douville  
712 et al., 2022; Lombard et al., 2023; Canesi et al., 2023).

713

#### 714 4 Spatial distribution of $A_T$ and $C_T$ : a global view from the SNAPO-CO2 dataset

715

716 The surface distribution in the global ocean based on the SNAPO-CO2 dataset is presented in Figure 7  
717 for  $A_T$  and  $C_T$ . In the open ocean, high  $A_T$  concentrations are identified in the subtropics in all basins (Jiang et al.,  
718 2014; Takahashi et al., 2014) with highest concentrations up to  $2484 \mu\text{mol kg}^{-1}$  in the central North Atlantic  
719 (STRASSE cruise in August 2012,  $26^\circ\text{N}/36^\circ\text{W}$ ). In surface and at depth, the  $A_T$ /Salinity and  $A_T/C_T$  relationships  
720 are clearly identified and structured at regional scale (Figure 8).

721

722

723

724

725

726

727

728

729

730

731

732

733

734

735

736

737

738

739

740

741

742

743

744

745

746

747

748

749

750

751

752

753

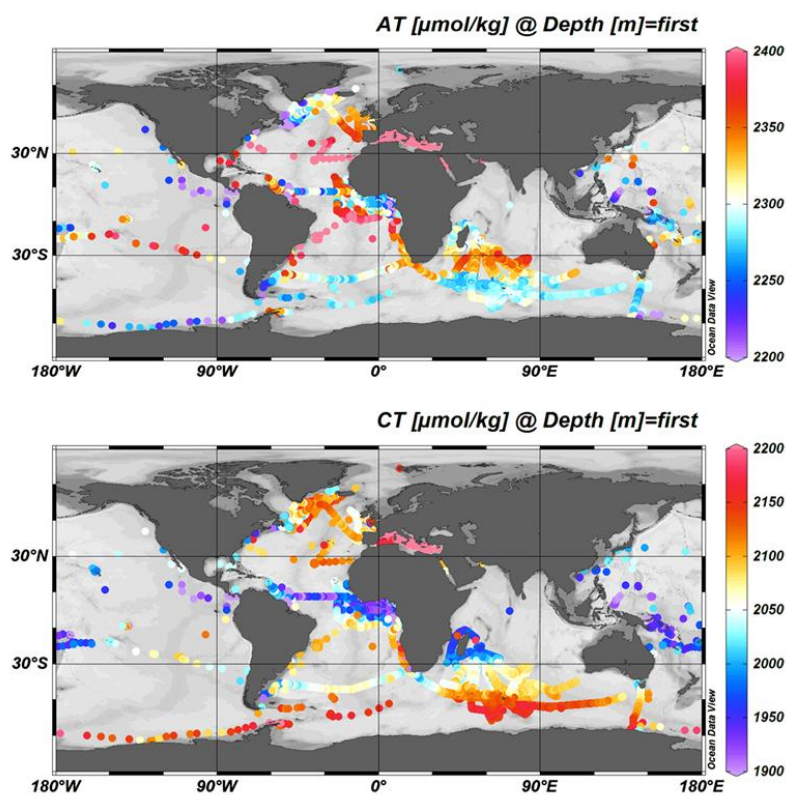


**Figure 7:** Distribution of  $A_T$  (top) and  $C_T$  (bottom) concentrations ( $\mu\text{mol.kg}^{-1}$ ) in surface waters (0-10m). Only data with flag 2 are presented in these figures. Figures produced with ODV (Schlitzer, 2018).



754  
 755  
 756  
 757  
 758  
 759  
 760  
 761  
 762  
 763  
 764  
 765  
 766  
 767  
 768  
 769  
 770  
 771  
 772  
 773  
 774  
 775  
 776  
 777  
 778  
 779  
 780  
 781  
 782  
 783  
 784  
 785  
 786  
 787  
 788  
 789  
 790  
 791  
 792  
 793  
 794  
 795  
 796  
 797  
 798  
 799  
 800  
 801  
 802  
 803  
 804  
 805  
 806  
 807  
 808

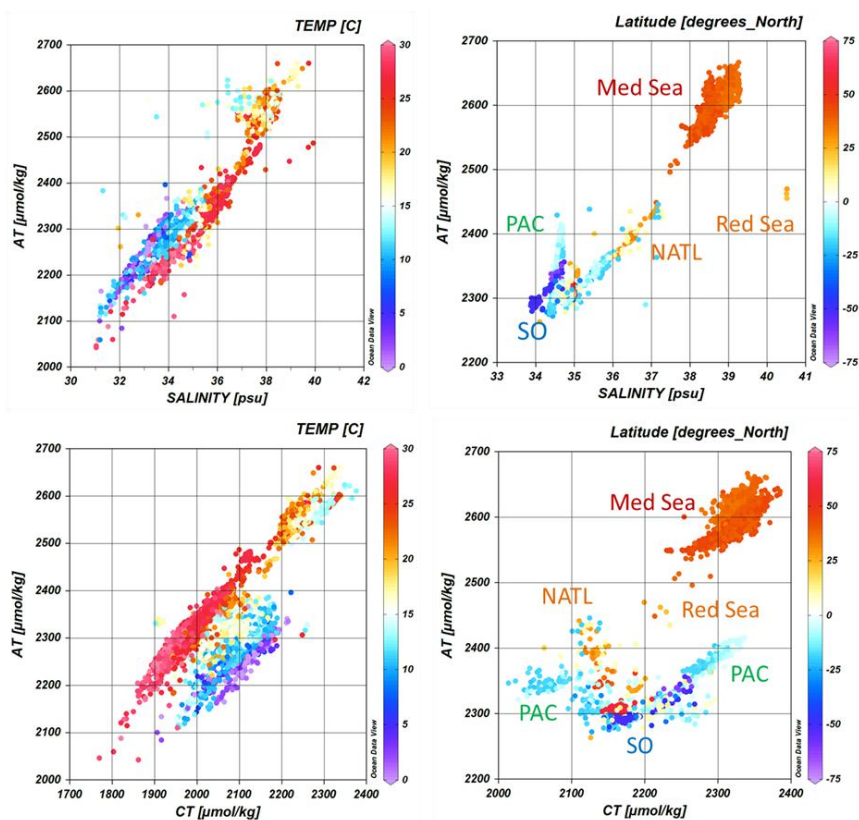


**Figure 8:** Relationships between  $A_T$  and Salinity (upper panel) and  $A_T$  versus  $C_T$  (lower panel) for samples in surface waters (0-10m and SSS > 31) (left) and in the water column below 100m (right). Only data with flag 2 are presented. The color scales correspond to the temperature (left) or the latitude (right). Some location of data are identified: Mediterranean Sea (Med Sea), Red Sea, Tropical Pacific (PAC), North Atlantic (NATL) and Southern Ocean (SO). Figures produced with ODV (Schlitzer, 2018).

In the eastern tropical Atlantic (ETA) where the Congo River impacts the salinity field (Vangriesheim et al., 2009),  $A_T$  concentrations range between 2100 and 2400  $\mu\text{mol kg}^{-1}$ . The regional  $A_T$ /Salinity relationship in the ETA based on data from the EGEE cruises in 2005-2007 (Koffi et al., 2010) is robust and validated with more recent measurements from PIRATA-FR cruises in 2010-2019 (Lefevre et al., 2021). The strong  $A_T$ /Salinity relationship in the ETA was also recognized using data from the TARA-MICROBIOME cruise in May-July 2022 (Figure S7). Low salinity (< 30) and low  $A_T$  (1700-2200  $\mu\text{mol kg}^{-1}$ ) are also observed in the western tropical Atlantic near the Amazon River plume. The  $A_T$ /Salinity relationships in both river plume regions are very similar (Figure S7).

For  $C_T$ , the lowest concentrations were observed in the coastal regions of the Tropical Atlantic, on the eastern side in the Gulf of Guinea (BIOZAIRE cruise in 2003, 6°S/11°E,  $C_T=1390 \mu\text{mol kg}^{-1}$ , Vangriesheim et al., 2009) and on the western side in coastal zone off French Guyana (PLUMAND cruise in 2007, 5°N/51°W,  $C_T=1512 \mu\text{mol kg}^{-1}$ , Lefèvre et al., 2010). Such low  $C_T$  concentrations were also observed around 5°N/51°W in the Amazon River plume during the recent EUREC4A-OA cruise in 2020 and the TARA-MICROBIOME cruise in 2021 ( $C_T=1451 \mu\text{mol kg}^{-1}$ ) leading to low oceanic  $f\text{CO}_2$  (< 350  $\mu\text{atm}$ ) and a  $\text{CO}_2$  sink in this region (Olivier et al., 2022).



809 The high  $C_T$  concentrations were mainly observed in the Southern Ocean (OISO and ACE cruises)  
810 south of the Polar Front around 50°S linked to the upwelling of  $C_T$ -rich deep water (Figure 7, Metzl et al., 2006;  
811 Wu et al., 2019; Chen et al., 2022). This leads to a high  $C_T/A_T$  ratio and a high Revelle factor in the Southern  
812 Ocean (Figure 9, Fassbender et al., 2017). The high  $C_T$  content and low temperature in the Southern Ocean also  
813 lead to low calcite and aragonite saturation state ( $\Omega$ ) (Takahashi et al., 2014; Jiang et al., 2015) but at present the  
814 surface ocean is not under-saturated with regard to aragonite (Figure 10); however, under-saturation levels ( $\Omega$ -  
815  $Ar < 1$ ) were found around 500 m in the Southern Ocean (ACE cruise in 2017, MODYDICK cruise in 2018),  
816 1000 m in the Tropical Pacific (PANDORA 2012 and OUTPACE 2015 cruises) and 2200 m in the North  
817 Atlantic (OVIDE 2012 and 2014 cruises, see also Turk et al., 2017) (Figure 10). Samples at 400 m from the  
818 TARA-Oceans cruise in 2009-2012 also indicated aragonite under-saturation in the Equatorial Atlantic,  
819 Equatorial Pacific, as well as off South America (73°W-34°S, Chile) associated to equatorial or eastern boundary  
820 upwelling systems (Feely et al., 2012; Lauvset et al., 2020).

821 In surface,  $\Omega - Ar > 3$  is found in the latitudinal band 45°S-54°N and  $\Omega - Ar < 3$ , below the critical  
822 threshold of  $\Omega - Ar = 3.25$  that represents a limit for distribution of tropical coral reefs (Hoegh-Guldberg et al.,  
823 2007) is observed at very few locations in the tropics.

824

825

826

827

828

829

830

831

832

833

834

835

836

837

838

839

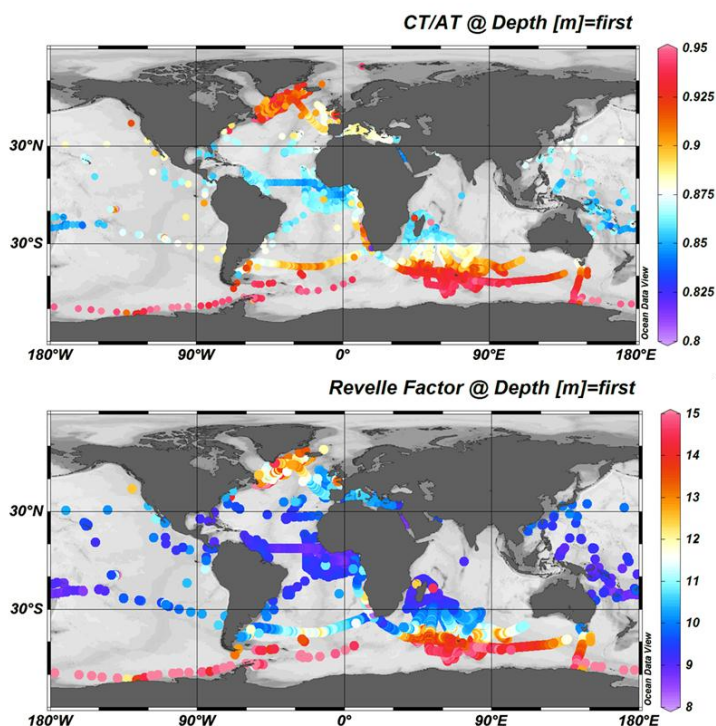
840

841

842

843

844



845 **Figure 9:** Distribution of the  $C_T/A_T$  ratio (top) and the Revelle factor (bottom) in surface waters (0-10m). Only  
846 data with flag 2 were used. Figures produced with ODV (Schlitzer, 2018).



847  
848  
849  
850  
851  
852  
853  
854  
855  
856  
857  
858  
859  
860  
861  
862  
863  
864  
865  
866  
867  
868  
869  
870  
871  
872  
873  
874  
875  
876  
877  
878  
879  
880  
881  
882  
883  
884  
885  
886  
887  
888  
889  
890  
891  
892  
893  
894  
895

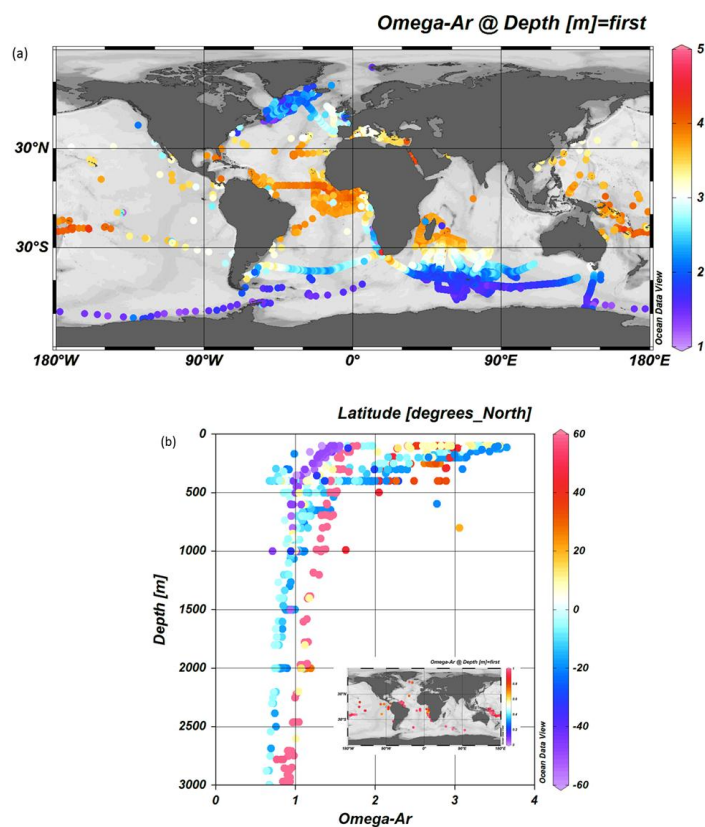


**Figure 10:** (a): Distribution of the aragonite saturation state ( $\Omega$ -Ar) in surface waters (0-10m). Only data with flag 2 were used. (b): Depth profiles (100-3000m) of  $\Omega$ -Ar at few locations in the Tropical Pacific, Atlantic and Southern Oceans. Stations where under-saturation is detected ( $\Omega$ -Ar<1) at depth are identified in the inserted map. Figures produced with ODV (Schlitzer, 2018).

Compared to the open ocean,  $A_T$  concentrations are much higher in the Mediterranean Sea (Copin-Montégut, 1993; Schneider et al., 2007; Álvarez et al., 2023) with values up to 2600  $\mu\text{mol kg}^{-1}$  (Figure 8). The  $A_T$  and  $C_T$  data obtained in 1998-2019 show on average a clear contrast between the northern and southern regions of the western Mediterranean sea (Figure 11 a, b) with higher concentration in the Ligurian Sea and the Gulf of Lion (Gemayel et al., 2015). However, the basin scale average distribution view smoothed the meso-scale signals recognized in the Mediterranean Sea (e.g. Bosse et al., 2017; Petrenko et al., 2017). In the Gulf of Lion the synthesis of 11 cruises conducted from May 2010 to June 2011 (CARBORHONE, CASCADE, LATEX, MOLA, MOOSE-GE) highlights the contrasting distributions of  $A_T$  and  $C_T$  in the coastal zones and off shore (Figure 11 c, d). The averaging of all data in 1998-2019 also smoothed the seasonal signal and the inter-annual variability described below.



896  
897  
898  
899  
900  
901  
902  
903  
904  
905  
906  
907  
908  
909  
910  
911  
912  
913  
914  
915  
916  
917  
918  
919  
920  
921  
922  
923  
924  
925  
926  
927  
928  
929  
930  
931  
932  
933  
934  
935  
936  
937  
938

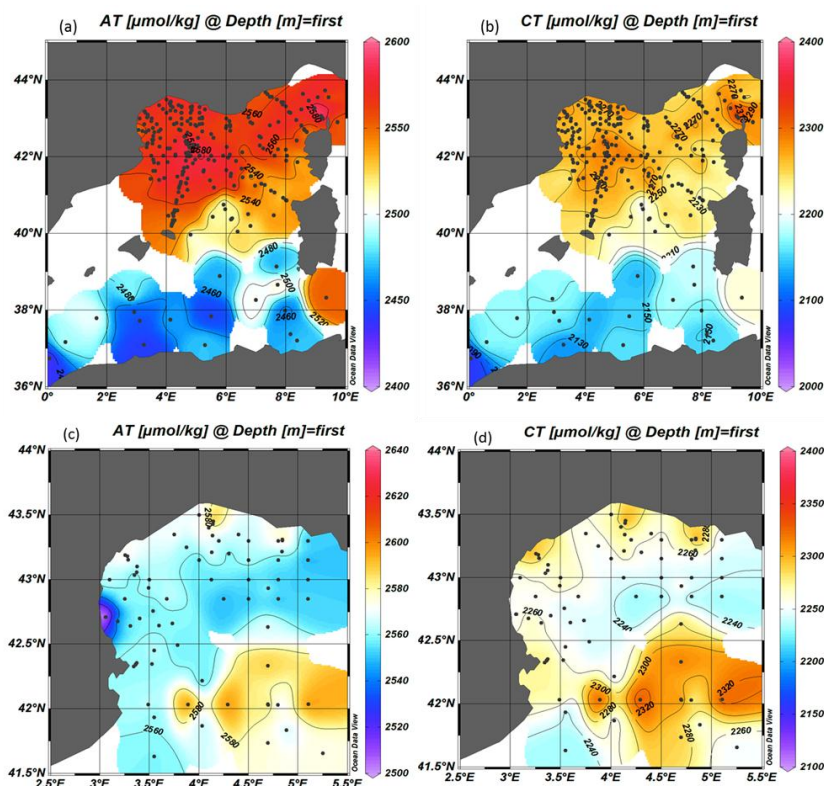


**Figure 11:** Distribution of  $A_T$  (a) and  $C_T$  (b) in  $\mu\text{mol.kg}^{-1}$  in surface waters of the western Mediterranean Sea (0-10m) from all data for 1998-2019. Detailed distribution of  $A_T$  (c) and  $C_T$  (d) in  $\mu\text{mol.kg}^{-1}$  in surface waters of the Gulf of Lion for the period 2010-2011 only (cruises CARBORHONE, CASCADE, LATEX, MOLA, MOOSE-GE). Figures produced with ODV (Schlitzer, 2018).

### 5 Temporal variations of $A_T$ and $C_T$ : examples from the SNAPO-CO2 dataset

Time-series stations such as BATS, ESTOC, HOT, in the Irminger Sea or in the Iceland Sea are the only way to detect the long-term change in the ocean carbonate system in the surface and the water column (Bates et al., 2014). These important time-series help to understand driving processes (e.g. Hagens and Middelburg, 2016) and are often used to validate the  $p\text{CO}_2$ ,  $A_T$ ,  $C_T$ , or pH reconstructed fields (e.g. Rödenbeck et al., 2013; Broullón et al., 2019, 2020; Keppler et al., 2020; Gregor and Gruber, 2021; Chau et al., 2023; Ma et al., 2023).

Here we show examples of the temporal surface variations at locations where data were obtained for more than 10 years (Figure 12). We thus selected the following contrasting regions: the North Atlantic Subpolar Gyre (NASPG around  $60^\circ\text{N}/30^\circ\text{W}$ , period 1993-2018), the Equatorial Atlantic (at  $2^\circ\text{N}-2^\circ\text{S}/12^\circ\text{W}-8^\circ\text{W}$ , period 2005-2017), the Indian Ocean subtropical sector ( $26-35^\circ\text{S}/50-56^\circ\text{E}$ , period 1998-2018), the Indian Ocean high latitude ( $54-60^\circ\text{S}/60-70^\circ\text{E}$ , period 1998-2018), the Ligurian Sea (around DYFAMED station,  $43.5-42.5^\circ\text{N}/5.5-9^\circ\text{E}$ , period 1998-2019) and times-series stations in the coastal zones off Brittany (period 2008-2019).



939  
 940  
 941  
 942  
 943  
 944  
 945  
 946  
 947  
 948  
 949  
 950  
 951  
 952  
 953  
 954  
 955  
 956  
 957  
 958  
 959  
 960  
 961  
 962

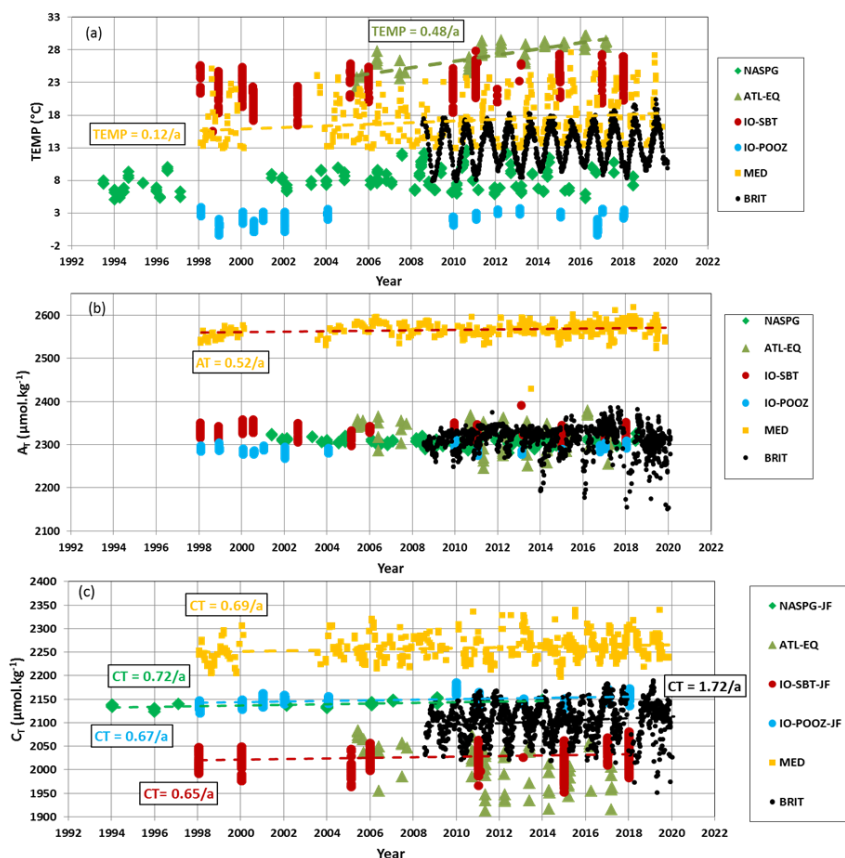


**Figure 12:** Time-series of (a) sea surface temperature ( $^{\circ}\text{C}$ ), (b)  $A_T$  ( $\mu\text{mol.kg}^{-1}$ ) and (c)  $C_T$  ( $\mu\text{mol.kg}^{-1}$ ) in 6 regions: the North Atlantic Subpolar Gyre (NASPG 1993-2018, green diamond), the Equatorial Atlantic (ATL-EQ, 2005-2017, green triangle), the Indian subtropical sector (IO-SBT, red circle) and high latitude (IO-POOZ, blue circle) (1998-2018), the Ligurian Sea (MED, 1998-2019, orange square) and times-series stations in the coastal zones off Brittany (BRIT, period 2008-2019, black dots). Trends (dashed lines) are shown when relevant for the discussion ( $C_T$  trends listed in Table 6).

**Table 6:** Trend of  $C_T$  ( $\mu\text{mol kg}^{-1} \text{ yr}^{-1}$ ) and corresponding standard error in 5 selected regions where data were available for more than 10 years (data are shown in Figure 12). The projects/cruises for selection of the data in each domain are indicated.

Region	Period	$C_T$ trend $\mu\text{mol kg}^{-1} \text{ yr}^{-1}$	Season	Projects/Cruises
NASPG	1994-2014	+0.719 (0.168)	Jan-Feb	SURATLANT
Indian SBT	1998-2018	+0.646 (0.117)	Jan-Feb	OISO
Indian High Lat	1998-2018	+0.668 (0.042)	Jan-Feb	OISO
Ligurian Sea	1998-2019	+0.686 (0.181)	All seasons	DYFAMED, BOUSSOLE, MOOSE-GE
Coast Brittany	2008-2019	+1.720 (0.281)	All seasons	Brest, Roscoff, ECOSCOPIA, PENZE

985  
 986



987 In the 6 regions, there was a progressive warming most clearly detected in the Mediterranean Sea (e.g.  
988 Nykjaer, 2009). From 1998 to 2019 the warming in the Ligurian Sea was  $+0.1208^{\circ}\text{C yr}^{-1}$  ( $\pm 0.0227$ ) (Figure 12).  
989 In the equatorial Atlantic, the apparent rapid increase of temperature of  $+0.48^{\circ}\text{C yr}^{-1}$  ( $\pm 0.04$ ) in 2005-2017 from  
990 the selected data indicated a change in water masses and circulation. The colder sea surface in 2005 was  
991 associated with the so-called Atlantic Cold Tongue (ACT) which was one of the most intense ATC since 1982  
992 (Caniaux et al., 2011). The ACT also leads to significant changes in oceanic  $f\text{CO}_2$  and air-sea  $\text{CO}_2$  fluxes (Parard  
993 et al., 2010; Koseki et al., 2023) and explained the high  $C_T$  concentrations observed in 2005 in this region  
994 (Figure 12, Koffi et al., 2010).

995 Alkalinity presents rather homogenous concentrations in the NASGP and the south Indian Ocean. Inter-  
996 annual variability of  $A_T$  is pronounced in the equatorial Atlantic ranging between 2245 and 2378  $\mu\text{mol kg}^{-1}$ . This  
997 is mainly related to salinity as normalized  $A_T$  values ( $N-A_T$ , for salinity= 35) do not show such inter-annual  
998 variability (Mean  $N-A_T = 2295.7 \pm 4.6 \mu\text{mol kg}^{-1}$ ,  $n = 67$  for 2005-2017, not shown). In the coastal zones off  
999 Brittany, the  $A_T$  is also highly variable (Salt et al., 2016; Gac et al., 2021) ranging between 2150 and 2386  $\mu\text{mol}$   
1000  $\text{kg}^{-1}$  (Figure 12).

1001 An interesting signal is the progressive increase of  $A_T$  in the Mediterranean Sea. The positive  $A_T$  trend  
1002 of  $+0.53$  ( $\pm 0.11$ )  $\mu\text{mol kg}^{-1} \text{ yr}^{-1}$  ( $n=538$ ) in 1998-2019 in the region offshore was also observed at the coastal  
1003 station SOMLIT-Point-B in 2007-2015 but with a faster increase of  $+2.08$  ( $\pm 0.19$ )  $\mu\text{mol kg}^{-1} \text{ yr}^{-1}$  (Kapsenberg et  
1004 al., 2017). Close to the DYFAMED site, at station SOMLIT-Point-B, the  $A_T$  trend was not linked to salinity  
1005 temporal changes as a positive  $N-A_T$  trend was also reported,  $+0.52$  ( $\pm 0.07$ )  $\mu\text{mol kg}^{-1} \text{ yr}^{-1}$  (not shown). Based  
1006 on data from the PERLE cruises in 2018-2021 a significant increase in  $A_T$  was also identified in the Eastern  
1007 Mediterranean Sea (Wimart-Rousseau et al., 2021). Along with the increase of  $C_T$  and the warming, the  $A_T$   
1008 increase would impact on the  $f\text{CO}_2$ , air-sea  $\text{CO}_2$  fluxes and pH temporal changes (Merlivat et al., 2018).  
1009 Processes explaining the  $A_T$  increase in the Mediterranean Sea are still unexplained and deserve further  
1010 investigations (Coppola et al., 2019).

1011 As expected, because of the anthropogenic  $\text{CO}_2$  uptake the  $C_T$  concentrations increased in most regions  
1012 (Figure 12, Table 6). This is identified in the Indian Ocean (in the subtropics and the high latitude), in the  
1013 Mediterranean Sea, and in coastal waters off Brittany. However, the signal is more complex in the NASPG. As  
1014 previously shown the  $C_T$  trend in the NASPG depends on seasons and decades (Metzl et al., 2010; Reverdin et  
1015 al., 2018; Fröb et al., 2019; Leseurre et al., 2020). Here we selected only the data in January-February from the  
1016 SURATLANT cruises leading a  $C_T$  trend of  $+0.719$  ( $\pm 0.168$ )  $\mu\text{mol kg}^{-1} \text{ yr}^{-1}$ . Compared to the regions further  
1017 north the  $C_T$  trend in the NASPG is about half the  $C_T$  trends of  $+1.44$  ( $\pm 0.23$ )  $\mu\text{mol kg}^{-1} \text{ yr}^{-1}$  observed in the  
1018 Iceland Sea (Olafsson et al., 2009) or  $+1.48$  ( $\pm 0.22$ )  $\mu\text{mol kg}^{-1} \text{ yr}^{-1}$  at station M in the Norwegian Sea (Skjelvan  
1019 et al., 2022).

1020 In the coastal zones off Brittany, although there are large seasonal and inter-annual variabilities (Gac et  
1021 al., 2021), an annual  $C_T$  trend of  $+1.72$  ( $\pm 0.28$ )  $\mu\text{mol kg}^{-1} \text{ yr}^{-1}$  is detected over 10 years (2009 to 2019). The same  
1022 is observed in the Mediterranean Sea where the  $C_T$  offshore trend of  $+0.69$  ( $\pm 0.18$ )  $\mu\text{mol kg}^{-1} \text{ yr}^{-1}$  is low  
1023 compared to what was observed in the coastal zone (SOMLIT-Point-B,  $+2.97$  ( $\pm 0.20$ )  $\mu\text{mol kg}^{-1} \text{ yr}^{-1}$ , Kapsenberg  
1024 et al., 2017).

1025 In the southern Indian Ocean,  $C_T$  concentrations also increased in both subtropical and high latitudes,  
1026 two regions where the primary productivity is relatively low (oligotrophic regime in the subtropics and High  
1027 Nutrient Low Chlorophyll regime, HNLC, south of the Polar Front). With the data selected for austral summer





1028 (January-February) the  $C_T$  trends appeared almost similar in these two regions, around  $+0.65 \mu\text{mol kg}^{-1} \text{yr}^{-1}$   
1029 (Table 6).

1030 Finally, in the Equatorial Atlantic the selected data around  $0^\circ$ - $10^\circ\text{W}$  highlighted the large variability  
1031 linked to the oceanic circulation. Detecting a  $C_T$  trend as well as a possible link with anthropogenic carbon  
1032 uptake, at least with the data available in 2005-2017, appears to be intricate as it has been previously discussed  
1033 for the period 2006-2013 (Lefèvre et al., 2016). However, the signal of the  $C_T$  increase is better identified north  
1034 or south of the Equator in the eastern tropical Atlantic sector (Lefèvre et al., 2021).

1035 In the water column  $A_T$ - $C_T$  data from dedicated cruises were used to evaluate the  $C_{\text{ant}}$  distribution and  
1036 pH change since pre-industrial era (e.g. PANDORA cruise, Ganachaud et al., 2017; OUTPACE cruise, Wagener  
1037 et al., 2018; SOMBA cruise, Keraghel et al., 2020). Time-series at DYFAMED station also enabled to  
1038 investigate the temporal variability of  $C_T$ ,  $A_T$  and  $C_{\text{ant}}$  in the water column (Touratier and Goyet, 2009; Coppola  
1039 et al., 2020; Fourrier et al., 2022). As an example of the observed temporal variations at depth we selected the  
1040 data in the layer 950-1050m in the Ligurian Sea from different cruises (Figure 13). At that depth both  $A_T$  and  $C_T$   
1041 present some large anomalies especially noticed in 2013 (lower  $A_T$  and  $C_T$  in February 2013, DEWEX cruise)  
1042 and in 2018 (lower  $A_T$  and  $C_T$  in May 2018, MOOSE-GE cruise) the later probably linked to episodic convective  
1043 process that occurred in winter 2018 (Fourrier et al., 2022). In this region the long-term increase of  $A_T$  indicates  
1044 that in addition to the anthropogenic  $\text{CO}_2$  signal another process is at play to explain the rapid  $C_T$  trend of  $+1.20$   
1045 ( $\pm 0.12$ )  $\mu\text{mol kg}^{-1} \text{yr}^{-1}$  at depth compared to that observed in surface (Figure 12). The signal at depth is probably  
1046 linked to the variations of the deep convection and mixing with Levantine intermediate water (LIW, Margirier et  
1047 al., 2020) with higher  $A_T$  and  $C_T$  concentrations. The long-term increase of  $A_T$  and  $C_T$  at depth (here at 1000m,  
1048 Figure 13) was also observed below 2000m (Coppola et al., 2020) a signal that has to be investigated in  
1049 dedicated analysis using other properties ( $\text{O}_2$ , nutrients, following Fourrier et al. (2022) for the period 2012-  
1050 2020) and a larger dataset in the Mediterranean Sea (e.g. CARIMED).

1051

1052

1053

1054

1055

1056

1057

1058

1059

1060

1061

1062

1063

1064

1065

1066

1067

1068

1069

1070

1071

1072

1073

1074

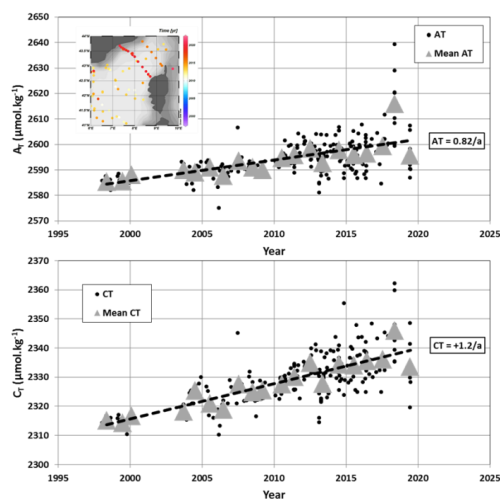


**Figure 13:** Time-series of  $A_T$  ( $\mu\text{mol.kg}^{-1}$ ) and  $C_T$  ( $\mu\text{mol.kg}^{-1}$ ) in the Ligurian Sea (1998-2019) in the layer 950-1050m. Annual mean (grey triangles) was calculated from all data each year (black dots). The trends (dashed line) based on annual mean are  $+0.82$  ( $\pm 0.15$ )  $\mu\text{mol.kg}^{-1}.\text{yr}^{-1}$  for  $A_T$  and  $+1.20$  ( $\pm 0.12$ )  $\mu\text{mol.kg}^{-1}.\text{yr}^{-1}$  for  $C_T$ . In this layer data selected are from cruises ANTARES, CASCADE, DEWEX, DYFAMED, MOOSE-GE and PEACETIME (location of stations shown in the inserted map).



## 1075 **6 Using $A_T$ and $C_T$ data to validate observations from autonomous instruments**

1076

1077 The dataset presented in this synthesis would also offer interesting observations to validate properties  
1078 ( $A_T$  and  $C_T$ ) derived from BG-ARGO floats equipped with pH sensors (e.g. Bushinsky et al., 2019; Mazloff et  
1079 al., 2023; Mignot et al., 2023). The water column in situ  $A_T$ - $C_T$  data obtained during the Antarctic Circumpolar  
1080 Expedition (ACE) in 2016-2017 were collected at location where SOCCOM floats were launched (Walton and  
1081 Thomas, 2018). A SOCCOM float (WMO ID 5905069) was launched on January 11<sup>th</sup> 2017 at 55°S-96°E south  
1082 of the Polar Front in the southern Indian Ocean. The pH, temperature and salinity data from the float were then  
1083 used to derive  $A_T$  and  $C_T$  profiles (here using the MLR method, Williams et al., 2016, 2017). In the top layers the  
1084 discrete ACE data (Figure 14) present large variability of  $A_T$  and  $C_T$  concentrations not captured in the records  
1085 derived from the float (MLR method somehow smooth the profiles). However, given the uncertainty in  
1086 reconstructed  $A_T$  from float data ( $5.6 \mu\text{mol kg}^{-1}$ ) the average values in the first 100m were almost identical ( $A_T$ -  
1087  $_{ACE} = 2285.1 (\pm 4.4) \mu\text{mol kg}^{-1}$  and  $A_T$ - $_{float} = 2278.3 (\pm 0.7) \mu\text{mol kg}^{-1}$ ;  $C_T$ - $_{ACE} = 2139.7 (\pm 9.2) \mu\text{mol kg}^{-1}$  and  $C_T$ -  
1088  $_{float} = 2141.1 (\pm 3.2) \mu\text{mol kg}^{-1}$ ). Moreover below 200m, profiles from the float are coherent compared to the  $A_T$ -  
1089  $C_T$  measurements (Figure 14). This is encouraging for using float data to explore the seasonal variability of  $A_T$   
1090 and  $C_T$  in the Southern Ocean (e.g. Williams et al., 2018; Johnson et al., 2022) and the estimation of  
1091 anthropogenic  $\text{CO}_2$  in the water column in this sector (Figure 14). Here the  $C_{ant}$  concentrations were calculated  
1092 below 200m (corresponding to the temperature minimum of the winter in the SO and using the TrOCA  
1093 method, Touratier et al., 2007). The float data suggest that  $C_{ant}$  concentrations are positive down to about 1000m,  
1094 with maximum values in subsurface. In 2017 the mean  $C_{ant}$  concentration at 200m was  $49.1 (\pm 9.0) \mu\text{mol kg}^{-1}$ .  
1095 Below that depth,  $C_{ant}$  decreased and reduced to  $+29.8 (\pm 8.5) \mu\text{mol kg}^{-1}$  in the layer 300-400m. To complement  
1096 the  $C_{ant}$  inventories based on GLODAP data-product (e.g. Gruber et al., 2019)  $C_{ant}$  estimates derived from BG-  
1097 ARGO floats as evaluated here in the Southern Ocean could be applied in other locations as was previously  
1098 tested in the North Pacific (Li et al., 2019).

1099 In surface water as the  $A_T$  derived from the float data are deduced using MLR or LIAR methods  
1100 (Williams et al., 2017; Carter et al., 2016), the  $A_T$  data in the SNAPO-CO<sub>2</sub> synthesis could also be used to  
1101 identify  $A_T$  anomalies not always captured from floats. This is particularly relevant in coccolithophores blooms  
1102 areas when low  $A_T$  concentrations and high pCO<sub>2</sub> are observed (e.g. Balch et al., 2016 in the Southern Ocean;  
1103 Robertson et al., 1994 in the North Atlantic).

1104

## 1105 **7 Summary and suggestions**

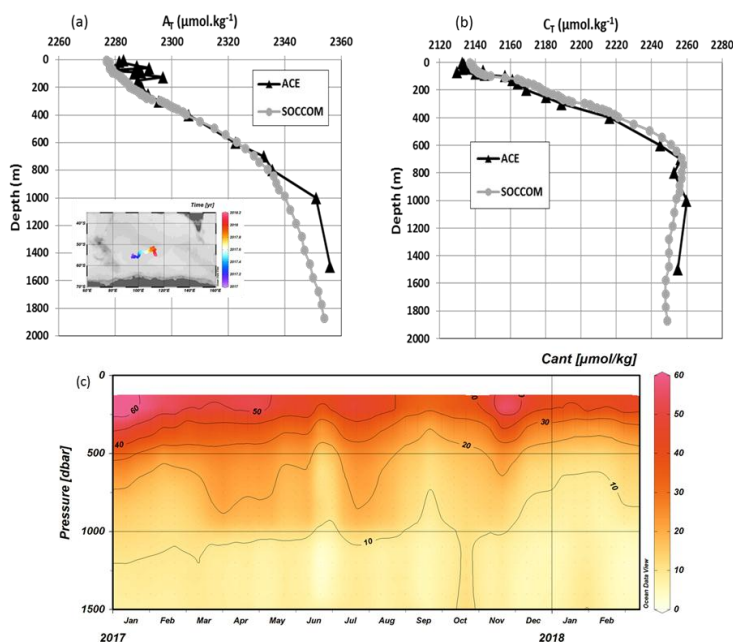
1106

1107 The ocean data synthesized in this product are based on measurements of  $A_T$  and  $C_T$  performed in 1993-  
1108 2022 with an accuracy of  $\pm 4 \mu\text{mol kg}^{-1}$ . It offers a large data set of  $A_T$  and  $C_T$  for the global ocean and regional  
1109 biogeochemical studies. It includes more than 44 400 surface and water column observations in all oceanic  
1110 basins, in the Mediterranean Sea, in the coastal zones, near coral reef, and in rivers. For the open ocean this  
1111 complements the SOCAT and GLODAP data-products (Bakker et al., 2016; Lauvset et al., 2021) and for the  
1112 Mediterranean Sea the ongoing CARIMED dataset. For the coastal sites this also complements the synthesis of  
1113 coastal time-series only done around North America (Fassbender et al., 2018; Jiang et al., 2020; OCADS, 2023).

1114



1115  
1116  
1117  
1118  
1119  
1120  
1121  
1122  
1123  
1124  
1125  
1126  
1127  
1128  
1129  
1130  
1131  
1132  
1133



1134 **Figure 14:** Profiles of (a)  $A_T$  ( $\mu\text{mol.kg}^{-1}$ ) and (b)  $C_T$  ( $\mu\text{mol.kg}^{-1}$ ) observed at station ACE-20 (55°S-95°E,  
1135 11/1/17, black triangles) compared with the profiles deduced from the SOCCOM float (WMO code 5905069)  
1136 launched at that location (first data on January 12<sup>th</sup> 2017, grey circles). The location/drift of the float in 2017-  
1137 2018 is shown on the inserted map. (c) Hovmöller section (Pressure/time) of anthropogenic CO<sub>2</sub> concentrations  
1138 ( $C_{\text{ant}}$  in  $\mu\text{mol.kg}^{-1}$ ) estimated from the float data ( $A_T$ ,  $C_T$ , O<sub>2</sub>, T) below 200m (period January 2017-February  
1139 2018). Section produced with ODV (Schlitzer, 2018).  
1140

1141 The SNAPO-CO<sub>2</sub> dataset enables to investigate seasonal variations to decadal trends of  $A_T$  and  $C_T$  in  
1142 various oceanic provinces. In regions where data are available for more than 2 decades in surface water (North  
1143 Atlantic, Ligurian Sea, Southern Indian Ocean, and coastal regions), all time-series show an increase in  $C_T$ .  
1144 Excepted in the Mediterranean Sea,  $A_T$  appears relatively constant over time, although the  $A_T$  content present  
1145 significant inter-annual variability such as in the NASPG or in the coastal zones including near the Congo and  
1146 Amazon Rivers plumes.

1147 This dataset represents independent data for validation of reconstructed  $A_T$  or  $C_T$  fields using various  
1148 methods (e.g. Rödenbeck et al., 2013, 2015; Sauzède et al., 2017; Turk et al., 2017; Bittig et al., 2018; Broullón  
1149 et al., 2019, 2020; Land et al., 2019; Keppler et al., 2020; Fourier et al., 2020; Gregor and Gruber, 2021; Sims et  
1150 al., 2023; Chau et al., 2023). It is also useful to validate Earth System Models (ESM) that currently present bias  
1151 to reproduce the seasonal cycle of  $C_T$  and  $A_T$  due to inadequate representation of biogeochemical cycles,  
1152 including the coupling of biological and physical processes (e.g. Pilcher et al., 2015; Mongwe et al., 2018;  
1153 Lerner et al., 2021). This should be resolved for confident in future projections of the productivity, ocean  
1154 acidification, and the responses of the marine ecosystems (e.g. Kwiatowkki et al., 2020). Recall that OBG  
1155 or ESM models calculate pCO<sub>2</sub> from  $A_T$ - $C_T$  pairs and the simulated annual CO<sub>2</sub> flux might be correct when  
1156 compared to observations but for wrong reasons (e.g. Goris et al., 2018, Lerner et al., 2021). For example, it has  
1157 been shown that biases in  $A_T$  in ESM models led to an overestimation of the oceanic fCO<sub>2</sub> trend and thus  
1158 uncertainty when predicting the oceanic anthropogenic CO<sub>2</sub> uptake (Lebehot et al., 2019). The simulated



1159 seasonal cycle of  $p\text{CO}_2$  is also uncertain in ESM models especially in high latitudes (e.g. Joos et al., 2023). It is  
1160 thus important to attempt validating ESM models with  $A_T$ - $C_T$  data such as presented in this synthesis.

1161 This dataset would also serve for validating autonomous platforms capable of measuring pH and  $p\text{CO}_2$   
1162 variables and, along with SOCAT and GLODAP datasets, provides an additional reference dataset for the  
1163 development and validation of regional biogeochemical models for simulating air-sea  $\text{CO}_2$  fluxes. It is also  
1164 essential for training and validating neural networks capable of predicting variables in the carbonate system,  
1165 thereby enhancing observations of marine  $\text{CO}_2$  at different spatial and temporal scales.

1166 The data presented here are available online on the Seanoë server (Metzl et al., 2023,  
1167 <https://doi.org/10.17882/95414>) and is divided in two files: one for the Global Ocean, and one for the  
1168 Mediterranean Sea. The sources of the original datasets (doi) with the associated references are listed in the  
1169 Supplementary Material (Table S3, S4). We invite the users to comment on any anomaly that would have not  
1170 been detected or to suggest potential misqualification of data in the present product (e.g. data probably good  
1171 although assigned with Flag 3, probably wrong). The SNAPO- $\text{CO}_2$  dataset will be regularly updated on Seanoë  
1172 data server with new observations controlled and archived.

1173

#### 1174 **8 Data availability**

1175 Data presented in this study are available at Seanoë: <https://www.seanoë.org>, <https://doi.org/10.17882/95414>  
1176 (Metzl et al., 2023).

1177

1178 *Author contributions.* NM prepared the data synthesis, the figures and wrote the draft of the manuscript with  
1179 contributions from all authors. JF measured the discrete samples since 2014, with the help from CM and CLM,  
1180 and prepared the individual reports for each project. NM and JF pre-qualified the discrete  $A_T$ - $C_T$  data. CLM and  
1181 NM are co-Is of the ongoing OISO project and qualified the underway  $A_T$ - $C_T$  data from OISO cruises. All  
1182 authors have contributed either to organizing cruises, sample collection or data qualification.

1183

1184 *Competing interest.* The authors declare that they have no conflict of interest.

1185

1186 *Acknowledgments.* The  $A_T$  and  $C_T$  data presented in this study were measured at the SNAPO- $\text{CO}_2$  facility  
1187 (Service National d'Analyse des Paramètres Océaniques du  $\text{CO}_2$ ) housed by the LOCEAN laboratory and part of  
1188 the OSU ECCE Terra at Sorbonne University and INSU/CNRS analytical services. Support by INSU/CNRS, by  
1189 OSU ECCE Terra and by LOCEAN, is gratefully acknowledged as well as support by different French "Services  
1190 nationaux d'Observations", such as OISO/CARAUS, SOMLIT, PIRATA, SSS and MOOSE. We thank the  
1191 research infrastructure ICOS (Integrated Carbon Observation System) France for funding a large part of the  
1192 analyses. We acknowledge the MOOSE program (Mediterranean Ocean Observing System for the Environment,  
1193 <https://campagnes.flotteoceanographique.fr/series/235/fr/>) coordinated by CNRS-INSU and the Research  
1194 Infrastructure ILICO (CNRS-IFREMER). AWIPEV- $\text{CO}_2$  was supported by the Coastal Observing System for  
1195 Northern and Arctic Seas (COSYNA), the two Helmholtz large-scale infrastructure projects ACROSS and  
1196 MOSES, the French Polar Institute (IPEV) as well as the European Union's Horizon 2020 research and  
1197 innovation projects Jericho-Next (No 871153 and 951799), INTAROS (No 727890) and FACE-IT (No 869154).  
1198 Support from the French *Agence Nationale de la Recherche* (ANR) is also acknowledged through their funding  
1199 of the BIOCAREX project. The EURECA4-OA cruise was also supported by the EURECA4-OA JPI Ocean and  
1200 Climate program. The OISO program was supported by the French institutes INSU (Institut National des



1201 Sciences de l'Univers) and IPEV (Institut Polaire Paul-Emile Victor), OSU Ecce-Terra (at Sorbonne Université),  
1202 and the French program SOERE/Great-Gases. We thank the French oceanographic fleet ("Flotte  
1203 océanographique française") for financial and logistic support for all cruises listed in this synthesis and for the  
1204 OISO program (<https://campagnes.flotteoceanographique.fr/series/228/>). Data from the float launched during the  
1205 ACE cruise were made freely available by the Southern Ocean Carbon and Climate Observations and Modeling  
1206 (SOCCOM) Project funded by the National Science Foundation, Division of Polar Programs (NSF PLR -  
1207 1425989), supplemented by NASA, and by the International Argo Program and the NOAA programs that  
1208 contribute to it. The Argo Program is part of the Global Ocean Observing System  
1209 (<http://doi.org/10.17882/42182>, <http://argo.jcompos.org>). We thank Frédéric Merceur (IFREMER) for preparing  
1210 the page and data availability on Seanoe. We thank Patrick Raimbault (retired, former at MIO, Marseille) for  
1211 managing the MOOSE project until 2019. We thank all colleagues and students who participated to the cruises  
1212 and have carefully collected the precious seawater samples. We warmly acknowledge our colleague Christian  
1213 Brunet (retired) for his supportive help for the analysis since the start of the Service facility SNAPO-CO2. We  
1214 would like to pay tribute to our late colleague Frédéric Diaz who contributed to the LATEX cruise in 2010.

1215

#### 1216 **References**

1217

1218 Álvarez, M., Catalá, T. S., Civitarese, G., Coppola, L., Hassoun, A. E.R., Ibello, V., Lazzari, P., Lefevre, D.,  
1219 Macías, D., Santinelli, C. and Ulses, C.: Chapter 11 - Mediterranean Sea general biogeochemistry, Editor(s):  
1220 Katrin Schroeder, Jacopo Chiggiato, Oceanography of the Mediterranean Sea, Elsevier, Pages 387-451,  
1221 <https://doi.org/10.1016/B978-0-12-823692-5.00004-2>, 2023.

1222

1223 Bakker, D. C. E., Pfeil, B., Smith, K., Hankin, S., Olsen, A., Alin, S. R., Cosca, C., Harasawa, S., Kozyr, A.,  
1224 Nojiri, Y., O'Brien, K. M., Schuster, U., Telszewski, M., Tilbrook, B., Wada, C., Akl, J., Barbero, L., Bates, N.  
1225 R., Boutin, J., Bozec, Y., Cai, W.-J., Castle, R. D., Chavez, F. P., Chen, L., Chierici, M., Currie, K., De Baar, H.  
1226 J. W., Evans, W., Feely, R. A., Fransson, A., Gao, Z., Hales, B., Hardman-Mountford, N. J., Hoppema, M.,  
1227 Huang, W.-J., Hunt, C. W., Huss, B., Ichikawa, T., Johannessen, T., Jones, E. M., Jones, S., Jutterstrøm, S.,  
1228 Kitidis, V., Körtzinger, A., Landschützer, P., Lauvset, S. K., Lefèvre, N., Manke, A. B., Mathis, J. T., Merlivat,  
1229 L., Metzl, N., Murata, A., Newberger, T., Omar, A. M., Ono, T., Park, G.-H., Paterson, K., Pierrot, D., Ríos, A.  
1230 F., Sabine, C. L., Saito, S., Salisbury, J., Sarma, V. V. S. S., Schlitzer, R., Sieger, R., Skjelvan, I., Steinhoff, T.,  
1231 Sullivan, K. F., Sun, H., Sutton, A. J., Suzuki, T., Sweeney, C., Takahashi, T., Tjiputra, J., Tsurushima, N., Van  
1232 Heuven, S. M. A. C., Vandemark, D., Vlahos, P., Wallace, D. W. R., Wanninkhof, R. and Watson, A. J.: An  
1233 update to the Surface Ocean CO<sub>2</sub> Atlas (SOCAT version 2). Earth System Science Data, 6, 69-90.  
1234 doi:10.5194/essd-6-69-2014. 2014

1235

1236 Bakker, D. C. E., Pfeil, B., Landa, C. S., Metzl, N., O'Brien, K. M., Olsen, A., Smith, K., Cosca, C., Harasawa,  
1237 S., Jones, S. D., Nakaoka, S.-I., Nojiri, Y., Schuster, U., Steinhoff, T., Sweeney, C., Takahashi, T., Tilbrook, B.,  
1238 Wada, C., Wanninkhof, R., Alin, S. R., Balestrini, C. F., Barbero, L., Bates, N. R., Bianchi, A. A., Bonou, F.,  
1239 Boutin, J., Bozec, Y., Burger, E. F., Cai, W.-J., Castle, R. D., Chen, L., Chierici, M., Currie, K., Evans, W.,  
1240 Featherstone, C., Feely, R. A., Fransson, A., Goyet, C., Greenwood, N., Gregor, L., Hankin, S., Hardman-  
1241 Mountford, N. J., Harlay, J., Hauck, J., Hoppema, M., Humphreys, M. P., Hunt, C. W., Huss, B., Ibánhez, J. S.  
1242 P., Johannessen, T., Keeling, R., Kitidis, V., Körtzinger, A., Kozyr, A., Krasakopoulou, E., Kuwata, A.,  
1243 Landschützer, P., Lauvset, S. K., Lefèvre, N., Lo Monaco, C., Manke, A., Mathis, J. T., Merlivat, L., Millero, F.  
1244 J., Monteiro, P. M. S., Munro, D. R., Murata, A., Newberger, T., Omar, A. M., Ono, T., Paterson, K., Pearce, D.,  
1245 Pierrot, D., Robbins, L. L., Saito, S., Salisbury, J., Schlitzer, R., Schneider, B., Schweitzer, R., Sieger, R.,  
1246 Skjelvan, I., Sullivan, K. F., Sutherland, S. C., Sutton, A. J., Tadokoro, K., Telszewski, M., Tuma, M., Van  
1247 Heuven, S. M. A. C., Vandemark, D., Ward, B., Watson, A. J., and Xu, S.: A multi-decade record of high-quality  
1248 fCO<sub>2</sub> data in version 3 of the Surface Ocean CO<sub>2</sub> Atlas (SOCAT), Earth Syst. Sci. Data, 8, 383-413,  
1249 doi:10.5194/essd-8-383-2016. 2016.

1250



- 1251 Bakker, D.C.E., Alin, S.R., Bates, N.R., Becker, M., Feely, R. A., Gritzalis, T., Jones, S. D., Kozyr, A., Lauvset,  
1252 S. K., Metzl, N., Munro, D.R., Nakaoka, S.-I., Nojiri, Y., O'Brien, K., Olsen, A., Pierrot, D., Rehder, G.,  
1253 Steinhoff, T., Sutton, A., Sweeney, C., Tilbrook, B., Wada, C., Wanninkhof, R., and all >100 SOCAT  
1254 contributors: An alarming decline in the ocean CO<sub>2</sub> observing capacity. Available at [www.socat.info](http://www.socat.info), 2023.  
1255
- 1256 Balch, W.M., Bates, N.R., Lam, P.J., Twining, B.S., Rosengard, S. Z., Bowler, B.C., Drapeau, D.T., Garley, R.,  
1257 Lubelczyk, L.C., Mitchell, C. and Rauschenberg S.: Factors regulating the Great Calcite Belt in the Southern  
1258 Ocean and its biogeochemical significance. *Global Biogeochem. Cycles*, 30, doi:10.1002/2016GB005414, 2016  
1259
- 1260 Beaufort, L., Probert, I., de Garidel-Thoron, T., Bendif, E.M., Ruiz-Pino, D., Metzl, N., Goyet, C., Buchet, N.,  
1261 Coupel, P., Grelaud, M., Rost, B., Rickaby, R.E.M., and de Vargas C.: Sensitivity of coccolithophores to  
1262 carbonate chemistry and ocean acidification. *Nature*, doi:10.1038/nature10295. 2011  
1263
- 1264 Bittig, H.C., Steinhoff, T., Claustre, H., Fiedler, B., Williams, N.L., Sauzède, R., Körtzinger, A. and Gattuso, J.-  
1265 P.: An Alternative to Static Climatologies: Robust Estimation of Open Ocean CO<sub>2</sub> Variables and Nutrient  
1266 Concentrations From T, S, and O<sub>2</sub> Data Using Bayesian Neural Networks. *Front. Mar. Sci.* 5:328. doi:  
1267 10.3389/fmars.2018.00328, 2018  
1268
- 1269 Bockmon, E. E., and Dickson, A. G.: An inter-laboratory comparison assessing the quality of seawater carbon  
1270 dioxide measurements. *Marine Chemistry*, 171, 36-43, doi:10.1016/j.marchem.2015.02.002, 2015.  
1271
- 1272 Bosse, A., Testor, P., Mayot, N., Prieur, L., D'Ortenzio, F., Mortier, L., Le Goff, H., Gourcuff, C., Coppola, L.,  
1273 Lavigne, H. and Raimbault, P.: A submesoscale coherent vortex in the Ligurian Sea: From dynamical barriers to  
1274 biological implications. *J. Geophys. Res. Oceans*, 122, doi:10.1002/2016JC012634., 2017.  
1275
- 1276 Bozec, Y., Merlivat, L., Baudoux, A.-C., Beaumont, L., Blain, S., Bucciarelli, E., Danguy, T., Grossteffan, E.,  
1277 Guillot, A., Guillou, J., Répécaud, M., and Tréguer, P.: Diurnal to inter-annual dynamics of pCO<sub>2</sub> recorded by a  
1278 CARIOCA sensor in a temperate coastal ecosystem (2003–2009). *Marine Chemistry*, 126, 1-4, 13-26,  
1279 10.1016/j.marchem.2011.03.003. 2011  
1280
- 1281 Broullón, D., Pérez, F. F., Velo, A., Hoppema, M., Olsen, A., Takahashi, T., Key, R. M., Tanhua, T., González-  
1282 Dávila, M., Jeansson, E., Kozyr, A., and van Heuven, S. M. A. C.: A global monthly climatology of total  
1283 alkalinity: a neural network approach, *Earth Syst. Sci. Data*, 11, 1109–1127, [https://doi.org/10.5194/essd-11-](https://doi.org/10.5194/essd-11-1109-2019)  
1284 1109-2019. 2019  
1285
- 1286 Broullón, D., Pérez, F. F., Velo, A., Hoppema, M., Olsen, A., Takahashi, T., Key, R. M., Tanhua, T., Santana-  
1287 Casiano, J. M., and Kozyr, A.: A global monthly climatology of oceanic total dissolved inorganic carbon: a  
1288 neural network approach, *Earth Syst. Sci. Data*, 12, 1725–1743, <https://doi.org/10.5194/essd-12-1725-2020>.  
1289 2020  
1290
- 1291 Bushinsky, S. M., Landschützer, P., Rödenbeck, C., Gray, A. R., Baker, D., Mazloff, M. R., Resplandy L.,  
1292 Johnson K. S., and Sarmiento, J. L.: Reassessing Southern Ocean air-sea CO<sub>2</sub> flux estimates with the addition of  
1293 biogeochemical float observations. *Global Biogeochemical Cycles*, 33. doi: 10.1029/2019GB006176, 2019.  
1294
- 1295 Canesi, M., Douville, E., Montagna, P., Taviani, M., Stolarski, J., Bordier, L., Dapoigny, A., Coulibaly, G. E. H.,  
1296 Simon, A.-C., Agelou, M., Fin, J., Metzl, N., Iwankow, G., Allemand, D., Planes, S., Moulin, C., Lombard, F.,  
1297 Bourdin, G., Troublé, R., Agostini, S., Banaigs, B., Boissin, E., Boss, E., Bowler, C., de Vargas, C., Flores, M.,  
1298 Forcioli, D., Furla, P., Gilson, E., Galand, P. E., Pesant, S., Sunagawa, S., Thomas, O., Thurber, R. V., Voolstra,  
1299 C. R., Wincker, P., Zoccola, D., and Reynaud, S.: Differences in carbonate chemistry up-regulation of long-lived  
1300 reef-building corals. *Sci. Rep.* 13, 11589, Doi: 10.1038/s41598-023-37598-9, 2023.  
1301
- 1302 Caniaux, G., Giordani, H., Redelsperger, J.-L., Guichard, F., Key, E. and Wade, M.: Coupling between the  
1303 Atlantic cold tongue and the West African monsoon in boreal spring and summer. *J. Geophys. Res.*, 119,  
1304 C04003, doi:10.1029/2010JC006570., 2011.



- 1305  
1306 Cariou, T., and Bozec, Y.: COMOR-CARBORHONE 1 cruise, RV L'Europe,  
1307 <https://doi.org/10.17600/11060060>, 2011a.  
1308  
1309 Cariou, T., and Bozec, Y.: COMOR-CARBORHONE 2 cruise, RV Téthys II,  
1310 <https://doi.org/10.17600/11450150>, 2011b.  
1311  
1312 Cariou, T., and Bozec, Y.: CARBORHONE 3 cruise, RV Téthys II, <https://doi.org/10.17600/12450020>, 2012a.  
1313  
1314 Cariou, T., and Bozec Y.: CARBORHONE 4 cruise, RV Téthys II, <https://doi.org/10.17600/12450140>, 2012b.  
1315  
1316 Carter, B. R., Williams, N. L., Gray, A. R., and Feely, R. A.: Locally interpolated alkalinity regression for global  
1317 alkalinity estimation, *Limnol. Oceanogr. Methods*, 14(4), 268–277, doi:10.1002/lom3.10087, 2016.  
1318  
1319 Chau, T.-T.-T., Gehlen, M., Metzl, N., and Chevallier, F.: CMEMS-LSCE: A global 0.25-degree, monthly  
1320 reconstruction of the surface ocean carbonate system, *Earth Syst. Sci. Data Discuss.* [preprint],  
1321 <https://doi.org/10.5194/essd-2023-146>, in review, 2023.  
1322  
1323 Chen, H., Haumann, F. A., Talley, L. D., Johnson, K. S., and Sarmiento, J. L.: The deep ocean's carbon exhaust.  
1324 *Global Biogeochemical Cycles*. doi: <https://doi.org/10.1002/essoar.10507757.1>, 2022  
1325  
1326 Cheng, L. J., Abraham, J., Zhu, J., Trenberth, K. E., Fasullo, J., Boyer, T., Locarnini, R., Zhang, B., Yu, F. J.,  
1327 Wan, L. Y., Chen, X. R., Song, X. Z., Liu, Y. L., and Mann, M. E.: Record-setting ocean warmth continued in  
1328 2019, *Adv. Atmos. Sci.*, 37, 137–142. <https://doi.org/10.1007/s00376-020-9283-7>, 2020  
1329  
1330 Claustre, H., Johnson, K. S., and Takeshita, Y.: Observing the Global Ocean with Biogeochemical-Argo. *Annual*  
1331 *Review of Marine Science*, 12: 23-48 | DOI: [10.1146/annurev-marine-010419-010956](https://doi.org/10.1146/annurev-marine-010419-010956), 2020.  
1332  
1333 Conan, P., Guieux, A., and Vuillemin, R.: MOOSE (MOLA), <https://doi.org/10.18142/234>, 2020.  
1334  
1335 Copin-Montégut, C.: Alkalinity and carbon budgets in the Mediterranean Sea, *Global Biogeochemical Cycles*,  
1336 vol. 7, pp. 915–925, 1993.  
1337  
1338 Copin-Montégut, C., and Bégovic, M.: Distributions of carbonate properties and oxygen along the water column  
1339 (0–2000 m) in the central part of the NW Mediterranean Sea (Dyfamed site): influence of the winter vertical  
1340 mixing on air–sea CO<sub>2</sub> and O<sub>2</sub> exchanges. *Deep-Sea Research II* 49, 2049–2066, [https://doi.org/10.1016/S0967-](https://doi.org/10.1016/S0967-0645(02)00027-9)  
1341 [0645\(02\)00027-9](https://doi.org/10.1016/S0967-0645(02)00027-9), 2002.  
1342  
1343 Coppola, L., and Diamond-Riquier, E.: MOOSE (DYFAMED), <https://doi.org/10.18142/131>, 2008.  
1344  
1345 Coppola, L., Raimbault, P., Mortier, L., and Testor, P.: Monitoring the environment in the northwestern  
1346 Mediterranean Sea, *Eos*, 100, <https://doi.org/10.1029/2019EO125951>. Published on 25 July 2019.  
1347  
1348 Coppola, L., Boutin, J., Gattuso, J.-P., Lefèvre, D., and Metzl, N.: The Carbonate System in the Ligurian Sea. In  
1349 *The Mediterranean Sea in the Era of Global Change: Evidence from 30 years of multidisciplinary study of the*  
1350 *Ligurian Sea*, C. Migon, P. Nival, A. Sciandra, Eds. (ISTE Science Publishing LTD, London, UK, 2020), vol. 1,  
1351 chap. 4, pp. 79–104. ISBN: 9781786304285. <https://doi.org/10.1002/9781119706960.ch4>, 2020.  
1352  
1353 Corbière, A., Metzl, N., Reverdin, G., Brunet, C., and Takahashi, T.: Interannual and decadal variability of the  
1354 oceanic carbon sink in the North Atlantic subpolar gyre. *Tellus B*, Vol. 59, issue 2, 168–179, DOI:  
1355 [10.1111/j.1600-0889.2006.00232](https://doi.org/10.1111/j.1600-0889.2006.00232), 2007.  
1356  
1357 D'Ortenzio, F. and Taillandier, V.: BIO-ARGO-MED-2018 cruise, RV Téthys II,  
1358 <https://doi.org/10.17600/18000550>, 2018.



- 1359  
1360 De Carlo, E. H., Mousseau, L., Passafiume, O., Drupp, P. and Gattuso J.-P.: Carbonate chemistry and air-sea  
1361 CO<sub>2</sub> flux in a NW Mediterranean bay over a four-year period: 2007-2011. *Aquatic Geochemistry*  
1362 doi:10.1007/s10498-013-9217-4, 2013.  
1363  
1364 Dickson, A. G., Sabine, C. L., and Christian, J. R.: Guide to best practices for ocean CO<sub>2</sub> measurements, North  
1365 Pacific Marine Science Organization, Sidney, British Columbia, 191, <https://doi.org/10.25607/OBP-1342>, 2007.  
1366  
1367 Division Plans de DMI – SHOM: PROTEUS2010\_LEG1 cruise, RV Pourquoi pas ?,  
1368 <https://doi.org/10.17600/10030040>, 2010.  
1369  
1370 Division Plans de DMI – SHOM: PROTEUSMED\_PERLE\_2018 cruise, RV L'Atalante,  
1371 <https://campagnes.flotteoceanographique.fr/campaign>, 2018.  
1372  
1373 Doney, S. C., Fabry, V. J., Feely, R. A., and Kleypas, J. A., Ocean acidification: The other CO<sub>2</sub> problem. *Annual*  
1374 *Review of Marine Science*, 1(1), 169–192. 10.1146/annurev.marine.010908.163834, 2009  
1375  
1376 Doney, S. C., Busch, D. S., Cooley, S. R., and Kroeker, K. J.: The Impacts of Ocean Acidification on Marine  
1377 Ecosystems and Reliant Human Communities. *Annual Review of Environment and Resources* 45:1,  
1378 <https://doi.org/10.1146/annurev-environ-012320-083019>. 2020  
1379  
1380 Douville, E., Bourdin, G., Lombard, F., Gorsky, G., Fin, J., Metzl, N., Pesant, S., and Tara Pacific Consortium:  
1381 Seawater carbonate chemistry dataset collected during the Tara Pacific Expedition 2016-2018. PANGAEA,  
1382 <https://doi.org/10.1594/PANGAEA.944420>. 2022.  
1383  
1384 Durrieu de Madron, X.: CASCADE cruise, RV L'Atalante, <https://doi.org/10.17600/11010020>, 2011.  
1385  
1386 Durrieu de Madron, X., and Conan, P.: PERLE2 cruise, RV Pourquoi pas ?, <https://doi.org/10.17600/18000865>,  
1387 2018  
1388  
1389 Edmond, J. M.: High precision determination of titration alkalinity and total carbon dioxide content of sea water  
1390 by potentiometric titration, *Deep-Sea Res.*, 17, 737–750, [https://doi.org/10.1016/0011-7471\(70\)90038-0](https://doi.org/10.1016/0011-7471(70)90038-0), 1970.  
1391  
1392 Eldin, G. : PANDORA cruise, RV L'Atalante, <https://doi.org/10.17600/12010050>, 2012.  
1393  
1394 Eyring, V., Righi, M., Lauer, A., Evaldsson, M., Wenzel, S., Jones, C., Anav, A., Andrews, O., Cionni, I., Davin,  
1395 E. L., Deser, C., Ehbrecht, C., Friedlingstein, P., Gleckler, P., Gottschaldt, K.-D., Hagemann, S., Juckes, M.,  
1396 Kindermann, S., Krasting, J., Kunert, D., Levine, R., Loew, A., Mäkelä, J., Martin, G., Mason, E., Phillips, A. S.,  
1397 Read, S., Rio, C., Roehrig, R., Senftleben, D., Sterl, A., van Ulft, L. H., Walton, J., Wang, S., and Williams, K.  
1398 D.: ESMValTool (v1.0) – a community diagnostic and performance metrics tool for routine evaluation of Earth  
1399 system models in CMIP, *Geosci. Model Dev.*, 9, 1747-1802, doi:10.5194/gmd-9-1747-2016, 2016.  
1400  
1401 Fabry, V. J., Seibel, B. A., Feely, R. A. and Orr, J. C.: Impacts of ocean acidification on marine fauna and  
1402 ecosystem processes. *ICES J. Mar. Sci.* 65, 414–432. <https://doi.org/10.1093/icesjms/fsn048>, 2008.  
1403  
1404 Fassbender, A. J., Sabine, C. L., and Palevsky, H. I.: Nonuniform ocean acidification and attenuation of the  
1405 ocean carbon sink, *Geophys. Res. Lett.*, 44, 8404–8413, doi:10.1002/2017GL074389., 2017.  
1406  
1407 Fassbender, A. J., Alin, S. R., Feely, R. A., Sutton, A. J., Newton, J. A., Krembs, C., Bos, J., Keyzers, M., Devol,  
1408 A., Ruef, W., and Pelletier, G.: Seasonal carbonate chemistry variability in marine surface waters of the US  
1409 Pacific Northwest, *Earth Syst. Sci. Data*, 10, 1367–1401, <https://doi.org/10.5194/essd-10-1367-2018>, 2018.  
1410





- 1411 Feely, R. A., Sabine, C. L., Byrne, R. H., Millero, F. J., Dickson, A. G., Wanninkhof, R., et al.: Decadal changes  
1412 in the aragonite and calcite saturation state of the Pacific Ocean. *Global Biogeochemical Cycles*, 26, GB3001.  
1413 <https://doi.org/10.1029/2011GB004157>, 2012.
- 1414  
1415 Fleury, E., Petton, S., Benabdelmouna, A., and Pouvreau, S., (coord.): Observatoire national du cycle de vie de  
1416 l'huître creuse en France. Rapport annuel ECOSCOPA 2022. R.INT.BREST RBE/PFOM/PI 2023-1, 2023.
- 1417  
1418 Fourier, M., Coppola, L., Claustre, H., D'Ortenzio, F., Sauzède, R. and Gattuso, J.-P.: A regional neural  
1419 network approach to estimate water-column nutrient concentrations and carbonate system variables in the  
1420 Mediterranean Sea: CANYON-MED. *Frontiers in Marine Science*, 7:620,  
1421 <https://www.frontiersin.org/articles/10.3389/fmars.2020.00620>, 2020.
- 1422  
1423 Fourier, M., Coppola, L., D'Ortenzio, F., Migon, C., and Gattuso, J.-P.: Impact of intermittent convection in the  
1424 northwestern Mediterranean Sea on oxygen content, nutrients, and the carbonate system. *Journal of Geophysical*  
1425 *Research: Oceans*, 127, e2022JC018615. <https://doi.org/10.1029/2022JC018615>, 2022
- 1426  
1427 Friedlingstein, P., O'Sullivan, M., Jones, M. W., Andrew, R. M., Gregor, L., Hauck, J., Le Quééré, C., Luijkx, I.  
1428 T., Olsen, A., Peters, G. P., Peters, W., Pongratz, J., Schwingshackl, C., Sitch, S., Canadell, J. G., Ciais, P.,  
1429 Jackson, R. B., Alin, S. R., Alkama, R., Arneeth, A., Arora, V. K., Bates, N. R., Becker, M., Bellouin, N., Bittig,  
1430 H. C., Bopp, L., Chevallier, F., Chini, L. P., Cronin, M., Evans, W., Falk, S., Feely, R. A., Gasser, T., Gehlen,  
1431 M., Gkritzalis, T., Gloege, L., Grassi, G., Gruber, N., Gürses, Ö., Harris, I., Hefner, M., Houghton, R. A., Hurtt,  
1432 G. C., Iida, Y., Ilyina, T., Jain, A. K., Jersild, A., Kadono, K., Kato, E., Kennedy, D., Klein Goldewijk, K.,  
1433 Knauer, J., Korsbakken, J. I., Landschützer, P., Lefèvre, N., Lindsay, K., Liu, J., Liu, Z., Marland, G., Mayot, N.,  
1434 McGrath, M. J., Metzl, N., Monacchi, N. M., Munro, D. R., Nakaoka, S.-I., Niwa, Y., O'Brien, K., Ono, T.,  
1435 Palmer, P. I., Pan, N., Pierrot, D., Pockock, K., Poulter, B., Resplandy, L., Robertson, E., Rödenbeck, C.,  
1436 Rodriguez, C., Rosan, T. M., Schwinger, J., Séférian, R., Shutler, J. D., Skjelvan, I., Steinhoff, T., Sun, Q.,  
1437 Sutton, A. J., Sweeney, C., Takao, S., Tanhua, T., Tans, P. P., Tian, X., Tian, H., Tilbrook, B., Tsujino, H.,  
1438 Tubiello, F., van der Werf, G. R., Walker, A. P., Wanninkhof, R., Whitehead, C., Willstrand Wranne, A.,  
1439 Wright, R., Yuan, W., Yue, C., Yue, X., Zaehle, S., Zeng, J., and Zheng, B.: Global Carbon Budget 2022, *Earth*  
1440 *Syst. Sci. Data*, 14, 4811–4900, <https://doi.org/10.5194/essd-14-4811-2022>, 2022.
- 1441  
1442 Fröb, F., Olsen, A., Becker, M., Chafik, L., Johannessen, T., Reverdin, G., and Omar, A.: Wintertime fCO<sub>2</sub>  
1443 variability in the subpolar North Atlantic since 2004. *Geophysical Research Letters*, 46,  
1444 <https://doi.org/10.1029/2018GL080554>, 2019.
- 1445  
1446 Gac, J.-P., Marrec, P., Cariou, T., Guillerm, C., Macé, E., Vernet, M., and Bozec, Y.: Cardinal buoys: An  
1447 opportunity for the study of air-sea CO<sub>2</sub> fluxes in coastal ecosystems. *Front. Mar. Sci.* doi:  
1448 10.3389/fmars.2020.00712. 2020.
- 1449  
1450 Gac, J.-P., Marrec, P., Cariou, T., Grosstefan, E., Macé, E., Rimmelin-Maury, P., Vernet, M., and Bozec, Y.:  
1451 Decadal Dynamics of the CO<sub>2</sub> System and Associated Ocean Acidification in Coastal Ecosystems of the North  
1452 East Atlantic Ocean. *Front. Mar. Sci.* 8:688008. doi:10.3389/fmars.2021.688008, 2021.
- 1453  
1454 Ganachaud, A., Cravatte, S., Sprintall, J., Germineaud, C., Albery, M., Jeandel, C., Eldin, G., Metzl, N., Bonnet,  
1455 S., Benavides, M., Heimburger, L.-E., Lefèvre, J., Michael, S., Resing, J., Quéroüé, F., Sarthou, G., Rodier, M.,  
1456 Berthelot, H., Baurand, F., Grelet, J., Hasegawa, T., Kessler, W., Kilepak, M., Lacan, F., Privat, E., Send, U.,  
1457 Van Beek, P., Souhaut, M. and Sonke, J. E.: The Solomon Sea: its circulation, chemistry, geochemistry and  
1458 biology explored during two oceanographic cruises. *Elem Sci Anth*, 5: 33, DOI:  
1459 <https://doi.org/10.1525/elementa.221>, 2017.
- 1460  
1461 Gattuso, J.-P., Magnan, A., Billé, R., Cheung, W. W. L., Howes, E. L., Joos, F., Allemand, D., Bopp, L., Cooley,  
1462 S., Eakin, M., Hoegh-Guldberg, O., Kelly, R. P., Pörtner, H.-O., Rogers, A. D., Baxter, J. M., Laffoley, D.,  
1463 Osborn, D., Rankovic, A., Rochette, J., Sumaila, U. R., Treyer, S., and Turley, C.: Contrasting futures for ocean



- 1464 and society from different anthropogenic CO<sub>2</sub> emissions scenarios. *Science* 349:aac4722.doi:  
1465 10.1126/science.aac4722, 2015.  
1466  
1467 Gattuso, J.-P., Alliouane, S., and Mousseau, L.: Seawater carbonate chemistry in the Bay of Villefranche, Point  
1468 B (France), January 2007 - September 2020. PANGAEA, <https://doi.org/10.1594/PANGAEA.727120>, 2021.  
1469  
1470 Gattuso, J.-P., Alliouane, S., and Fischer, P.: High-frequency, year-round time series of the carbonate chemistry  
1471 in a high-Arctic fjord (Svalbard), *Earth Syst. Sci. Data*, 15, 2809–2825, [https://doi.org/10.5194/essd-15-2809-](https://doi.org/10.5194/essd-15-2809-2023)  
1472 [2023](https://doi.org/10.5194/essd-15-2809-2023), 2023.  
1473  
1474 Gattuso, J.-P., Alliouane, S., and Fischer, P.: High-frequency, year-round time series of the carbonate chemistry  
1475 in a high-Arctic fjord (Svalbard) v2. PANGAEA, <https://doi.org/10.1594/PANGAEA.960131>, 2023.  
1476  
1477 Gemayel, E., Hassoun, A. E. R., Benallal, M. A., Goyet, C., Rivaro, P., Abboud-Abi Saab, M., Krasakopoulou,  
1478 E., Touratier, F., and Ziveri, P.: Climatological variations of total alkalinity and total inorganic carbon in the  
1479 Mediterranean Sea surface waters. *Earth Syst. Dynam.*, 6, 789–800, doi:10.5194/esd-6-789-2015, 2015.  
1480  
1481 Golbol, M., Vellucci, V., and Antoine, D.: BOUSSOLE, <https://doi.org/10.18142/1>, 2000.  
1482  
1483 Golbol M., Boutin J., Merlivat L., Vellucci, V., and Antoine, D.: Dissolved Inorganic Carbon and Total  
1484 Alkalinity sampled at Boussole site in the Mediterranean Sea. SEANOE. <https://doi.org/10.17882/71911>, 2020.  
1485  
1486 Goris, N., Tjiputra, J. F., Olsen, A., Schwinger, J., Lauvset, S. K. and Jeansson, E.: Constraining projection-  
1487 based estimates of the future North Atlantic carbon uptake, *J. Climate*, 31, 3959–3978,  
1488 <https://doi.org/10.1175/JCLI-D-17-0564.1>, 2018.  
1489  
1490 Goyet, C., Beauverger, C., Brunet, C., and Poisson, A.: Distribution of carbon dioxide partial pressure in surface  
1491 waters of the Southwest Indian Ocean, *Tellus B: Chemical and Physical Meteorology*, 43:1, 1–11, DOI:  
1492 [10.3402/tellusb.v43i1.15242](https://doi.org/10.3402/tellusb.v43i1.15242), 1991.  
1493  
1494 Gregor, L. and Gruber, N.: OceanSODA-ETHZ: a global gridded data set of the surface ocean carbonate system  
1495 for seasonal to decadal studies of ocean acidification, *Earth Syst. Sci. Data*, 13, 777–808,  
1496 <https://doi.org/10.5194/essd-13-777-2021>, 2021.  
1497  
1498 Gruber, N., Clement, D., Carter, B. R., Feely, R. A., van Heuven, S., Hoppema, M., Ishii, M., Key, R. M.,  
1499 Kozyr, A., Lauvset, S. K., Lo Monaco, C., Mathis, J. T., Murata, A., Olsen, A., Perez, F. F., Sabine, C. L.,  
1500 Tanhua, T., and Wanninkhof, R.: The oceanic sink for anthropogenic CO<sub>2</sub> from 1994 to 2007, *Science* vol. 363  
1501 (issue 6432), pp. 1193–1199. DOI: 10.1126/science.aau5153, 2019.  
1502  
1503 Guieu, C., Desboeufs, K., Albani, S., et al.: BIOGEOCHEMICAL dataset collected during the PEACETIME  
1504 cruise. SEANOE. <https://doi.org/10.17882/75747>, 2020.  
1505  
1506 Hagens, M., and Middelburg, J. J.: Attributing seasonal pH variability in surface ocean waters to governing  
1507 factors, *Geophys. Res. Lett.*, 43, doi:10.1002/2016GL071719, 2016.  
1508  
1509 Henson, S. A., Painter, S. C., Holliday, N. P., Stinchcombe, M. C., and Giering, S. L. C.: Unusual subpolar  
1510 North Atlantic phytoplankton bloom in 2010: Volcanic fertilization or North Atlantic Oscillation?, *J. Geophys.*  
1511 *Res. Oceans*, 118, 4771–4780, doi:10.1002/jgrc.20363, 2013.  
1512  
1513 Hoegh-Guldberg, O., Mumby, P.J., Hooten, A.J., Steneck, R.S., Greenfield, P., Gomez, E., Harvell, C.D., Sale,  
1514 P.F., Edwards, A.J., Caldeira, K., Knowlton, N., Eakin, C.M., Iglesias-Prieto, R., Muthiga, N., Bradbury, R.H.,  
1515 Dubi, A., and Hatziolos, M.E.: Coral reefs under rapid climate change and ocean acidification. *Science* 14,  
1516 1737–1742. <https://doi.org/10.1126/science.1152509>, 2007.  
1517



- 1518 Hood, E.M., and Merlivat, L.: Annual to interannual variations of  $f\text{CO}_2$  in the northwestern Mediterranean  
1519 Sea: Results from hourly measurements made by CARIOCA buoys, 1995-1997, *Journal Of Marine Research*,  
1520 59, 113-131, doi: 10.1357/002224001321237399. 2001
- 1521
- 1522 Howes, E., Stemmann, L., Assailly, C., Irisson, J.-O., Dima, M., Bijma, J., Gattuso, J.-P.: Pteropod time series  
1523 from the North Western Mediterranean (1967-2003): impacts of pH and climate variability. *Mar Ecol Prog Ser*  
1524 531: 193-206, doi: 10.3354/meps11322. 2015.
- 1525
- 1526 Howes, E. L., Eagle, R., Gattuso, J.-P., and Bijma, J.: Comparison of Mediterranean pteropod shell biometrics  
1527 and ultrastructure from historical (1910 and 1921) and present day (2012) samples provides baseline for  
1528 monitoring effects of global change. *PLoS ONE* 12:e0167891. 2017.
- 1529
- 1530 IPCC. Changing Ocean, Marine Ecosystems, and Dependent Communities. in *The Ocean and Cryosphere in a*  
1531 *Changing Climate* 447–588 (Cambridge University Press, 2022). doi:10.1017/9781009157964.007. 2022
- 1532
- 1533 Jiang, Z.-P., Tyrrell, T., Hydes, D. J., Dai, M., and Hartman, S. E.: Variability of alkalinity and the alkalinity-  
1534 salinity relationship in the tropical and subtropical surface ocean, *Global Biogeochem. Cycles*, 28, 729–742,  
1535 doi:10.1002/2013GB004678, 2014.
- 1536
- 1537 Jiang, L.-Q., Feely, R. A., Carter, B. R., Greeley, D. J., Gledhill, D. K., and Arzayus K. M.: Climatological  
1538 distribution of aragonite saturation state in the global oceans, *Global Biogeochem. Cycles*, 29, 1656–1673,  
1539 doi:10.1002/2015GB005198, 2015.
- 1540
- 1541 Jiang, L.-Q., Carter, B. R., Feely, R. A., Lauvset, S. K. and Olsen, A.: Surface ocean pH and buffer capacity:  
1542 past, present and future, *Sci Rep*, 9(1), 1–11, doi:10.1038/s41598-019-55039-4. 2019.
- 1543
- 1544 Jiang, L.Q., Feely, R. A., Wanninkhof, R., et al.: Coastal Ocean Data Analysis Product in North America  
1545 (CODAP-NA, Version 2021) (NCEI Accession 0219960). [indicate subset used]. NOAA National Centers for  
1546 Environmental Information. Dataset. <https://doi.org/10.25921/531n-c230>. Accessed [date]. 2020.
- 1547
- 1548 Jiang, L.-Q., Dunne, J., Carter, B. R., Tjiputra, J. F., Terhaar, J., Sharp, J. D., et al.: Global surface ocean  
1549 acidification indicators from 1750 to 2100. *Journal of Advances in Modeling Earth Systems*, 15,  
1550 e2022MS003563. <https://doi.org/10.1029/2022MS003563>, 2023a
- 1551
- 1552 Jiang, L.Q., Kozyr, A., Relph, J.M. *et al.* The Ocean Carbon and Acidification Data System. *Sci Data* 10, 136.  
1553 <https://doi.org/10.1038/s41597-023-02042-0>, 2023b
- 1554
- 1555 Johnson, K. S., Mazloff, M. R., Bif, M. B., Takeshita, Y., Jannasch, H. W., Maurer, T. L., et al.: Carbon to  
1556 nitrogen uptake ratios observed across the Southern Ocean by the SOCCOM profiling float array. *Journal of*  
1557 *Geophysical Research: Oceans*, 127, e2022JC018859. <https://doi.org/10.1029/2022JC018859>, 2022.
- 1558
- 1559 Joos, F., Hameau, A., Frölicher, T. L., and Stephenson, D. B.: Anthropogenic attribution of the  
1560 increasing seasonal amplitude in surface ocean  $p\text{CO}_2$ . *Geophysical Research Letters*, 50, e2023GL102857.  
1561 <https://doi.org/10.1029/2023GL102857>, 2023.
- 1562
- 1563 Joyce, T. and Corry, C., eds: Requirements for WOCE Hydrographic Programme Data Reporting. WHPO  
1564 Publication 90-1 Revision 2, WOCE Report 67/91, Woods Hole, Mass., USA, May 1994.
- 1565
- 1566 Kapsenberg, L., Alliouane, S., Gazeau, F., Mousseau, L., and Gattuso, J.-P.: Coastal ocean acidification and  
1567 increasing total alkalinity in the northwestern Mediterranean Sea, *Ocean Sci.*, 13, 411-426, doi:10.5194/os-13-  
1568 411-2017, 2017.
- 1569
- 1570 Keppler, L., Landschützer, P., Gruber, N., Lauvset, S. K., and Stemmler, I.: Seasonal carbon dynamics in the  
1571 near-global ocean. *Global Biogeochemical Cycles*, 34, e2020GB006571. doi:10.1029/2020GB006571, 2020.



- 1572  
1573 Keppler, L., Landschützer, P., Lauvset, S.K., and Gruber, N.: Recent trends and variability in the oceanic storage  
1574 of dissolved inorganic carbon. *Global Biogeochemical Cycles*, 37, e2022GB007677. Doi:  
1575 10.1029/2022GB007677, 2023.  
1576  
1577 Keraghel, M. A., Louanchi, F., Zerrouki, M., Kaci, M. A., Aït-Ameur, N., Labaste, M., Legoff, H., Taillandier,  
1578 V., Harid, R., and Mortier, L.: Carbonate system properties and anthropogenic carbon inventory in the Algerian  
1579 Basin during SOMBA cruise (2014): Acidification estimate, *Marine Chemistry*,  
1580 <https://doi.org/10.1016/j.marchem.2020.103783>. 2020.  
1581  
1582 Key, R. M., Kozyr, A., Sabine, C. L., Lee, K., Wanninkhof, R., Bullister, J. L., Feely, R. A., Millero, F. J.,  
1583 Mordy, C., and Peng, T. H.: A global ocean carbon climatology: Results from Global Data Analysis Project  
1584 (GLODAP), *Global Biogeochemical Cycles*, 18, GB4031, <https://doi.org/10.1029/2004GB002247>, 2004.  
1585  
1586 Key, R. M., Tanhua, T., Olsen, A., Hoppema, M., Jutterström, S., Schirnick, C., van Heuven, S., Kozyr, A., Lin,  
1587 X., Velo, A., Wallace, D. W. R., and Mintrop, L.: The CARINA data synthesis project: introduction and  
1588 overview, *Earth Syst. Sci. Data*, 2, 105–121, <https://doi.org/10.5194/essd-2-105-2010>, 2010.  
1589  
1590 Khatiwala, S., Tanhua, T., Mikaloff Fletcher, S., Gerber, M., Doney, S. C., Graven, H. D., Gruber, N.,  
1591 McKinley, G. A., Murata, A., Ríos, A. F., and Sabine, C. L.: Global ocean storage of anthropogenic carbon,  
1592 *Biogeosciences*, 10, 2169–2191, <https://doi.org/10.5194/bg-10-2169-2013>, 2013.  
1593  
1594 Kitidis, V., Shutler, J. D., Ashton, I., Warren, M., Brown, I., Findlay, H., Hartman, S. E., Sanders, R.,  
1595 Humphreys, M., Kivimäe, C., Greenwood, N., Hull, T., Pearce, D., McGrath, T., Stewart, B. M., Walsham, P.,  
1596 McGovern, E., Bozec, Y., Gac, J.-P., van Heuven, S., Hoppema, M., Schuster, U., Johannessen, T., Omar, A.,  
1597 Lauvset, S. K., Skjelvan, I., Olsen, A., Steinhoff, T., Körtzinger, A., Becker, M., Lefèvre, N., Diverrès, D.,  
1598 Gkritzalis, T., Cattrijsse, A., Petersen, W., Voynova, Y., Chapron, B., Grouazel, A., Land, P. E., Sharples, J., and  
1599 Nightingale, P. D.: Winter weather controls net influx of atmospheric CO<sub>2</sub> on the north-west European shelf. *Sci*  
1600 *Rep* 9, 20153, doi:10.1038/s41598-019-56363-5. 2019.  
1601  
1602 Koffi U., Lefevre, N., Kouadio, G., and Boutin, J.: Surface CO<sub>2</sub> parameters and air-sea CO<sub>2</sub> fluxes distribution  
1603 in the eastern equatorial Atlantic Ocean. *J. Marine Systems*, doi:10.1016/j.jmarsys/2010.04.010. 2010.  
1604  
1605 Koffi, U., Georges, K., and Boutin, J.: Partial pressure (or fugacity) of carbon dioxide, dissolved inorganic  
1606 carbon, alkalinity, temperature, salinity and other variables collected from Surface underway, discrete sample  
1607 and profile observations using CTD, Carbon dioxide (CO<sub>2</sub>) gas analyzer and other instruments from ANTEA  
1608 and L'ATALANTE in the Gulf of Guinea, North Atlantic Ocean and South Atlantic Ocean from 2005-06-09 to  
1609 2007-09-30 (NCEI Accession 0108086). [indicate subset used]. NOAA National Centers for Environmental  
1610 Information. Dataset. [https://doi.org/10.3334/cdiac/otg.egee1\\_6](https://doi.org/10.3334/cdiac/otg.egee1_6). Accessed [date]., 2013  
1611  
1612 Koseki, S., Tjiputra, J., Fransner, F. et al.: Disentangling the impact of Atlantic Niño on sea-air CO<sub>2</sub> flux. *Nat*  
1613 *Commun* 14, 3649. <https://doi.org/10.1038/s41467-023-38718-9>, 2023.  
1614  
1615 Kwiatkowski, L., Torres, O., Bopp, L., Aumont, O., Chamberlain, M., Christian, J. R., Dunne, J. P., Gehlen, M.,  
1616 Ilyina, T., John, J. G., Lenton, A., Li, H., Lovenduski, N. S., Orr, J. C., Palmieri, J., Santana-Falcón, Y.,  
1617 Schwinger, J., Séférian, R., Stock, C. A., Tagliabue, A., Takano, Y., Tjiputra, J., Toyama, K., Tsujino, H.,  
1618 Watanabe, M., Yamamoto, A., Yool, A., and Ziehn, T.: Twenty-first century ocean warming, acidification,  
1619 deoxygenation, and upper-ocean nutrient and primary production decline from CMIP6 model projections,  
1620 *Biogeosciences*, 17, 3439–3470, <https://doi.org/10.5194/bg-17-3439-2020>, 2020.  
1621  
1622 Land, P. E., Findlay, H. S., Shutler, J. D., Ashton, I. G., Holding, T., Grouazel, A., Girard-Ardhuin, F., Reul, N.,  
1623 Piolle, J. F., Chapron, B., and Quilfen, Y.: Optimum satellite remote sensing of the marine carbonate system  
1624 using empirical algorithms in the global ocean, the Greater Caribbean, the Amazon Plume and the Bay of  
1625 Bengal. *Remote Sensing of Environment*, 235, p.111469, doi: 10.1016/j.rse.2019.111469, 2019.



- 1626  
1627 Lange, N., Fiedler, B., Álvarez, M., Benoit-Cattin, A., Benway, H., Buttigieg, P. L., Coppola, L., Currie, K.,  
1628 Flecha, S., Honda, M., Huertas, I. E., Lauvset, S. K., Muller-Karger, F., Körtzinger, A., O'Brien, K. M.,  
1629 Ólafsdóttir, S. R., Pacheco, F. C., Rueda-Roa, D., Skjelvan, I., Wakita, M., White, A., and Tanhua, T.: Synthesis  
1630 Product for Ocean Time-Series (SPOTS) – A ship-based biogeochemical pilot, *Earth Syst. Sci. Data Discuss.*  
1631 [preprint], <https://doi.org/10.5194/essd-2023-238>, in review, 2023.  
1632  
1633 Lauvset, S. K., Gruber, N., Landschützer, P., Olsen, A., and Tjiputra, J.: Trends and drivers in global surface  
1634 ocean pH over the past 3 decades. *Biogeosciences*, 12, 1285-1298, doi:10.5194/bg-12-1285-2015, 2015  
1635  
1636 Lauvset, S. K., Carter, B. R., Perez, F. F., Jiang, L.-Q., Feely, R. A., Velo, A., and Olsen, A.: Processes Driving  
1637 Global Interior Ocean pH Distribution, *Global Biogeochem. Cycles*, 34, e2019GB006 229,  
1638 <https://doi.org/10.1029/2019GB006229>, 2020.  
1639  
1640 Lauvset, S. K., Lange, N., Tanhua, T., Bittig, H. C., Olsen, A., Kozyr, A., Álvarez, M., Becker, S., Brown, P. J.,  
1641 Carter, B. R., Cotrim da Cunha, L., Feely, R. A., van Heuven, S., Hoppema, M., Ishii, M., Jeansson, E.,  
1642 Jutterström, S., Jones, S. D., Karlsen, M. K., Lo Monaco, C., Michaelis, P., Murata, A., Pérez, F. F., Pfeil, B.,  
1643 Schirnack, C., Steinfeldt, R., Suzuki, T., Tilbrook, B., Velo, A., Wanninkhof, R., Woosley, R. J., and Key, R. M.:  
1644 An updated version of the global interior ocean biogeochemical data product, GLODAPv2.2021, *Earth Syst. Sci.*  
1645 *Data*, 13, 5565–5589, <https://doi.org/10.5194/essd-13-5565-2021>, 2021.  
1646  
1647 Lebehot, A. D., Halloran, P. R., Watson, A. J., McNeill, D., Ford, D. A., Landschützer, P., Lauvset, S. K.,  
1648 and Schuster, U.: Reconciling Observation and Model Trends in North Atlantic Surface CO<sub>2</sub>, *Global*  
1649 *Biogeochem. Cy.*, 33, 1204–1222, <https://doi.org/10.1029/2019GB006186>, 2019.  
1650  
1651 Lee, K., Wanninkhof, R., Feely, R. A., Millero, F. J., and Peng, T.-H.: Global relationships of total inorganic  
1652 carbon with temperature and nitrate in surface seawater, *Global Biogeochem. Cy.*, 14, 979–994,  
1653 <https://doi.org/10.1029/1998GB001087>, 2000.  
1654  
1655 Lee, K., Tong, L.T., Millero, F.J., Sabine, C.L., Dickson, A.G., Goyet, C., Park, G.H., Wanninkhof, R., Feely,  
1656 R.A., and Key, R.M.: Global relationships of total alkalinity with salinity and temperature in surface waters of  
1657 the world's oceans. *Geophys. Res. Lett.* 33, L19605. doi10.1029/2006GL027207. 2006.  
1658  
1659 Lefèvre, D.: MOOSE (ANTARES), <https://doi.org/10.18142/233>, 2010.  
1660  
1661 Lefèvre, N., Guillot, A., Beaumont, L., and Danguy, T.: Variability of fCO<sub>2</sub> in the Eastern Tropical Atlantic  
1662 from a moored buoy. *J. of Geophysical Research-Oceans*, Volume: 113 Issue: C1, DOI:  
1663 10.1029/2007JC004146. 2008.  
1664  
1665 Lefèvre N., and Merlivat, L.: Carbon and oxygen net community production in the eastern tropical Atlantic  
1666 estimated from a moored buoy. *Global biogeochemical cycles*, 26(1), 1-14.  
1667 <https://doi.org/10.1029/2010GB004018>. 2012.  
1668  
1669 Lefèvre, N., Diverres, D., and Gallois, F.: Origin of CO<sub>2</sub> undersaturation in the western tropical Atlantic: *Tellus*  
1670 *Series B Chemical and Physical Meteorology*. Volume: 62 Issue: 5 Special Issue: SI Pages: 595-607 DOI:  
1671 10.1111/j.1600-0889.2010.00475.x, 2010.  
1672  
1673 Lefèvre N.: Carbon parameters along a zonal transect. SEANOE. <https://doi.org/10.17882/58575>, 2010.  
1674  
1675 Lefèvre, N., Veleda, D., Araujo, M., Caniaux, G.: Variability and trends of carbon parameters at a time series in  
1676 the eastern tropical Atlantic. *Tellus B*, Co-Action Publishing, 68, pp.30305. 10.3402/tellusb.v68.30305. 2016.  
1677



- 1678 Lefèvre, N., Mejia, C., Khvorostyanov, D., Beaumont, L., and Koffi, U.: Ocean Circulation Drives the  
1679 Variability of the Carbon System in the Eastern Tropical Atlantic. *Oceans*, 2021, 2, 126–148.  
1680 <https://doi.org/10.3390/oceans2010008>, 2021.
- 1681
- 1682 Lefèvre, N.: Discrete profile measurements of dissolved inorganic carbon, total alkalinity, temperature and  
1683 salinity collected from R/V Antea French PIRATA cruise in Eastern Tropical Atlantic Ocean from 2009-07-10  
1684 to 2010-10-01 (NCEI Accession 0171193), 2018a.
- 1685
- 1686 Lefèvre, N.: Discrete surface measurements of dissolved inorganic carbon, total alkalinity, temperature and  
1687 salinity collected from R/V Le Suroit French PIRATA cruise in Eastern Tropical Atlantic Ocean from 2011-05-  
1688 03 to 2011-05-25 (NCEI Accession 0171197), 2018b.
- 1689
- 1690 Lefèvre, N.: Discrete profile measurements of dissolved inorganic carbon, total alkalinity, temperature and  
1691 salinity collected from R/V Le Suroit French PIRATA cruise in Eastern Tropical Atlantic Ocean from 2012-03-  
1692 21 to 2012-04-30 (NCEI Accession 0171195), 2018c.
- 1693
- 1694 Lefèvre, N.: Discrete surface measurements of dissolved inorganic carbon, total alkalinity, temperature and  
1695 salinity collected from R/V Le Suroit French PIRATA cruise in Eastern Tropical Atlantic Ocean from 2013-05-  
1696 11 to 2013-06-18 (NCEI Accession 0171189), 2018d.
- 1697
- 1698 Lefèvre, N.: Discrete profile measurements of dissolved inorganic carbon, total alkalinity, temperature and  
1699 salinity collected from R/V Le Suroit French PIRATA cruise in Eastern Tropical Atlantic Ocean from 2014-04-  
1700 10 to 2014-05-19 (NCEI Accession 0171194), 2018e.
- 1701
- 1702 Lefèvre, N.: Discrete surface measurements of dissolved inorganic carbon, total alkalinity, temperature and  
1703 salinity collected from R/V Thalassa French PIRATA cruise in Eastern Tropical Atlantic Ocean from 2015-03-  
1704 18 to 2015-04-15 (NCEI Accession 0171196), 2018f.
- 1705
- 1706 Lefèvre, N.: Discrete surface measurements of dissolved inorganic carbon, total alkalinity, temperature and  
1707 salinity collected from R/V Thalassa French PIRATA cruise in Eastern Tropical Atlantic Ocean from 2016-03-  
1708 08 to 2016-04-11 (NCEI Accession 0171190), 2018g.
- 1709
- 1710 Lefèvre, N.: Discrete surface measurements of dissolved inorganic carbon, total alkalinity, temperature and  
1711 salinity collected from R/V Thalassa French PIRATA cruise in Eastern Tropical Atlantic Ocean from 2017-02-  
1712 26 to 2017-03-30 (NCEI Accession 0171191), 2018h.
- 1713
- 1714 Le Quéré, C., Moriarty, R., Andrew, R. M., Canadell, J. G., Sitch, S., Korsbakken, J. I., Friedlingstein, P., Peters,  
1715 G. P., Andres, R. J., Boden, T. A., Houghton, R. A., House, J. I., Keeling, R. F., Tans, P., Arneeth, A., Bakker, D.  
1716 C. E., Barbero, L., Bopp, L., Chang, J., Chevallier, F., Chini, L. P., Ciais, P., Fader, M., Feely, R. A., Gkritzalis,  
1717 T., Harris, I., Hauck, J., Ilyina, T., Jain, A. K., Kato, E., Kitidis, V., Klein Goldewijk, K., Koven, C.,  
1718 Landschützer, P., Lauvset, S. K., Lefèvre, N., Lenton, A., Lima, I. D., Metzl, N., Millero, F., Munro, D. R.,  
1719 Murata, A., Nabel, J. E. M. S., Nakaoka, S., Nojiri, Y., O'Brien, K., Olsen, A., Ono, T., Pérez, F. F., Pfeil, B.,  
1720 Pierrot, D., Poulter, B., Rehder, G., Rödenbeck, C., Saito, S., Schuster, U., Schwinger, J., Séférian, R., Steinhoff,  
1721 T., Stocker, B. D., Sutton, A. J., Takahashi, T., Tilbrook, B., van der Laan-Luijkx, I. T., van der Werf, G. R., van  
1722 Heuven, S., Vandemark, D., Viovy, N., Wiltshire, A., Zaehle, S., and Zeng, N.: Global Carbon Budget 2015,  
1723 *Earth Syst. Sci. Data*, 7, 349–396, <https://doi.org/10.5194/essd-7-349-2015>, 2015.
- 1724
- 1725 Lerner, P., Romanou, A., Kelley, M., Romanski, J., Ruedy, R., and Russell, G.: Drivers of Air-Sea CO<sub>2</sub> Flux  
1726 Seasonality and its Long-Term Changes in the NASA-GISS model CMIP6 submission. *Journal of Advances in*  
1727 *Modeling Earth Systems*, 13, e2019MS002028. [Doi:10.1029/2019MS002028](https://doi.org/10.1029/2019MS002028), 2021.
- 1728
- 1729 Leseurre, C., Lo Monaco, C., Reverdin, G., Metzl, N., Fin, J., Olafsdottir, S., and Racapé, V.: Ocean carbonate  
1730 system variability in the North Atlantic Subpolar surface water (1993–2017), *Biogeosciences*, 17, 2553–2577,  
1731 <https://doi.org/10.5194/bg-17-2553-2020>, 2020
- 1732
- 1733 Leseurre, C., Lo Monaco, C., Reverdin, G., Metzl, N., Fin, J., Mignon, C., and Benito, L.: Summer trends and  
1734 drivers of sea surface fCO<sub>2</sub> and pH changes observed in the southern Indian Ocean over the last two decades  
1735 (1998–2019), *Biogeosciences*, 19, 2599–2625, <https://doi.org/10.5194/bg-19-2599-2022>, 2022.



- 1736  
1737 Lherminier, P., Mercier, H., Gourcuff, C., Alvarez, M., Bacon, S., and Kermabon, C.: Transports across the 2002  
1738 Greenland-Portugal OVIDE section and comparison with 1997. *J. Geophys. Res.*, 112(C7), C07003,  
1739 [doi:10.1029/2006JC003716](https://doi.org/10.1029/2006JC003716). 2007  
1740  
1741 Li, B. F., Watanabe, Y. W., Hosoda, S., Sato, K., and Nakano, Y.: Quasireal-time and high-resolution  
1742 spatiotemporal distribution of ocean anthropogenic CO<sub>2</sub>. *Geophysical Research Letters*, 46, 4836–4843.  
1743 <https://doi.org/10.1029/2018GL081639>. 2019.  
1744  
1745 Lo Monaco, C., Álvarez, M., Key, R. M., Lin, X., Tanhua, T., Tilbrook, B., Bakker, D. C. E., van Heuven, S.,  
1746 Hoppema, M., Metzl, N., Ríos, A. F., Sabine, C. L., and Velo, A.: Assessing the internal consistency of the  
1747 CARINA database in the Indian sector of the Southern Ocean, *Earth Syst. Sci. Data*, 2, 51–70,  
1748 <https://doi.org/10.5194/essd-2-51-2010>, 2010.  
1749  
1750 Lo Monaco, C., Metzl, N., Fin, J., and Tribollet, A.: Sea surface measurements of dissolved inorganic carbon  
1751 (DIC) and total alkalinity (TALK), temperature and salinity during the R/V Marion-Dufresne cruise CLIM-  
1752 EPARSE (EXPOCODE 35MV20190405) in the Indian Ocean and Mozambique Channel from 2019-04-04 to  
1753 2019-04-30. (NCEI Accession 0212218). [indicate subset used]. NOAA National Centers for Environmental  
1754 Information. Dataset. <https://doi.org/10.25921/26rw-w185>. Accessed [date]. 2020.  
1755  
1756 Lo Monaco, C., Metzl, N., Fin, J., Mignon, C., Cuet, P., Douville, E., Gehlen, M., Trang Chau, T.T., and  
1757 Tribollet, A.: Distribution and long-term change of the sea surface carbonate system in the Mozambique Channel  
1758 (1963-2019), *Deep-Sea Research Part II*, <https://doi.org/10.1016/j.dsr2.2021.104936>, 2021  
1759  
1760 Lombard, F., Bourdin, G., Pesant, S., Agostini, S., Baudena, A., Boissin, E., Cassar, N., Clampitt, M., Conan,  
1761 P., Da Silva, O., Dimier, C., Douville, E., Elineau, A., Fin, J., Flores, J.-M., Ghiglione, J.-F., Hume, B. C. C.,  
1762 Jalabert, L., John, S. G., Kelly, R. L., Koren, I., Lin, Y., Marie, D., McMinds, R., Méridet, Z., Metzl, N., Paz-  
1763 García, D. A., Luiza Pedrotti, M., Poulain, J., Pujo-Pay, M., Ras, J., Reverdin, G., Romac, S., Röttinger, E.,  
1764 Vardi, A., Voolstra, C. R., Moulin, C., Iwankow, G., Banaigs, B., Bowler, C., de Vargas, C., Forcioli, D., Furla,  
1765 P., Galand, P. E., Gilson, E., Reynaud, S., Sunagawa, S., Thomas, O., Troublé, R., Vega Thurber, R., Wincker,  
1766 P., Zoccola, D., Allemand, D., Planes, S., Boss, E., and Gorsky, G.: Open science resources from the Tara  
1767 Pacific expedition across the surface ocean and coral reef ecosystems. *Sci Data* 10, 324 (2023).  
1768 <https://doi.org/10.1038/s41597-022-01757-w>, 2022.  
1769  
1770 Ma, D., Gregor, L., and Gruber, N.: Four decades of trends and drivers of global surface ocean acidification.  
1771 *Global Biogeochemical Cycles*, 37, e2023GB007765. [10.1029/2023GB007765](https://doi.org/10.1029/2023GB007765), 2023.  
1772  
1773 Maier, C., Watremez, P., Taviani, M., Weinbauer, M. G., and Gattuso, J.-P.: Calcification rates and the effect of  
1774 ocean acidification on Mediterranean cold-water corals. *Proceedings of the Royal Society B-Biological Sciences*,  
1775 279(1734), 1716-1723, [doi:10.1098/rspb.2011.1763](https://doi.org/10.1098/rspb.2011.1763). 2012.  
1776  
1777 Margirier, F., Testor, P., Heslop, E. et al. : Abrupt warming and salinification of intermediate waters interplays  
1778 with decline of deep convection in the Northwestern Mediterranean Sea. *Sci Rep* 10, 20923. [10.1038/s41598-020-77859-5](https://doi.org/10.1038/s41598-020-77859-5), 2020.  
1779  
1780  
1781 Marrec, P., Cariou, T., Collin, E., Durand, A., Latimier, M., Macé, E., Morin, P., Raimund, S., Vernet, M., and  
1782 Bozec, Y.: Seasonal and latitudinal variability of the CO<sub>2</sub> system in the western English Channel based on  
1783 Voluntary Observing Ship (VOS) measurements. *Marine Chemistry*, 155 (2013): 29–41. 2013.  
1784  
1785 Marrec, P., Cariou, T., Latimier, M., Macé, E., Morin, P., Vernet, M., and Bozec, Y.: Spatio-temporal dynamics  
1786 of biogeochemical processes and air–sea CO<sub>2</sub> fluxes in the Western English Channel based on two years of  
1787 FerryBox deployment. *Journal of Marine Systems*, Special Issue: 5<sup>th</sup> FerryBox Workshop.  
1788 [10.1016/j.jmarsys.2014.05.010](https://doi.org/10.1016/j.jmarsys.2014.05.010). 2014.  
1789



- 1790 Marrec, P., Cariou, T., Macé, E., Morin, P., Salt, L. A., Vernet, M., Taylor, B., Paxman, K., and Y. Bozec:  
1791 Dynamics of air–sea CO<sub>2</sub> fluxes in the northwestern European shelf based on voluntary observing ship and  
1792 satellite observations, *Biogeosciences*, 12, 5371–5391, doi:10.5194/bg-12-5371-2015. 2015  
1793  
1794 Marrec, P., and Bozec, Y.: Partial pressure (or fugacity) of carbon dioxide, dissolved inorganic carbon, alkalinity  
1795 and salinity collected from Surface underway observations using Carbon dioxide (CO<sub>2</sub>) gas analyzer and other  
1796 instruments from ARMORIQUE in the English Channel from 2012-04-25 to 2013-01-03 (NCEI Accession  
1797 0157472). Version 1.1. NOAA National Centers for Environmental Information. Dataset. doi:10.3334/CDIAC/OTG.COAST\_FERRYBOX\_ROSCOFF\_PLYMOUTH\_2012 [access date]. 2016a.  
1798  
1799  
1800 Marrec, P., and Bozec, Y.: Partial pressure (or fugacity) of carbon dioxide, dissolved inorganic carbon, alkalinity  
1801 and salinity collected from Surface underway observations using Carbon dioxide (CO<sub>2</sub>) gas analyzer and other  
1802 instruments from ARMORIQUE in the English Channel from 2013-03-15 to 2013-12-22 (NCEI Accession  
1803 0157444). Version 1.1. NOAA National Centers for Environmental Information. Dataset. doi:10.3334/CDIAC/OTG.COAST\_FERRYBOX\_ROSCOFF\_PLYMOUTH\_2013 [access date]. 2016b.  
1804  
1805  
1806 Marrec, P., and Bozec, Y.: Partial pressure (or fugacity) of carbon dioxide, dissolved inorganic carbon, alkalinity  
1807 and salinity collected from surface underway observations using Carbon dioxide (CO<sub>2</sub>) gas analyzer and other  
1808 instruments from ARMORIQUE in the English Channel from 2014-03-18 to 2014-10-09 (NCEI Accession  
1809 0163193). Version 1.1. NOAA National Centers for Environmental Information. Dataset. doi:10.3334/CDIAC/OTG.COAST\_FERRYBOX\_ROSCOFF\_PLYMOUTH\_2014 [access date]. 2017.  
1810  
1811  
1812 Mazloff, M. R., Verdy, A., Gille, S. T., Johnson, K. S., Cornuelle, B. D., and Sarmiento, J.: Southern Ocean  
1813 acidification revealed by biogeochemical-Argo floats. *Journal of Geophysical Research: Oceans*, 128,  
1814 e2022JC019530. <https://doi.org/10.1029/2022JC019530>, 2023.  
1815  
1816 McCulloch, M., Trotter, J., Montagna, P., Falter, J., Dunbar, R., Freiwald, A., Försterra, G., López Correa, M.,  
1817 Maier, C., Rüggeberg, A., and Taviani, M.: Resilience of cold-water scleractinian corals to ocean acidification:  
1818 Boron isotopic systematics of pH and saturation state up-regulation. *Geochimica et Cosmochimica Acta*, Volume  
1819 87, 21–34. <http://dx.doi.org/10.1016/j.gca.2012.03.027>. 2012  
1820  
1821 McKinley, G. A., Fay, A. R., Takahashi, T., and Metzl, N.: Convergence of atmospheric and North Atlantic  
1822 carbon dioxide trends on multidecadal timescales. *Nature Geoscience*. doi:10.1038/NGEO1193. 2011.  
1823  
1824 McKinley, G. A., Ritzer, A. L. and Lovenduski, N. S.: Mechanisms of northern North Atlantic biomass  
1825 variability, *Biogeosciences*, 15(20), 6049–6066, doi:<https://doi.org/10.5194/bg-15-6049-2018>, 2018.  
1826  
1827 Meier, K. J. S., Beaufort, L., Heussner, S., and Ziveri, P.: The role of ocean acidification in *Emiliania huxleyi*  
1828 coccolith thinning in the Mediterranean Sea, *Biogeosciences*, 11, 2857–2869, [https://doi.org/10.5194/bg-11-](https://doi.org/10.5194/bg-11-2857-2014)  
1829 2857-2014, 2014.  
1830  
1831 Mercier, H., Lherminier, P., Sarafanov, A., Gaillard, F., Daniault, N., Desbruyères, D., Falina, A., Ferron, B.,  
1832 Huck, T., and Thierry, V.: Variability of the meridional overturning circulation at the Greenland-Portugal Ovide  
1833 section from 1993 to 2010. *Progress in Oceanography*, 132, 250–261, doi:10.1016/j.pocean.2013.11.001. 2015  
1834  
1835 Merlivat, L., Boutin, J., Antoine, D., Beaumont, L., Golbol, M., and Vellucci, V.: Increase of dissolved inorganic  
1836 carbon and decrease in pH in near-surface waters in the Mediterranean Sea during the past two decades,  
1837 *Biogeosciences*, 15, 5653–5662, <https://doi.org/10.5194/bg-15-5653-2018>, 2018.  
1838  
1839 Metzl, N., Brunet, C., Jabaud-Jan, A., Poisson, A., and Schauer, B.: Summer and winter air–sea CO<sub>2</sub> fluxes in  
1840 the Southern Ocean *Deep Sea Res I*, 53, 1548–1563, doi:10.1016/j.dsr.2006.07.006. 2006.  
1841





- 1842 Metzl, N., Tilbrook, B., Bakker, D., Le Quééré, C., Doney, S., Feely, R., Hood M., and Dargaville, R.: Global  
1843 Changes in Ocean Carbon: Variability and Vulnerability. *Eos, Transactions of the American Geophysical Union*  
1844 88 (28): 286-287. doi: 10.1029/2007EO280005, 2007.
- 1845  
1846 Metzl, N., Corbière, A., Reverdin, G., Lenton, A., Takahashi, T., Olsen, A., Johannessen, T., Pierrot, D.,  
1847 Wanninkhof, R., Ólafsdóttir, S. R., Ólafsson, J., and Ramonet, M.: Recent acceleration of the sea surface fCO<sub>2</sub>  
1848 growth rate in the North Atlantic subpolar gyre (1993-2008) revealed by winter observations, *Global*  
1849 *Biogeochem. Cycles*, 24, GB4004, doi:10.1029/2009GB003658, 2010.
- 1850  
1851 Metzl, N., and Lo Monaco, C.: OISO - OCÉAN INDIEN SERVICE D'OBSERVATION,  
1852 <https://doi.org/10.18142/228>, 1998.
- 1853  
1854 Metzl, N., Pierre, C., and Vangriesheim, A.: Hydrographic and Chemical measurements during the R/V  
1855 L'Atalante BIOZAIRE III Cruise in the Atlantic Ocean (14 December, 2003 - 7 January 2004).  
1856 <http://cdiac.esd.ornl.gov/ftp/oceans/BIOZAIRE3>. Carbon Dioxide Information Analysis Center, Oak Ridge  
1857 National Laboratory, US Department of Energy, Oak Ridge, Tennessee. doi:  
1858 10.3334/CDIAC/OTG.BIOZAIRE3, 2016.
- 1859  
1860 Metzl, N., Ferron, B. Lherminier, P. Sarthou, G. Thierry, V.: Discrete profile measurements of dissolved  
1861 inorganic carbon (DIC), total alkalinity (TALK), temperature and salinity during the multiple ships Observatoire  
1862 de la variabilité interannuelle et décennale en Atlantique Nord (OVIDE) project, OVIDE-2006, OVIDE-2008,  
1863 OVIDE-2010, OVIDE-2012, OVIDE-2014 cruises in the North Atlantic Ocean from 2006-05-23 to 2014-06-30  
1864 (NCEI Accession 0177219). Version 1.1. NOAA National Centers for Environmental Information. Dataset.  
1865 doi:10.25921/v0qt-ms48 [access date], 2018.
- 1866  
1867 Metzl, N., Fin, J., Lo Monaco, C., et al.: SNAPO-CO<sub>2</sub> data-set: A synthesis of total alkalinity and total dissolved  
1868 inorganic carbon observations in the global ocean (1993-2022). *SEANOE*. <https://doi.org/10.17882/95414>, 2023.
- 1869  
1870 Mignot, A., Claustre, H., Cossarini, G., D'Ortenzio, F., Gutknecht, E., Lamouroux, J., Lazzari, P., Perruche, C.,  
1871 Salon, S., Sauzède, R., Taillandier, V., and Teruzzi, A.: Using machine learning and Biogeochemical-Argo  
1872 (BGC-Argo) floats to assess biogeochemical models and optimize observing system design, *Biogeosciences*, 20,  
1873 1405–1422, <https://doi.org/10.5194/bg-20-1405-2023>, 2023.
- 1874  
1875 Millero, F. J., Lee, K. and Roche, M.: Distribution of alkalinity in the surface waters of the major oceans. *Mar.*  
1876 *Chem.* **60**, 111–130. [https://doi.org/10.1016/S0304-4203\(97\)00084-4](https://doi.org/10.1016/S0304-4203(97)00084-4), 1998.
- 1877  
1878 Mongwe, N. P., Vichi, M., and Monteiro, P. M. S: The seasonal cycle of pCO<sub>2</sub> and CO<sub>2</sub> fluxes in the Southern  
1879 Ocean: Diagnosing anomalies in CMIP5 earth system models. *Biogeosciences*, 15(9), 2851–2872.  
1880 <https://doi.org/10.5194/bg-15-2851-2018>, 2018.
- 1881  
1882 Mortier, L., Ait Ameer, N., and Taillandier, V.: SOMBA-GE-2014 cruise, RV Téthys II,  
1883 <https://doi.org/10.17600/14007500>, 2014.
- 1884  
1885 Moutin, T., and Bonnet, S.: OUTPACE cruise, RV L'Atalante, <https://doi.org/10.17600/15000900>, 2015.
- 1886  
1887 Moutin, T., Wagener, T., Caffin, M., Fumenia, A., Gimenez, A., Baklouti, M., Bouruet-Aubertot, P., Pujo-Pay,  
1888 M., Leblanc, K., Lefevre, D., Helias Nunige, S., Leblond, N., Grosso, O., and de Verneil, A.: Nutrient  
1889 availability and the ultimate control of the biological carbon pump in the western tropical South Pacific Ocean,  
1890 *Biogeosciences*, 15, 2961-2989, <https://doi.org/10.5194/bg-15-2961-2018>, 2018.
- 1891  
1892 Newton, J.A., Feely, R. A., Jewett, E. B., Williamson, P. and Mathis, J.: Global Ocean Acidification Observing  
1893 Network: Requirements and Governance Plan. Second Edition, GOA-ON, [http://www.goa-on.org/docs/GOA-ON\\_plan\\_print.pdf](http://www.goa-on.org/docs/GOA-ON_plan_print.pdf), 2015.
- 1894



- 1895 Nykjaer, L.: Mediterranean Sea surface warming 1985–2006. *Clim. Res.* 39, 11–17. doi: 10.3354/cr00794, 2009.
- 1896
- 1897 Obernosterer, I.: MOBYDICK-THEMISTO cruise, RV Marion-Dufresne, <https://doi.org/10.17600/18000403>,
- 1898 2018.
- 1899
- 1900 OCADS: Coastal Carbon Data, [https://www.ncei.noaa.gov/access/ocean-carbon-acidification-data-](https://www.ncei.noaa.gov/access/ocean-carbon-acidification-data-system/oceans/coastal_carbon_data.html)
- 1901 [system/oceans/coastal\\_carbon\\_data.html](https://www.ncei.noaa.gov/access/ocean-carbon-acidification-data-system/oceans/coastal_carbon_data.html), 2023
- 1902
- 1903 Olafsson, J., Olafsdottir, S.R., Benoit-Cattin, A., Danielsen, M., Arnarson, T.S., and Takahashi, T.: Rate of
- 1904 Iceland Sea acidification from time series measurements. *Biogeosciences* 6, 2661–2668.
- 1905 <https://doi.org/10.5194/bg-6-2661-2009>, 2009.
- 1906
- 1907 Olivier, L., Boutin, J., Reverdin, G., Lefèvre, N., Landschützer, P., Speich, S., Karstensen, J., Labaste, M.,
- 1908 Noisel, C., Ritschel, M., Steinhoff, T., and Wanninkhof, R.: Wintertime process study of the North Brazil
- 1909 Current rings reveals the region as a larger sink for CO<sub>2</sub> than expected, *Biogeosciences*, 19, 2969–2988,
- 1910 <https://doi.org/10.5194/bg-19-2969-2022>, 2022.
- 1911
- 1912 Olsen, A., Key, R. M., van Heuven, S., Lauvset, S. K., Velo, A., Lin, X., Schirnick, C., Kozyr, A., Tanhua, T.,
- 1913 Hoppema, M., Jutterström, S., Steinfeldt, R., Jeansson, E., Ishii, M., Pérez, F. F., and Suzuki, T.: The Global
- 1914 Ocean Data Analysis Project version 2 (GLODAPv2) – an internally consistent data product for the world ocean,
- 1915 *Earth Syst. Sci. Data*, 8, 297–323, <https://doi.org/10.5194/essd-8-297-2016>, 2016.
- 1916
- 1917 Olsen, A., Lange, N., Key, R. M., Tanhua, T., Álvarez, M., Becker, S., Bittig, H. C., Carter, B. R., Cotrim da
- 1918 Cunha, L., Feely, R. A., van Heuven, S., Hoppema, M., Ishii, M., Jeansson, E., Jones, S. D., Jutterström, S.,
- 1919 Karlsen, M. K., Kozyr, A., Lauvset, S. K., Lo Monaco, C., Murata, A., Pérez, F. F., Pfeil, B., Schirnick, C.,
- 1920 Steinfeldt, R., Suzuki, T., Telszewski, M., Tilbrook, B., Velo, A., and Wanninkhof, R.: GLODAPv2.2019 – an
- 1921 update of GLODAPv2, *Earth Syst. Sci. Data*, 11, 1437–1461, <https://doi.org/10.5194/essd-11-1437-2019>, 2019.
- 1922
- 1923 Olsen, A., Lange, N., Key, R. M., Tanhua, T., Bittig, H. C., Kozyr, A., Álvarez, M., Azetsu-Scott, K., Becker, S.,
- 1924 Brown, P. J., Carter, B. R., Cotrim da Cunha, L., Feely, R. A., van Heuven, S., Hoppema, M., Ishii, M.,
- 1925 Jeansson, E., Jutterström, S., Landa, C. S., Lauvset, S. K., Michaelis, P., Murata, A., Pérez, F. F., Pfeil, B.,
- 1926 Schirnick, C., Steinfeldt, R., Suzuki, T., Tilbrook, B., Velo, A., Wanninkhof, R., and Woosley, R. J.: An updated
- 1927 version of the global interior ocean biogeochemical data product, GLODAPv2.2020, *Earth Syst. Sci. Data*, 12,
- 1928 3653–3678, <https://doi.org/10.5194/essd-12-3653-2020>, 2020.
- 1929
- 1930 Orr, J. C., Epitalon, J.-M., and Gattuso, J.-P.: Comparison of ten packages that compute ocean carbonate
- 1931 chemistry, *Biogeosciences*, 12(5), 1483–1510, doi:10.5194/bg-12-1483-2015, 2015.
- 1932
- 1933 Parard, G., Lefèvre, N., and Boutin, J.: Sea water fugacity of CO<sub>2</sub> at the PIRATA mooring at 6°S, 10°W. *Tellus-*
- 1934 *B*, DOI: 10.1111/j.1600-0889.2010.00503.x. 2010.
- 1935
- 1936 Pérez F. F., Vázquez-Rodríguez, M., Mercier, H., Velo, A., Lherminier, P. and Ríos, A. F.: Trends of
- 1937 anthropogenic CO<sub>2</sub> storage in North Atlantic water masses. *Biogeosciences*, 7, 1789–1807, doi:10.5194/bg-7-
- 1938 [1789-2010](https://doi.org/10.5194/bg-7-1789-2010), 2010.
- 1939
- 1940 Pérez, F. F., Mercier, H., Vazquez-Rodriguez, M., Lherminier, P., Velo, A., Pardo, P., Roson, G., and Rios, A.:
- 1941 Reconciling air-sea CO<sub>2</sub> fluxes and anthropogenic CO<sub>2</sub> budgets in a changing North Atlantic. *Nature*
- 1942 *Geosciences*, 6, 146–152, doi:10.1038/ngeo1680, 2013.
- 1943
- 1944 Pérez, F., Fontela, M., García-Ibáñez, M. et al. : Meridional overturning circulation conveys fast acidification to
- 1945 the deep Atlantic Ocean. *Nature* 554, 515–518. Doi: 10.1038/nature25493, 2018.
- 1946
- 1947 Pesant, S., Not, F., Picheral, M., Kandels-Lewis, S., Le Bescot, N., Gorsky, G., Iudicone, D., Karsenti, E.,
- 1948 Speich, S., Troublé, R., Dimier, C., Searson, S., and Tara Oceans Consortium Coordinators: Open science



- 1949 resources for the discovery and analysis of Tara Oceans data. *Scientific Data* 2:150023. doi:  
1950 10.1038/sdata.2015.23, 2015.  
1951  
1952 Petrenko, A.: LATEX10 cruise, RV Téthys II, <https://doi.org/10.17600/10450150>, 2010.  
1953  
1954 Petrenko, A.A., Doglioli, A.M., Nencioli, F., Kersalé, M., Hu, Z., and d'Ovidio, F.: A review of the LATEX  
1955 project: mesoscale to submesoscale processes in a coastal environment. *Ocean Dynam.*, doi: 10.1007/s10236-  
1956 017-1040-9, 2017.  
1957  
1958 Petton, S., Pouvreau, S., and Fleury, E.: ECOSCOPA network : high frequency environmental database.  
1959 SEANOE. <https://doi.org/10.17882/86131>, 2023.  
1960  
1961 Pfeil, B., Olsen, A., Bakker, D. C. E., Hankin, S., Koyuk, H., Kozyr, A., Malczyk, J., Manke, A., Metzl, N.,  
1962 Sabine, C. L., Akl, J., Alin, S. R., Bates, N., Bellerby, R. G. J., Borges, A., Boutin, J., Brown, P. J., Cai, W.-J.,  
1963 Chavez, F. P., Chen, A., Cosca, C., Fassbender, A. J., Feely, R. A., González-Dávila, M., Goyet, C., Hales,  
1964 B., Hardman-Mountford, N., Heinze, C., Hood, M., Hoppema, M., Hunt, C. W., Hydes, D., Ishii, M.,  
1965 Johannessen, T., Jones, S. D., Key, R. M., Körtzinger, A., Landschützer, P., Lauvset, S. K., Lefèvre, N.,  
1966 Lenton, A., Laurantou, A., Merlivat, L., Midorikawa, T., Mintrop, L., Miyazaki, C., Murata, A., Nakadate, A.,  
1967 Nakano, Y., Nakaoka, S., Nojiri, Y., Omar, A. M., Padin, X. A., Park, G.-H., Paterson, K., Perez, F. F., Pierrot,  
1968 D., Poisson, A., Ríos, A. F., Santana-Casiano, J. M., Salisbury, J., Sarma, V. V. S. S., Schlitzer, R.,  
1969 Schneider, B., Schuster, U., Sieger, R., Skjelvan, I., Steinhoff, T., Suzuki, T., Takahashi, T., Tedesco, K.,  
1970 Telszewski, M., Thomas, H., Tilbrook, B., Tjiputra, J., Vandemark, D., Veness, T., Wanninkhof, R., Watson,  
1971 A. J., Weiss, R., Wong, C. S., and Yoshikawa-Inoue, H.: A uniform, quality controlled Surface Ocean CO<sub>2</sub>  
1972 Atlas (SOCAT), *Earth Syst. Sci. Data*, 5, 125-143, doi:10.5194/essd-5-125-2013, 2013.  
1973  
1974 Picheral, M., Searson, S., Taillandier, V., Bricaud, A., Boss, E., Ras, J., Claustre, H., Ouhssain, M., Morin, P.,  
1975 Coppola, L., Gattuso, J.-P., Metzl, N., Thuillier, D., Gorsky, G., Tara Oceans Consortium, Coordinators; Tara  
1976 Oceans Expedition, Participants: Vertical profiles of environmental parameters measured on discrete water  
1977 samples collected with Niskin bottles during the Tara Oceans expedition 2009-2013.  
1978 doi:10.1594/PANGAEA.836319, 2014.  
1979  
1980 Pilcher, D. J., Brody, S. R., Johnson, L., and Bronselaer, B.: Assessing the abilities of CMIP5 models to  
1981 represent the seasonal cycle of surface ocean pCO<sub>2</sub>, *J. Geophys. Res. Oceans*, 120, 4625–4637,  
1982 doi:10.1002/2015JC010759, 2015.  
1983  
1984 Poisson, A., Culkin, F., and Ridout, P.: Intercomparison of CO<sub>2</sub> measurements. *Deep Sea Research Part A.*  
1985 *Oceanographic Research Papers*, 37, 10, 1647-1650, [https://doi.org/10.1016/0198-0149\(90\)90067-6](https://doi.org/10.1016/0198-0149(90)90067-6), 1990.  
1986  
1987 Pujo-Pay, M., Durrieu de Madron, X., and Conan, P.: PERLE3 cruise, RV Pourquoi pas ?,  
1988 <https://doi.org/10.17600/18001342>, 2020.  
1989  
1990 Pujo-Pay, M., Durrieu de Madron, X., and Conan, P.: PERLE4 cruise, RV L'Atalante,  
1991 <https://doi.org/10.17600/18001980>, 2021.  
1992  
1993 Rabouille C.: AMOR-BFLUX cruise, RV Téthys II, <https://doi.org/10.17600/15008700>, 2015.  
1994  
1995 Racapé, V., Metzl, N., Pierre, C., Reverdin, G., Quay, P.D., and Olafsdottir, S. R.: The seasonal cycle of the  
1996 d13C<sub>DIC</sub> in the North Atlantic Subpolar Gyre. *Biogeosciences*, 11, 6, 1683-1692, doi:10.5194/bg-11-1683-2014,  
1997 2014.  
1998  
1999 Revelle, R., and Suess, H. E.: Carbon dioxide exchange between atmosphere and ocean and the question of an  
2000 increase of atmospheric CO<sub>2</sub> during the past decades. *Tellus* 9, 18–27. doi:10.1111/j.2153-  
2001 3490.1957.tb01849.x., 1957.  
2002



- 2003 Reverdin, G.: STRASSE cruise, RV Thalassa, <https://doi.org/10.17600/12040060>, 2012.
- 2004
- 2005 Reverdin, G., Metzl, N., Olafsdottir, S., Racapé, V., Takahashi, T., Benetti, M., Valdimarsson, H., Benoit-Cattin,
- 2006 A., Danielsen, M., Fin, J., Naamar, A., Pierrot, D., Sullivan, K., Bringas, F., and Goni, G.: SURATLANT: a
- 2007 1993–2017 surface sampling in the central part of the North Atlantic subpolar gyre, *Earth Syst. Sci. Data*, 10,
- 2008 1901-1924, <https://doi.org/10.5194/essd-10-1901-2018>, 2018.
- 2009
- 2010 Reverdin, G., Metzl, N., Olafsdottir, S., Racapé, V., Takahashi, T., Benetti, M., Valdimarsson, H., Quay, P. D.,
- 2011 Benoit-Cattin, A., Danielsen, M., Fin, J., Naamar, A., Pierrot, D., Sullivan, K., Bringas, F., and Goni, G.:
- 2012 SURATLANT: a surface dataset in the central part of the North Atlantic subpolar gyre. *SEANOE*.
- 2013 <https://doi.org/10.17882/54517>, 2022.
- 2014
- 2015 Ridame, C., Dekaezemacker, J., Guieu, C., Bonnet, S., L'Helguen, S., and Malien, F.: Contrasted Saharan dust
- 2016 events in LNLC environments: impact on nutrient dynamics and primary production, *Biogeosciences*, 11, 4783–
- 2017 4800, <https://doi.org/10.5194/bg-11-4783-2014>, 2014.
- 2018
- 2019 Robertson, J. E., Robinson, C., Turner, D. R., Holligan, P., Watson, A. J., Boyd, P., Fernandez, E., and Finch,
- 2020 M.: The impact of a coccolithophore bloom on oceanic carbon uptake in the northeast Atlantic during summer
- 2021 1991, *Deep Sea Res., Part I*, 41(2), 297–314, 1994.
- 2022
- 2023 Rödenbeck, C., Keeling, R. F., Bakker, D. C. E., Metzl, N., Olsen, A., Sabine, C., and Heimann, M.: Global
- 2024 surface-ocean pCO<sub>2</sub> and sea–air CO<sub>2</sub> flux variability from an observation-driven ocean mixed-layer scheme,
- 2025 *Ocean Sci.*, 9, 193–216, <https://doi.org/10.5194/os-9-193-2013>, 2013.
- 2026
- 2027 Rödenbeck, C., Bakker, D. C. E., Gruber, N., Iida, Y., Jacobson, A.R., Jones, S., Landschützer, P., Metzl, N.,
- 2028 Nakaoka, S., Olsen, A., Park, G.-H., Peylin, P., Rodgers, K. B., Sasse, T. P., Schuster, U., Shutler, J. D., Valsala,
- 2029 V., Wanninkhof, R., Zeng, J. Data-based estimates of the ocean carbon sink variability – First results of the
- 2030 Surface Ocean pCO<sub>2</sub> Mapping intercomparison (SOCOM). *Biogeosciences* 12: 7251-7278. doi:10.5194/bg-12-
- 2031 7251-2015, 2015.
- 2032
- 2033 Sabine, C. L., Feely, R. A., Gruber, N., Key, R. M., Lee, K., Bullister, J. L., Wanninkhof, R., Wong, C. S.,
- 2034 Wallace, D. W. R., Tilbrook, B., Millero, F. J., Peng, T.-H., Kozyr, A., Ono, T., and Rios, A. F.: The Oceanic
- 2035 Sink for Anthropogenic CO<sub>2</sub>, *Science*, 305, 367-371, <https://doi.org/10.1126/science.1097403>, 2004.
- 2036
- 2037 Sabine, C. L., Hankin, S., Koyuk, H., Bakker, D. C. E., Pfeil, B., Olsen, A., Metzl, N., Kozyr, A., Fassbender,
- 2038 A., Manke, A., Malczyk, J., Akl, J., Alin, S. R., Bellerby, R. G. J., Borges, A., Boutin, J., Brown, P. J., Cai, W.-
- 2039 J., Chavez, F. P., Chen, A., Cosca, C., Feely, R.A., González-Dávila, M., Goyet, C., Hardman-Mountford, N.,
- 2040 Heinze, C., Hoppema, M., Hunt, C. W., Hydes, D., Ishii, M., Johannessen, T., Key, R. M., Körtzinger, A.,
- 2041 Landschützer, P., Lauvset, S. K., Lefèvre, N., Lenton, A., Lourantou, A., Merlivat, L., Midorikawa, T.,
- 2042 Mintrop, L., Miyazaki, C., Murata, A., Nakadate, A., Nakano, Y., Nakaoka, S., Nojiri, Y., Omar, A. M., Padin,
- 2043 X. A., Park, G.-H., Paterson, K., Perez, F. F., Pierrot, D., Poisson, A., Ríos, A. F., Salisbury, J., Santana-
- 2044 Casiano, J. M., Sarma, V. V. S. S., Schlitzer, R., Schneider, B., Schuster, U., Sieger, R., Skjelvan, I., Steinhoff,
- 2045 T., Suzuki, T., Takahashi, T., Tedesco, K., Telszewski, M., Thomas, H., Tilbrook, B., Vandemark, D., Veness,
- 2046 T., Watson, A. J., Weiss, R., Wong, C. S., and Yoshikawa-Inoue, H.: Surface Ocean CO<sub>2</sub> Atlas (SOCAT)
- 2047 gridded data products, *Earth Syst. Sci. Data*, 5, 145-153, doi:10.5194/essd-5-145-2013, 2013.
- 2048
- 2049 Salt, L. A., Beaumont, L., Blain, S., Bucciarelli, E., Grosstefan, E., Guillot, A., L'Helguen, S., Merlivat, L.,
- 2050 Répécaud, M., Quémener, L., Rimmelin-Maury, P., Tréguer, P., and Bozec, Y.: The annual and seasonal
- 2051 variability of the carbonate system in the Bay of Brest (Northwest Atlantic Shelf, 2008–2014). *Marine*
- 2052 *Chemistry*, doi:10.1016/j.marchem.2016.09.003. 2016.
- 2053
- 2054 Sasse, T. P., McNeil, B. I., and Abramowitz, G.: A novel method for diagnosing seasonal to inter-annual surface
- 2055 ocean carbon dynamics from bottle data using neural networks, *Biogeosciences*, 10, 4319–4340,
- 2056 <https://doi.org/10.5194/bg-10-4319-2013>, 2013.



- 2057  
2058 Sauzède, R., Claustre, H., Pasqueron de Fommervault, O., Bittig, H., Gattuso, J.-P., Legendre, L. and Johnson,  
2059 K. S.: Estimates of water-column nutrients and carbonate system parameters in the global ocean: A novel  
2060 approach based on neural networks. *Front. Mar. Sci.* 4:128. doi:10.3389/fmars.2017.00128, 2017.  
2061  
2062 Seelmann, K., Steinhoff, T., Aßmann, S., and Körtzinger, A.: Enhance Ocean Carbon Observations: Successful  
2063 Implementation of a Novel Autonomous Total Alkalinity Analyzer on a Ship of Opportunity. *Front. Mar. Sci.*  
2064 7:571301. doi: 10.3389/fmars.2020.571301, 2020.  
2065  
2066 Schlitzer, R.: Ocean Data View, Ocean Data View, <http://odv.awi.de> (last access: 13 March 2019), 2018.  
2067  
2068 Schneider, A., Wallace, D. W. R., and Körtzinger, A.: Alkalinity of the Mediterranean Sea, *Geophys. Res. Lett.*,  
2069 34, L15608, doi:10.1029/2006GL028842, 2007.  
2070  
2071 Schuster, U., Watson, A.J., Bates, N., Corbière, A., Gonzalez-Davila, M., Metzl, N., Pierrot, D. and Santana-  
2072 Casiano, M.: Trends in North Atlantic sea surface pCO<sub>2</sub> from 1990 to 2006. *Deep-Sea Res II*,  
2073 doi:10.1016/j.dsr2.2008.12.011, 2009.  
2074  
2075 Schuster, U., McKinley, G. A., Bates, N., Chevallier, F., Doney, S. C., Fay, A. R., González-Dávila, M., Gruber,  
2076 N., Jones, S., Krijnen, J., Landschützer, P., Lefèvre, N., Manizza, M., Mathis, J., Metzl, N., Olsen, A., Rios, A.  
2077 F., Rödenbeck, C., Santana-Casiano, J. M., Takahashi, T., Wanninkhof, R., and Watson, A. J.: An assessment of  
2078 the Atlantic and Arctic sea-air CO<sub>2</sub> fluxes, 1990–2009, *Biogeosciences*, 10, 607–627,  
2079 <https://doi.org/10.5194/bg-10-607-2013>, 2013.  
2080  
2081 Sims, R. P., Holding, T. M., Land, P. E., Piolle, J.-F., Green, H. L., and Shutler, J. D.: OceanSODA-UNEXE: a  
2082 multi-year gridded Amazon and Congo River outflow surface ocean carbonate system dataset, *Earth Syst. Sci.*  
2083 *Data*, 15, 2499–2516, <https://doi.org/10.5194/essd-15-2499-2023>, 2023.  
2084  
2085 Skjelvan, I., Lauvset, S.K., Johannessen, T., et al.: Decadal trends in Ocean Acidification from the Ocean  
2086 Weather Station M in the Norwegian Sea, *Journal of Marine Systems*,  
2087 <https://doi.org/10.1016/j.jmarsys.2022.103775>, 2022.  
2088  
2089 Speich, S., and The Embarked Science Team: EUREC4A-OA. Cruise Report. 19 January – 19 February 2020.  
2090 Vessel: L'ATALANTE. <https://doi.org/10.13155/80129>, 2021  
2091  
2092 Takahashi, T., Sutherland, S. C., Sweeney, C., Poisson, A., Metzl, N., Tilbrook, B., Bates, N., Wanninkhof, R.,  
2093 Feely, R. A., Sabine, C., Olafsson, J., and Nojiri, Y.: Global Sea-Air CO<sub>2</sub> Flux Based on Climatological Surface  
2094 Ocean pCO<sub>2</sub>, and Seasonal Biological and Temperature Effect. *Deep-Sea Res. II*, 49, 9-10, 1601-1622,  
2095 [https://doi.org/10.1016/S0967-0645\(02\)00003-6](https://doi.org/10.1016/S0967-0645(02)00003-6). 2002  
2096  
2097 Takahashi, T., Sutherland, S. C., Wanninkhof, R., Sweeney, C., Feely, R. A., Chipman, D. W., Hales, B.,  
2098 Friederich, G., Chavez, F., Sabine, C., Watson, A. J., Bakker, D. C., Schuster, U., Metzl, N., Yoshikawa-Inoue,  
2099 H., Ishii, M., Midorikawa, T., Nojiri, Y., Körtzinger, A., Steinhoff, T., Hoppema, M., Olafsson, J., Arnarson, T.  
2100 S., Tilbrook, B., Johannessen, T., Olsen, A., Bellerby, R., Wong, C., Delille, B., Bates, N., and de Baar, H. J.:  
2101 Climatological mean and decadal change in surface ocean pCO<sub>2</sub>, and net sea air CO<sub>2</sub> flux over the global  
2102 oceans. *Deep-Sea Res. II*, 56 (8-10), 554–577, <http://dx.doi.org/10.1016/j.dsr2.2008.12.009>. 2009.  
2103  
2104 Takahashi, T., Sutherland, S. C., Chipman, D. W., Goddard, J. G., Ho, C., Newberger, T., Sweeney, C. and  
2105 Munro, D. R.: Climatological distributions of pH, pCO<sub>2</sub>, total CO<sub>2</sub>, alkalinity, and CaCO<sub>3</sub> saturation in the  
2106 global surface ocean, and temporal changes at selected locations. *Marine Chemistry*, 164, 95–125,  
2107 doi:10.1016/j.marchem.2014.06.004. 2014.  
2108  
2109 Tanhua, T., Pouliquen, S., Hausman, J., O'Brien, K., Bricher, P., de Bruin, T., Buck, J. J. H., Burger, E. F.,  
2110 Carval, T., Casey, K. S., Diggs, S., Giorgetti, A., Glaves, H., Harscoat, V., Kinkade, D., Muelbert, J. H.,



- 2111 Novellino, A., Pfeil, B., Pulsifer, P. L., Van de Putte, A., Robinson, E., Schaap, D., Smirnov, A., Smith, N.,  
2112 Snowden, D., Spears, T., Stall, S., Tacoma, M., Thijsse, P., Tronstad, S., Vandenberghe, T., Wengren, M.,  
2113 Wyborn, L. and Zhao, Z.: Ocean FAIR Data Services. *Front. Mar. Sci.* 6:440. doi: 10.3389/fmars.2019.00440,  
2114 2019.  
2115  
2116 Tanhua, T., Lauvset, S.K., Lange, N. et al.: A vision for FAIR ocean data products. *Commun Earth Environ* 2,  
2117 136. <https://doi.org/10.1038/s43247-021-00209-4>, 2021  
2118  
2119 Testor, P., Bosse, A., and Coppola, L.: MOOSE-GE, <https://doi.org/10.18142/235>, 2010.  
2120  
2121 Testor, P.: DEWEX-MERMEX 2013 LEG1 cruise, RV Le Suroît, <https://doi.org/10.17600/13020010>, 2013.  
2122  
2123 Tilbrook, B., Jewett, E. B., DeGrandpre, M. D., Hernandez-Ayon, J. M., Feely, R. A., Gledhill, D. K., Hansson,  
2124 L., Isensee, K., Kurz, M. L., Newton, J. A., Siedlecki, S. A., Chai, F., Dupont, S., Graco, M., Calvo, E., Greeley,  
2125 D., Kapsenberg, L., Lebrech, M., Pelejero, C., Schoo, K. L., and Telszewski, M.: An Enhanced Ocean  
2126 Acidification Observing Network: From People to Technology to Data Synthesis and Information Exchange.  
2127 *Frontiers in Marine Science*, 6, 337, DOI:10.3389/fmars.2019.00337, 2019.  
2128  
2129 Touratier, F., Azouzi, L. and Goyet, C.: CFC-11,  $\Delta 14C$  and 3H tracers as a means to assess anthropogenic CO<sub>2</sub>  
2130 concentrations in the ocean. *Tellus B*, 59(2), 318–325, doi:10.1111/j.1600-0889.2006.00247.x, 2007.  
2131  
2132 Touratier, F., and Goyet, C.: Decadal evolution of anthropogenic CO<sub>2</sub> in the north western Mediterranean Sea  
2133 from the mid-1990's to the mid-2000's. *Deep Sea Research Part I*.doi:10.1016/j.dsr.2009.05.015, 2009.  
2134  
2135 Touratier, F., Goyet, C., Houpert, L., Durrieu de Madron, X., Lefèvre, D., Stabholz, M., and Guglielmi, V.: Role  
2136 of deep convection on anthropogenic CO<sub>2</sub> sequestration in the Gulf of Lions (northwestern Mediterranean Sea).  
2137 *Deep-Sea Research Part I*. doi.org/10.1016/j.dsr.2016.04.003, 2016.  
2138  
2139 Turk, D., Dowd, M., Lauvset, S. K., Koelling, J., Alonso-Pérez, F. and Pérez, F. F.: Can Empirical Algorithms  
2140 Successfully Estimate Aragonite Saturation State in the Subpolar North Atlantic? *Front. Mar. Sci.* 4:385. doi:  
2141 10.3389/fmars.2017.00385, 2017.  
2142  
2143 Ulses, C., Estournel, C., Marsaleix, P., Soetaert, K., Fourier, M., Coppola, L., Lefèvre, D., Touratier, F., Goyet,  
2144 C., Guglielmi, V., Kessouri, F., Testor, P., and Durrieu de Madron, X.: Seasonal dynamics and annual budget of  
2145 dissolved inorganic carbon in the northwestern Mediterranean deep convection region, *Biogeosciences Discuss.*  
2146 [preprint], <https://doi.org/10.5194/bg-2022-219>, in review, 2022.  
2147  
2148 UNESCO: Intercomparison of total alkalinity and total inorganic carbon determinations in seawater. UNESCO  
2149 Tech. Pap. Mar. Sci. 59., 1990  
2150  
2151 UNESCO: Reference materials for oceanic carbon dioxide measurements. UNESCO Tech. Pap. Mar. Sci. 60.,  
2152 1991  
2153  
2154 United Nations. The Sustainable Development Goals 2020, 68pp. <https://unstats.un.org/sdgs/report/2020/>, 2020  
2155  
2156 Vangriesheim A., Pierre, C., Aminot, A., Metzl, N., Baurand, F., and Caprais, J.-C.: The influence of Congo  
2157 river discharges in the surface and deep layers of the Gulf of Guinea. *Deep-Sea Res. II*, doi:  
2158 10.1016/j.dsr2.2009.04.002, 2009.  
2159  
2160 Vazquez-Rodriguez, M., Perez, F., Velo, A., Rios, A., and Mercier, H.: Observed acidification trends in the  
2161 North Atlantic water masses. *Biogeosciences*, 9, 5217-5230, doi:10.5194/bg-9-5217-2012, 2012.  
2162  
2163 Velo, A., Perez, F. F., Brown, P., Tanhua, T., Schuster, U., and Key, R. M.: CARINA alkalinity data in the  
2164 Atlantic Ocean, *Earth Syst. Sci. Data*, 1, 45–61, <https://doi.org/10.5194/essd-1-45-2009>, 2009.



- 2165  
2166 von Schuckmann, K., Cheng, L., Palmer, M. D., Hansen, J., Tassone, C., Aich, V., Adusumilli, S., Beltrami, H.,  
2167 Boyer, T., Cuesta-Valero, F. J., Desbruyères, D., Domingues, C., García-García, A., Gentine, P., Gilson, J.,  
2168 Gorfer, M., Haimberger, L., Ishii, M., Johnson, G. C., Killick, R., King, B. A., Kirchengast, G., Kolodziejczyk,  
2169 N., Lyman, J., Marzeion, B., Mayer, M., Monier, M., Monselesan, D. P., Purkey, S., Roemmich, D., Schweiger,  
2170 A., Seneviratne, S. I., Shepherd, A., Slater, D. A., Steiner, A. K., Straneo, F., Timmermans, M.-L., and Wijffels,  
2171 S. E.: Heat stored in the Earth system: where does the energy go?, *Earth Syst. Sci. Data*, 12, 2013–2041,  
2172 <https://doi.org/10.5194/essd-12-2013-2020>, 2020.  
2173  
2174 von Schuckmann, K., Minière, A., Gues, F., Cuesta-Valero, F. J., Kirchengast, G., Adusumilli, S., Straneo, F.,  
2175 Ablain, M., Allan, R. P., Barker, P. M., Beltrami, H., Blazquez, A., Boyer, T., Cheng, L., Church, J.,  
2176 Desbruyeres, D., Dolman, H., Domingues, C. M., García-García, A., Giglio, D., Gilson, J. E., Gorfer, M.,  
2177 Haimberger, L., Hakuba, M. Z., Hendricks, S., Hosoda, S., Johnson, G. C., Killick, R., King, B., Kolodziejczyk,  
2178 N., Korosov, A., Krinner, G., Kuusela, M., Landerer, F. W., Langer, M., Lavergne, T., Lawrence, I., Li, Y.,  
2179 Lyman, J., Marti, F., Marzeion, B., Mayer, M., MacDougall, A. H., McDougall, T., Monselesan, D. P., Nitzbon,  
2180 J., Otosaka, I., Peng, J., Purkey, S., Roemmich, D., Sato, K., Sato, K., Savita, A., Schweiger, A., Shepherd, A.,  
2181 Seneviratne, S. I., Simons, L., Slater, D. A., Slater, T., Steiner, A. K., Suga, T., Szekely, T., Thiery, W.,  
2182 Timmermans, M.-L., Vanderkelen, I., Wijffels, S. E., Wu, T., and Zemp, M.: Heat stored in the Earth system  
2183 1960–2020: where does the energy go?, *Earth Syst. Sci. Data*, 15, 1675–1709, [https://doi.org/10.5194/essd-15-](https://doi.org/10.5194/essd-15-1675-2023)  
2184 [1675-2023](https://doi.org/10.5194/essd-15-1675-2023), 2023.  
2185  
2186 Wagener, T., Metzl, N., Caffin, M., Fin, J., Helias Nunige, S., Lefevre, D., Lo Monaco, C., Rougier, G., and  
2187 Moutin, T.: Carbonate system distribution, anthropogenic carbon and acidification in the western tropical South  
2188 Pacific (OUTPACE 2015 transect), *Biogeosciences*, 15, 5221–5236, <https://doi.org/10.5194/bg-15-5221-2018>,  
2189 2018a.  
2190  
2191 Wagener, T., Metzl, N., Caffin, M., Fin, J., Helias Nunige, S., Lefevre, D., Lo Monaco, C., Rougier, G., and  
2192 Moutin, T.: Discrete profile measurements of dissolved inorganic carbon (DIC), total alkalinity (TALK),  
2193 temperature, salinity and other parameters during the R/V L'Atalante "Oligotrophy from Ultra-oligoTrophy  
2194 PACific Experiment" (OUTPACE) cruise (EXPCODE 35A320150218) in the South Pacific Ocean from 2015-  
2195 02-18 to 2015-04-03 (NCEI Accession 0177706). Version 1.1. NOAA National Centers for Environmental  
2196 Information. Dataset. doi:10.25921/wbkb-0q19 [access date], 2018b.  
2197  
2198 Walton, D. W. H., and Thomas, J.: Cruise Report - Antarctic Circumnavigation Expedition (ACE) 20th  
2199 December 2016 - 19th March 2017 (1.0). Zenodo. <https://doi.org/10.5281/zenodo.1443511>, 2018.  
2200  
2201 Wanninkhof, R., Park, G.-H., Takahashi, T., Sweeney, C., Feely, R., Nojiri, Y., Gruber, N., Doney, S. C.,  
2202 McKinley, G. A., Lenton, A., Le Quééré, C., Heinze, C., Schwinger, J., Graven, H., and Khatiwala, S.: Global  
2203 ocean carbon uptake: magnitude, variability and trends, *Biogeosciences*, 10, 1983–2000, doi:10.5194/bg-10-  
2204 1983-2013, 2013.  
2205  
2206 Watson, A. J., Schuster, U., Bakker, D. C. E., Bates, N., Corbiere, A., Gonzalez-Davila, M., Freidrich, T.,  
2207 Hauck, J., Heinze, C., Johannessen, T., Koertzinger, A., Metzl, N., Olafsson, J., Olsen, A., Oschlies, A., Padin,  
2208 X., Pfeil, B., Rios, A., Santana-Casiano, M., Steinhoff, T., Telszewski, M., Wallace, D. W. R., and Wanninkhof,  
2209 R.: Tracking the variable North Atlantic sink for atmospheric CO<sub>2</sub>, *Science*, 326, 1391,  
2210 doi:10.1126/science.1177394. 2009.  
2211  
2212 Watson, A. J., Schuster, U., Shutler, J.D. et al.: Revised estimates of ocean-atmosphere CO<sub>2</sub> flux are consistent  
2213 with ocean carbon inventory. *Nat Commun* 11, 4422, <https://doi.org/10.1038/s41467-020-18203-3>, 2020.  
2214  
2215 Williams, N. L., Juranek, L. W., Johnson, K. S., Feely, R. A., Riser, S. C., Talley, L. D., et al.: Empirical  
2216 algorithms to estimate water column pH in the Southern Ocean. *Geophysical Research Letters*, 43, 3415–3422.  
2217 <https://doi.org/10.1002/2016GL068539>, 2016.  
2218



- 2219 Williams, N. L., Juranek, L. W., Feely, R. A., Johnson, K. S., Sarmiento, J. L., Talley, L. D., Dickson,  
2220 A. G., Gray, A. R., Wanninkhof, R., Russell, J. L., Riser, S. C., and Takeshita, Y.: Calculating surface  
2221 ocean pCO<sub>2</sub> from biogeochemical Argo floats equipped with pH: An uncertainty analysis, *Global Biogeochem.*  
2222 *Cycles*, 31, 591–604, doi:10.1002/2016GB005541., 2017.  
2223
- 2224 Williams, N. L., Juranek, L. W., Feely, R. A., Russell, J. L., Johnson, K. S., and Hales, B.: Assessment of the  
2225 carbonate chemistry seasonal cycles in the Southern Ocean from persistent observational platforms. *Journal of*  
2226 *Geophysical Research: Oceans*, 123. <https://doi.org/10.1029/2017JC012917>, 2018.  
2227
- 2228 Wimart-Rousseau, C., Lajaunie-Salla, K., Marrec, P., Wagener, T., Raimbault, P., Lagadec, V., Lafont, M.,  
2229 Garcia, N., Diaz, F., Pinazo, C., Yohia, C., Garcia, F., Xueref-Remy, I., Blanc, P.-E., Armengaud, A., and  
2230 Lefèvre, D.: Temporal variability of the carbonate system and air-sea CO<sub>2</sub> exchanges in a Mediterranean human-  
2231 impacted coastal site. *Estuarine, Coastal and Shelf Science*. <https://doi.org/10.1016/j.ecss.2020.106641>, 2020a.  
2232
- 2233 Wimart-Rousseau, C., Wagener, T., Raimbault, P., Lagadec, V., Lafont, M., Garcia, N., and Lefèvre, D.:  
2234 Oceanic carbonate chemistry measurements from discrete samples collected at the SOLEMIO station (Bay of  
2235 Marseille - North western Mediterranean Sea) between 2016 and 2019. *SEANOE*.  
2236 <https://doi.org/10.17882/72356>, 2020b.  
2237
- 2238 Wimart-Rousseau, C., Wagener, T., Álvarez, M., Moutin, T., Fourier, M., Coppola, L., Niclas-Chirurgien, L.,  
2239 Raimbault, P., D'Ortenzio, F., Durrieu de Madron, X., Taillandier, V., Dumas, F., Conan, P., Pujo-Pay, M. and  
2240 Lefèvre, D.: Seasonal and Interannual Variability of the CO<sub>2</sub> System in the Eastern Mediterranean Sea: A Case  
2241 Study in the North Western Levantine Basin. *Front. Mar. Sci.* 8:649246. doi: 10.3389/fmars.2021.649246, 2021  
2242
- 2243 WMO/GCOS, 2018: <https://gcos.wmo.int/en/global-climate-indicators>, 2018  
2244
- 2245 Wu, Y., Hain, M. P., Humphreys, M. P., Hartman, S., and Tyrrell, T.: What drives the latitudinal gradient in  
2246 open-ocean surface dissolved inorganic carbon concentration?, *Biogeosciences*, 16, 2661-2681,  
2247 <https://doi.org/10.5194/bg-16-2661-2019>, 2019.  
2248